2019

CASCADIA SUBDUCTION ZONE COSEISMIC SUBSIDENCE ESTIMATES FROM NORTHERN CALIFORNIA AND WASHINGTON

Jason Scott Padgett
University of Rhode Island, jason_padgett@uri.edu

CASCADIA SUBDUCTION ZONE COSEISMIC SUBSIDENCE ESTIMATES FROM NORTHERN CALIFORNIA AND WASHINGTON

BY

JASON SCOTT PADGETT

A DISSERTATION SUBMITTED IN PARTIAL FULFILLMENT OF THE REQUIREMENTS FOR THE DEGREE OF

DOCTOR OF PHILOSOPHY

IN

BIOLOGICAL AND ENVIRONMENTAL SCIENCE

UNIVERSITY OF RHODE ISLAND

2019

DOCTOR OF PHILOSOPHY IN BIOLOGICAL AND ENVIORNMENTAL

SCIENCES

OF

JASON SCOTT PADGETT

APPROVED:

Dissertation Committee:

Major Professor Simon Englehart

Brian Savage

Rebecca Robinson

Robert Witter

Nasser H. Zawia
DEAN OF THE GRADUATE SCHOOL

UNIVERSITY OF RHODE ISLAND
2019

ABSTRACT

This study aims to supplement the paleogeodetic database of past Cascadia subduction zone earthquakes and further our understanding of the Cascadia subduction zone seismic and tsunami hazards. I first address a previously identified spatial gap within the Cascadia paleogeodetic database in southern Cascadia by refining the timing and magnitude of Cascadia subduction zone earthquakes over the past 2000 years in northern Humboldt Bay, California (~44.8°N, -124.2°W). There, I mapped wetland stratigraphy consistent with past megathrust earthquakes across three marshes; Jacoby Creek, McDaniel Creek, and Mad River Slough. To improve the existing paleoseismic chronology at northern Humboldt Bay, I employed Bayesian age modeling based on 21 minimum and maximum limiting ages of short-lived plant macrofossils. These AMS ages found above and below subsidence contacts coupled to the construction of Bayesian age models provide the tightest age distributions for stratigraphic evidence of plate boundary earthquakes along the southern Cascadia coastline over the last 2 ka. These subduction zone earthquakes are dated to CE 1700, ~870 cal yrs BP, ~1125 cal yrs BP, and ~1600 cal yrs BP. I also provide estimates of coseismic subsidence of 0.90 ±0.46m for the 1700 earthquake, 0.39±0.33 m for the ~870 cal yr BP earthquake, 0.99±0.44 m ~1125 cal yr BP earthquake, and ≥0.86 m for the ~1600 cal yr BP earthquake using a validated foraminiferal-based Bayesian transfer function (BTF).

To further improve our confidence in the BTF analysis required an evaluation of the stratigraphic and biostratigraphic variability preserved within the wetland stratigraphy across northern Humboldt Bay. Therefore, I compiled a large stratigraphic

and biostratigraphic dataset that allowed for inter- and intra-site variability and replicability assessments of foraminiferal BTF coseismic subsidence estimates. I analyzed 26 sediment cores containing the four mud-over-peat contacts; nine for the 1700 contact (average of 0.63 ±0.36 m subsidence), five for the ~870 cal yr BP earthquake (average of 0.39 ±0.35 m), six for the ~1125 cal yr BP earthquake (average of 0.7±0.39 m) and six for the ~1600 cal yr BP earthquake.(≥0.86 m). The estimate for the 1600 cal yr BP earthquake is a minimum because, across the estuary, the contact formed above the upper limit of foraminiferal habitation. Intra-site variability of coseismic subsidence estimates reached a maximum of 0.59 m for the 1700 earthquake at McDaniel Creek. Inter-site averaged coseismic subsidence variability reached a maximum of 0.47 ±0.48 m between McDaniel Creek (0.80 ±0.41 m) and Mad River Slough (0.33 ±0.25 m) for the 1700 earthquake. The maximum inter-site individual core site variability is 0.76 m from McDaniel Creek (1.04 ±0.42 m) to Mad River Slough (0.28 ±0.26 m). Based on the variability results, I recommend a minimum of two to ideally three RSL reconstruction across the same stratigraphic sequence to provide increased confidence in the subsidence estimate.

The lessons I learned from northern Humboldt Bay were then transferred to southwest Washington, where I focused on identifying the variability of subsidence during the CSZ 1700 earthquake at six new sites, spanning 75 km along-strike, within the CSZ 1700 BTF paleogeodetic database; Copalis River, Ocean Shores, Johns River, Smith Creek, Bone River, and Naselle River. I provide eight estimates (two are within-site replicates) of subsidence for the 1700 earthquake that range from 0.39 ±0.37 m at Johns River to 1.52 ±0.51 m at Smith Creek. The seven new estimates of

the CSZ 1700 earthquake from northern Humboldt Bay (1) and southwest Washington (6) were integrated into a margin-wide BTF paleogeodetic database (14), which increases the number of measurements by 50% to a total of 20 estimates margin wide. The updated BTF paleogeodetic data are used to constrain new 3-D elastic dislocation models that inform seismic and tsunami hazard assessments. In this work, we develop three alternate 3-D elastic dislocation models that improve modeled coseismic that identify multiple non-unique solutions that fit to the coastal coseismic subsidence estimates. Even with the new coseismic subsidence constraints, a four-patch slip distribution still the best hypothetical solution. Our results highlight the need for additional high-quality subsidence estimates within the remaining spatial gaps,.e.g., between Nehalem-Netarts, such as at Tillamook Bay.

ACKNOWLEDGMENTS

There exists a very long list of people who have influenced my path in life that has led me to this point. I am sincerely grateful for the experiences and interactions with them all.

I thank my advisor Simon Englehart. I consider myself very fortunate to have had the opportunity to learn from and work with Simon. Simon took a chance on me and I hope I was able to meet some of his expectations. I am eternally grateful for his patience, understanding, support, and all of his efforts that provided me with a world-class educational experience. I share this achievement with Simon.

I owe many thanks to each of my co-authors and dissertation committee members. Their contributions towards my learning are sincerely appreciated and will not be forgotten.

I thank the URI Geology Department, URI Sea Level Research Lab, and my office mates, e.g., Matthew Gerlach, Byron Halavik, Rachel Streans, Greta Janigian and Maxwell Meadows.

I sincerely thank my loving partner Savannah Harik, for her unwavering support, love, and understanding. I also thank my family for their support and understating my need to stay in school another five years. My partner and family have been an incredibly dynamic support system for me. Without their love and care this would not have been possible. I consider this achievement just as much theirs as it is mine.

PREFACE

This dissertation is written in manuscript form in accordance with the requirements of the Graduate School of the University of Rhode Island. This dissertation contains three chapters as three manuscripts. Chapter one, entitled Timing and the amount of Cascadia earthquake subsidence over the past 2,000 years at northern Humboldt Bay, California, USA is prepared for submission to the journal *GSA Bulletin*. Chapter two, entitled Variability of coseismic subsidence estimates from sites in northern Humboldt Bay, California (USA) is prepared for submission to the journal *Marine Micropaleontology*. Chapter three, entitled Expanding the Cascadia 1700 CE paleogeodetic database with subsidence estimates from southwest Washington and the implications for an elastic dislocation model is prepared for submission to the journal *Bulletin of the Seismological Society of America*.

TABLE OF CONTENTS

LIST OF TABLES

TABLE PAGE

CHAPTER 1

CHAPTER 2

CHAPTER 3

LIST OF FIGURES

FIGURE PAGE

CHAPTER 1

CHAPTER 3

CHAPTER 1

Timing and the amount of Cascadia earthquake subsidence over the past 2,000 years at northern Humboldt Bay, California, USA

J. Scott Padgett[1], Simon E. Engelhart[1], Harvey M. Kelsey[2], Robert C. Witter[3], and Niamh Cahill[4]

[1]Department of Geosciences, University of Rhode Island, Kingston, Rhode Island 02881, USA
[2]Department of Geology, Humboldt State University, Arcata, California 95524, USA
[3]U.S. Geological Survey, Alaska Science Center, 4210 University Drive, Anchorage, Alaska 99508, USA
[4]Department of Mathematics and Statistics, Maynooth University, Kildare, Ireland

This chapter/manuscript is prepared for submission to the journal *GSA Bulletin*.

ABSTRACT

Stratigraphic, lithologic, foraminiferal, and radiocarbon analyses indicate that at least four abrupt peat-to-mud contacts are recorded across three sites (Jacoby Creek, McDaniel Creek and Mad River Slough) in northern Humboldt Bay, California (~44.8°N, -124.2°W). The contacts record subsidence during past megathrust earthquakes at the southern Cascadia subduction zone, ~40 km north of the Mendocino Triple Junction. Maximum and minimum radiocarbon ages on plant macrofossils from above and below laterally extensive (>5 km) contacts suggest regional synchronicity of subsidence. The shallowest contact has radiocarbon ages consistent with the last great earthquake at Cascadia in 250 cal yr BP (CE 1700). Using Bchron and OxCal software, we model ages for the three older contacts of ~870, ~1,125 and ~1,600 cal yrs BP.

For each of the four earthquakes, we analyze foraminifera across representative sediment cores selected from McDaniel Slough. Changes in fossil foraminiferal assemblages across all four contacts reveal sudden relative sea-level (RSL) rise (land subsidence) with lasting submergence (decades to centuries). To estimate subsidence during each earthquake, we reconstructed RSL rise across the contacts using the fossil foraminiferal assemblages in a Bayesian transfer function. The coseismic subsidence estimates are 0.90 ±0.46m for the 1700 earthquake, 0.39±0.33 m for the ~870 cal yrs BP earthquake, 0.99±0.44 m ~1,125 cal yrs BP earthquake, and ≥0.86 m for the ~1,600 cal yrs BP earthquake. The estimate for the 1,600 cal yr BP earthquake is a minimum because the paleoenvironment likely formed above the upper limit of foraminiferal habitation. Although, the subsidence estimates for 1700 CE, ~1,125 cal

yrs BP, and ~1,600 cal yrs BP are similar, the estimate for ~870 cal yrs BP is lower, which suggests that subsidence varied over the past four earthquake cycles in southern Cascadia.

INTRODUCTION

Many of Cascadia's coastal wetlands host extensive stratigraphic evidence for coseismic subsidence induced by earthquake rupture on the subduction megathrust. Over three decades of coastal paleogeodetic research on these natural archives has greatly improved our understanding of Cascadia plate boundary processes (Atwater, 1987; Darienzo, 1987; Peterson and Darienzo, 1991; Atwater et al., 1992; Nelson, 1992; Nelson et al., 1996; Shennan et al. 1996; Atwater and Hemphill-Haley, 1997; Kelsey et al., 2002; Witter et al., 2003; Hawks et al., 2010, 2011; Engelhart et al., 2013, Wang et al., 2013; Milker et al., 2017). However, fundamental questions regarding past great (M_w >8.0) Cascadia subduction zone (CSZ) earthquake segmentation and magnitude remain unanswered. For example, 1) given better quality radiocarbon samples and improved radiocarbon age models, is the paleoseismic community achieving sufficient dating precision to distinguish separate subduction zone earthquake events both at-a-site and along a margin and 2) what coseismic deformation estimate resolution is needed in order to ascribe coseismic variability both at-a-site over multiple earthquake cycles and/or along-margin during one earthquake?

Stratigraphic correlation of wetland stratigraphy within a marsh, over 10-100's m, can be straightforward but becomes increasing difficult with distance, across multiple marshes within a single estuary and over 10-100's km among estuaries (Nelson et al., 1996; Milker et al., 2016). For earthquakes prior to the well-

documented 1700 CE (Common Era) earthquake, radiocarbon dating techniques aid with stratigraphic correlation within-and across-sites. However, in many cases radiocarbon age errors can be on the order of several hundred years, which presents difficulties when attempting to correlate stratigraphic earthquake contacts, that have 200-500 year reoccurrence intervals, among estuaries (Atwater, 1987; Adams, 1990; Nelson, 1992; Nelson et al., 1996; Shennan et al. 1996; Atwater and Hemphill-Haley, 1997; Goldfinger et al., 2001; Kelsey et al., 2002; Witter et al., 2003; Nelson et al., 2008; Goldfinger et al., 2012; Enkin et al., 2013; Milker et al., 2016). However, recent research has shown that incorporation of multiple minimum and maximum limiting ages of short-lived plant macrofossils found above and below subsidence contacts (Nelson et al., 2006; 2008; Kemp et al., 2013; Milker et al., 2017) and the construction of Bayesian age models offer possibilities to produce accurate chronologies with better precision of stratigraphic ages to aid in correlation (Kelsey et al., 2005; Bronk Ramsey, 2008; Parnell et al., 2008; Goldfinger, 2011; Enkin et al., 2013; Garrett et al., 2013; Milker et al., 2016; Dura et al., 2017).

Equally as important to defining the timing of past plate boundary rupture is quantifying the amount of coseismic vertical deformation. Early Cascadia coastal research utilized qualitative and semi-quantitative methods to estimate coseismic subsidence which have accompanying errors that are typically ±0.5 – 1.0 m and generally too large to distinguish differences between earthquakes cycles or between sites. In order to improve estimates of coseismic subsidence, subsequent research has focused on the development of fully quantitative microfossil-based transfer function primarily using foraminifera (e.g., Jennings and Nelson, 1992; Guilbault et al., 1995;

1996; Nelson et al., 2008; Hawkes et al., 2010, 2011; Milker et al., 2015, 2016, Engelhart et al., 2013, 2015). Cascadia foraminiferal-based transfer function analysis enable researchers to relate differences in coseismic subsidence estimates for one earthquake at many sites (Hawkes et al., 2011; Wang et al., 2013; Kemp et al., 2018) and over multiple earthquake cycles at a single site (e.g., Milker et al., 2016). For example, Wang et al. (2013) employ a foraminiferal transfer function and identify along-strike subsidence heterogeneity during the CE 1700 earthquake and highlight large spatial gaps within the paleogeodetic database, e.g., northern California and Washington. Recent refinement and expansion of the Cascadia foraminiferal-based transfer function has led to development of a Bayesian transfer function (BTF), which can model non-unimodal taxa-elevation relationships, improves the availability of modern analogues for fossil samples, and is capable of handling sediment and microfossil mixing through assigning simple informative priors based on lithology (Kemp et al., 2018).

Although northern Humboldt Bay, California, stratigraphy provoked early CSZ paleogeodetic research attention, the complicated stratigraphic record and disparate interpretations have dissuaded subsequent clarification. For example, there remains no consensus on the number of past CSZ earthquake-induced subsidence contacts and the magnitude of coseismic deformation archived within the wetland stratigraphy. These open questions have resulted in paleoseismic interpretations that range from three to six earthquakes over the past 1900 yr BP, (e.g., Vick 1988, Clark and Carver 1992; Valentine, 1992; Pritchard, 2004; Valentine et al., 2012). However, the development

improved chronostratigraphic methods and quantitative foraminiferal-based transfer functions can help refine the northern Humboldt Bay paleoseismic history.

The goals of this paper are, first, to provide high-quality age determinations for times of wetland subsidence within the northern Humboldt Bay estuary, second, to construct a paleoseismic chronology for the site, third, to provide high-precision estimates of subsidence during each subduction zone earthquake, and fourth, to reevaluate and update regional (43.5°-40.5°) correlations of paleoearthquakes in the southern Cascadia subduction zone. Our results suggest that northern Humboldt Bay has recorded four CSZ earthquakes over the past 2,000 years and that the magnitude of coseismic subsidence has varied over these earthquake deformation cycles.

SETTING

We studied stratigraphy beneath three tidal marshes that fringe the northern portion of Humboldt Bay, Mad River Slough, McDaniel Creek, and Jacoby Creek, which are protected and managed by U.S. Fish & Wildlife Service Humboldt Bay National Wildlife Refuge and the City Arcata, California (Fig.1). Northern Humboldt Bay is separated from the Pacific Ocean by the ~20-25 m high Lanphere-Ma-le'l Dunes (Fig. 1c; Vick, 1988; Pickart and Hesp, 2018). At the mouth of Mad River Slough a NOAA tide gauge station registers the semidiurnal tidal range (Mean Highest High Water, MHHW – Mean Lowest Low Water, MLLW) at 2.36 m (Fig. 1c; ID: 9418865). Because over half of northern Humboldt Bay surface area is exposed at low tide, most of the environments of the lagoon system are tidal channels and low-tide mud flats (Eicher, 1987). Low marshes form at elevations around mean high water

(MHW) and high marshes form at elevations around mean higher high water (MHHW; Pritchard, 2004).

Flora and fauna within northern Humboldt Bay are typical for Cascadia tidal wetland plant and animal distributions (Pritchard, 2004; Hawkes et al., 2010; Engelhart, 2015; Kemp et al., 2018). Plant communities of lower marsh environments, around MTL, include *Distichlis spicata*, *Salicornia virginica*, *Spartina densiflora*, and *Triglochin maritimum* (Eicher, 1987). In high marsh environments plant communities include *Castilleja exserta*, *Distichlis spicata*, *Grindelia spp*., *Jaumea carnosa, Spartina alterniflora*, and *Triglochin maritimum* (Eicher, 1987). Kemp et al., (2018) show that intertidal benthic foraminiferal communities are comparable along the west coast of North America from ~35.5 -50° N. Benthic foraminiferal communities differ along an intertidal gradient such that higher marsh environments, around MHHW, are often dominated by *Trochaminita spp.*, *Haplophragmoides spp.*, *Balticammina pseudomacrescens*, *Trochammina inflata*, and *Jadammina macrescens*. Whereas at elevations from ~MHW down to MTL, increasing percentages of *Miliammina fusca*, *Ammobaculites spp.*, *Reophax spp.,* and calcareous foraminifera species are reported (Guilbault et al., 1995; 1996; Nelson et al., 2008; Hawkes, 2010, 2011; Engelhart et al., 2013a, 2013b; Pilarcyk et al., 2014 et Milker et al., 2015a, 2015b, 2016; Kemp et al., 2018).

We selected our three study sites because the existing wetland stratigraphic framework reflects a complicated stratigraphic record of earthquake subsidence. The stratigraphic sections typically consist of repeated abrupt *mud-over-peat* and *mud-*

over-forest soil contacts, where a peat or forest soil is sharply overlain by tidal mud and then the tidal mud gradually grades into the next organic-rich unit.

RESEARCH APPROACH AND METHODS

Like many Cascadia wetlands, the sediment and stratigraphy at northern Humboldt Bay may record evidence of coseismic land-level changes during past great CSZ earthquakes. In order to evaluate if stratigraphy is evidence of megathrust-induced land-level changes, we utilize a strategy refined by over three decades of research along the Cascadia margin through the context of land-level changes expressed by contrasting stratigraphic units within intertidal sediments (Atwater, 1987; Hemphill-Haley, 1995; Nelson et al., 1996; Kelsey et al., 2002; Witter et al., 2003; Hawkes et al., 2011; Engelhart et al., 2013; Milker et al., 2017). Stratigraphic sections consisting of abrupt *mud-over-peat* and *mud-over-forest soil* contacts are the most common signature of coastal coseismic subsidence associated with CSZ megathrust deformation.

We consider six criteria after Hemphill-Haley (1995),Nelson et al., (1996) and Shennan et al., (2016) to test for regional coseismic subsidence of tidal marsh deposits. These criteria include suddenness of submergence, lasting submergence, amount of submergence, lateral extent of stratigraphic contacts, coincidence of tsunami deposit, and regional synchroneity of submergence by employing stratigraphic mapping, lithostratigraphic analysis, fossil foraminiferal analysis, and radiocarbon age estimates that correlate with other plate boundary earthquake records in southern Cascadia (Table 4; Fig. 4). We do not discuss the coincidence of tsunami deposit criterion because we found no evidence for a tsunami deposit above buried

organic-rich units. The ~20-25 m high, Lanphere-Ma-le'l Dunes have likely protected northern Humboldt Bay from tsunami inundation (Fig. 1c; Vick, 1988; Pickart and Hesp, 2019).

Our research approach is three-fold; 1) lithostratigraphic analysis (describe subsurface stratigraphy at multiple core locations across three sites), 2) Chronologic analysis using Bayesian age models (constrained by radiocarbon AMS ages of plant macrofossils) and 3) relative sea-level reconstructions (estimate paleoenvironmental elevation changes using fossil foraminiferal data and an existing BTF; Kemp et al., 2018).

Lithostratigraphic analysis

Stratigraphic description and sampling

We compiled stratigraphic descriptions from 31 core locations over a >6 km transect at Mad River (6), McDaniel Creek (15), and Jacoby Creek (10) moving west to east (landward) along the northern shore of northern Humboldt Bay. Wetland stratigraphy consists of clastic mud and interbedded organic-rich units. A clastic "mud" refers to a olive grey massive to finely (1-3mm) bedded silts and clays. An "organic-rich unit" refers to a dark oxidized salt marsh peat or a forest soil.

Using a 30 mm wide gouge core, we mapped sharp (<10mm) to abrupt (<1mm) *mud-over-peat* and *mud-over-forest soil* contacts up to ~4 m depth below the ground surface. Grain size, sedimentary structures, contacts, thickness, and facies changes were described in the field using general stratigraphic methods in combination with the Troels-Smith (1955) method for describing organic-rich sediment. Stratigraphic unit descriptions include peat, muddy peat, peaty mud, and

mud. Organic percentages determined by qualitative field assessment (Troels-Smith, 1955); for peat, muddy peat, and peaty mud are 100%-75%, 75%-50%, and 50%-25%, respectively. Silt and clay units that consist of <25% organics by volume are described as "mud". Samples were collected for radiometric and biostratigraphic analyses using either an Eijkelkamp peat sampler or a 60 mm gouge core.

Stratigraphic Imaging

Contact sharpness and continuity is not always clear from optical inspection. Therefore, we followed recent studies in Cascadia (e.g., Milker et al., 2016) and Alaska (e.g., Briggs et al., 2014) and obtained high-resolution imagery in order to analyze fossil core density contrasts. Computerized tomography (CT) scans were conducted at Oregon State University College of Veterinary Medicine and Rhode Island South County Hospital, following the methods outlined in Rothwell and Rack (2006) and Davies et al. (2011). Density measurements were performed using a Toshiba Aquilion 64 Slice. Scans were collected at 120 kVp and 200 mA and a pitch of 0.5s (100 mAs). For visualization purposes, the resulting images were processed with a "bone" algorithm to generate coronal images every millimeter across the core. X-radiation (X-ray) images, collected with a Shimadzu UD150B-40 and imaged with a Fuji FCR XL-2 at the University of Rhode Island Health Center, also illuminate density differences within the collected sediment cores. The cores were scanned in ~60 cm segments and then joined into composite imagery using Horos and Adobe software.

Surveying to sea-level datum

Sample elevations for each core were acquired using RTK-GPS. Data collected by the RTK-GPS was post-processed using Online Positioning User Service, (https://www.ngs.noaa.gov/OPUS/) to obtain North American Vertical Datum 1988 (NAVD88) orthometric elevations. To establish elevations with respect to a tidal datum, we took RTK-GPS measurements of the tidal benchmarks associated with the temporary tide gauge installation (12/01/1978 to 03/31/1979) at Mad River Slough (NOAA ID: 9418865).

Chronologic analysis

Radiocarbon dating

Plant macrofossils were collected from representative core material to provide bracketing maximum and/or minimum-ages for each organic-rich unit upper contact at all three sites. We focused on samples that were found in growth position and/or close (<3cm) to abrupt *mud-over-peat* and *mud-over-forest soil* contacts and that have the potential to tightly constrain the timing of the organic-rich unit burial, such as rhizomes of salt-marsh plants that have a known relationship to the surface of the marsh (n=13). We also collected detrital fragments of plants including stems (n=7) and wood fragments (n=1), and seeds and seed casings (n=2). Discrete stratigraphic intervals, that range from 0.5 cm to 1.5 cm, were sampled from cores and disaggregated on a glass plate under a binocular microscope. Occasionally, high-resolution CT scans and X-radiographic images aided in targeting organic materials to be extracted from sediments. Selected material, usually plant rhizome, stem, or seed, was cleaned of all attached sediment particles and rootlets; then oven dried at ~50° C for 24 hrs (Kemp et al., 2013; Nelson et al, 2015; Törnqvist et al., 2015). Once dried

and weighed, samples were sent to National Ocean Science Accelerator Mass Spectrometer (NOSAMS) laboratory at Woods Hole Oceanographic Institute for analysis. The AMS radiocarbon age results were calibrated with OxCal using the IntCal13 calibration curve (Reimer et al., 2013).

Bayesian Age-models

Two Bayesian age models with different assumptions are utilized to estimate time of subsidence, OxCal (version 4.2; Bronk Ramsey, 2009; Sequence command) and Bchron 4.1.2 (Haslett and Parnell, 2008). We incorporate maximum and minimum OxCal calibrated ages to develop an estuary-wide representative composite stratigraphy. We selected samples to be dated that were as close to the upper contacts of the buried organic-rich units as possible. Using the OxCal 4.2 'Sequence command' can be seen as a more conservative approach that uses stratigraphic order as prior information in composite stratigraphy. In contrast, Bchron incorporates sample depths to further constrain the age estimate by modeling a sedimentation rate between age constraint intervals. This trims the predicted age resulting in a more precise estimate. However, the accuracy will be dependent on an appropriate density of radiocarbon dates that can identify changes in sedimentation rate that may be expected post-earthquake and that exceed the long-term average. Using more than one Bayesian age model technique, with different assumptions, enables us to assess the impacts of utilizing different methods and the variability in age estimates that may be imposed by model choice.

Regional Paleoseismic Timing Correspondence

We compare the age distributions derived from OxCal results from northern Humboldt Bay with the timing of plate-boundary earthquakes at other sites along the southern Cascadia coastal estuarine and lacustrine environments from 43.5° - 40.5° N, which include Eel River (Li, 1992), southern Humboldt Bay (Patton, 2004), Lagoon Creek (Abramson, 1998; Garrison-Laney 1998), Sixes River (Kelsey et al., 2002) Bradley Lake (Kelsey et al., 2005), Coquille River (Witter et al., 2003), Talbot Creek, tributary to South Slough in the Coos Bay region of Southern Oregon (Milker et al, 2016). We also compare offshore turbidite data has been interpreted to reflect shaking produced by great earthquakes (Goldfinger et al., 2012). Bradley Lake and Lagoon Creek are coastal lacustrine environments that are inferred to have recorded tsunami inundation coincident with plate-boundary earthquakes. Eel River, southern and northern Humboldt Bay, Sixes River, Coquille River, and Talbot Creek are estuarine marshes that have recorded evidence for both coseismic land-level changes and occasionally subsequent tsunami inundation. Offshore turbidite chronology provides the longest stratigraphic records of CSZ paleoseismic history. Even though each of the environments uniquely document stratigraphic evidence for plate-boundary earthquakes and therefore each have unique magnitude thresholds necessary to trigger coseismic depositional processes, each record evidence of earthquakes over the past 2000 years (Fig. 4).

Relative sea-level reconstructions

Foraminifera

Fossil foraminifera specie assemblages can be indicative of paleo-intertidal environments. We followed standard sample preparation and analysis techniques of

fossil foraminiferal found within wetland stratigraphy (e.g. Scott and Medioli, 1982; de Rijk, 1995; Horton and Edwards, 2006). Fossil foraminifera were concentrated by sieving 1 cm intervals of sediment (~3cm^3) from collected cores over 500- and 63-micron sieves and retaining the material between those size fractions. The 500-micron sieve was checked for larger foraminifera before material was discarded. Fossil samples were analyzed until at least 200 dead foraminifera were identified, or until the entire sample was enumerated (Fatela and Taborda, 2002). Following after Kemp et al. (2018), only samples with >30 foraminifera were used in the production of quantitative RSL reconstructions because low abundances may reflect a non in-situ assemblage and/or may not be representative of the depositional environment. Foraminifera were identified following taxonomy based on Hawkes et al. (2010) and Milker et al. (2015). Additionally, we combine *Haplophragmoides spp* following Kemp et al. (2018).

Transfer Function

Sudden RSL change caused by subsidence during past great earthquakes along the Cascadia coastal margin can be quantified using fossil foraminifera (found within subsidence stratigraphy) and a transfer function (Guilbault et al., 1995; 1996; Nelson et al., 2008, Hawkes et al., 2010; 2011; Engelhart et al., 2013; Wang et al., 2013; Milker et al., 2016; Kemp et al., 2018). Early fossil foraminifera transfer functions utilized a local (same site) training set of foraminiferal assemblages and tidal elevations (Guilbault et al., 1995; 1996; Nelson et al., 2008). Later efforts progressed to regional modern training sets where taxa-elevation relationships were unimodal (Hawkes et al., 2010; 2011; Engelhart et al., 2013; Wang et al., 2013; Milker et al.,

2016). Generally, a larger modern dataset provides higher diversity of modern analogs and covers more natural variability but is often accompanied with reduced precision (Horton and Edwards, 2005). More recently, Kemp et al. (2018) developed a BTF that incorporates an extended West Coast modern foraminifera training set, allows for flexible species-response curves, and can formally incorporate prior information from additional proxies, e.g., other microfossil groups, $\delta^{13}C$, or stratigraphic context, which combine to produce improved precision of RSL reconstruction and extends applicability of the methodology (Cahill et al., 2016; Holden et al., 2017). We follow Kemp et al. (2018) and assign stratigraphic context as informative priors to RSL reconstructions. The stratigraphic context ranges from either clastic dominated (tidal flat) to low salt-marsh sediment, which accumulates at elevations between mean low water (MLW) and MHHW (20-200 SWLI), or organic-rich high salt marsh, which accumulates at elevations around MHW to the highest occurrence of foraminifera (HOF; 180-252 SWLI; Kemp et al., 2018). The BTF cannot incorporate a lithologic prior assignment of a forest or upland soil unit, as it occurs above HOF and foraminifera cannot inform such elevations. In order to evaluate if a fossil assemblage has a modern analog, we used the Bray-Curtis distance metric. Due to low species diversity, a threshold of less than the 20th percentile is appropriate for salt marsh foraminifera modern and fossil assemblage pairings (Kemp and Telford, 2015).

RESULTS

First, we describe wetland stratigraphy across the three sites. Then, we present radiocarbon ages that constrain the timing of organic-rich unit burial. Using the radiocarbon age results, we correlate the upper contacts of buried soils among all the

sites using lithology and age. Based on increasing depth, we refer to the upper contacts of organic rich units as contact A, B, C, D, and E. Next, we present radiocarbon age modeling in order to assign age ranges for the abrupt *mud-over-peat* and *mud-over-forest soil* contacts. Finally, we examine lithology, foraminiferal assemblages, and regional timing correlations in order to evaluate if a contact represents coseismic subsidence during an Cascadia subduction zone earthquake.

Wetland Stratigraphy

Throughout the northern Humboldt Bay estuary, we mapped abrupt (~1mm) to sharp (<3mm) *mud-over-peat* and *mud-over-forest soil* contacts (Fig. 2). In cores, we observed grey mud units sharply overlying organic-rich units, which we refer to as a buried organic-rich unit. The organic-rich units contain relatively abundant plant macrofossils. The clastic muds contain sparse plant macrofossils and were often massive and occasionally finely bedded. We did not observe any sand layers in-between an organic-rich unit and overlying mud across the estuary. In general, the shallowest subsidence contact and underlying organic-rich unit is well-defined and widespread, while deeper subsidence contacts and underlying organic-rich units are often less distinct with a more restricted lateral extent. Our reconnaissance core descriptions revealed five buried organic-rich units at Mad River Slough, four buried organic-rich units at McDaniel Creek and three buried organic-rich units at Jacoby Creek (Fig. 2; Table 1). We reoccupy previously described wetland stratigraphic sections (Vick, 1988; Clarke and Carver, 1992; Valentine, 1992; Pritchard, 2004; Valentine et al., 2012) and further extend the spatial extent of wetland stratigraphic mapping in northern Humboldt Bay. In doing so, we document buried organic-rich

units that have not been previously described at McDaniel Creek and Jacoby Creek marshes. For lab analysis, we selected representative stratigraphic segments (50cm) of key stratigraphic intervals that visually contained the sharpest contacts between the clastic-over-organic units and/or abundant short-lived plant macro fossils.

Mad River Slough

Vick (1988) was the first to describe the wetland stratigraphy of Mad River Slough at 12 sites and identified four-to-five subsidence sequences in the southern section of the marsh and one subsidence sequence at the northern portion of the marsh. Subsequent investigations reoccupied several Vick (1988) sites and developed both similar (Valentine, 1992; Clarke and Carver, 1992;) and diverging (Pritchard, 2004; Valentine, 2012) conclusions. We reoccupied six coring sites of Vick (1988) in the southern portion of Mad River Slough and observed similar stratigraphy.

We observed five organic-rich units in individual cores; but based on lithology and depth, we can correlate four of the organic-rich units with sharp upper contacts across the six-location survey at Mad River Sough (Figs. 1 and 2b). Core top elevations differ from the west to the east side of the main tidal channel, 2.1 m and 1.4 m respectively (NAVD88). The shallowest organic-rich unit was observed at 100-150 cm depths at every core location, has an abrupt to sharp upper contact, and is a bold 15-35 cm thick peat. At core sites *MR.2* and *MR.7*, at 169 and 174 cm core depths, we observed the second deepest organic-rich unit; a 3-4 cm thick bold organic-rich unit in sharp upper contact with a 5 cm and 7 cm thick overlying mud (DR1). The third deepest organic-rich unit was identified at every core location between depth intervals of 184-227 cm, is 10-20 cm thick, has an abrupt-to-sharp upper contact, and ranges

from a peat at the top of the unit to a rooted mud at the base. The fourth organic-rich unit is represented within four of the six core locations, observed between the cores depth of 245-275 cm, has a sharp upper contact, and is a 15-20 cm thick organic-rich unit that ranges from a muddy peat to a peat between core locations. The fifth and deepest organic rich-unit was observed on the east side of the main channel at two proximate core locations, *MR.2* and *MR.7*, with a sharp upper contacts between 293 - 303 cm core depths, and is a 4-12 cm thick highly humified decomposed-peat.

Five organic-rich units were observed at two core locations, three buried organic-rich units were observed at two core locations, and two buried organic-rich units were observed at two core locations. Mad River Slough archives the highest amount of stratigraphic variability throughout the estuary.

McDaniel Creek

Pritchard (2004) was the first to describe wetland stratigraphy from McDaniel Creek slough across four sites and described two subsidence sequences south of the reclaimed farm land dike. We expanded upon these initial descriptions by describing a further 15 core locations further west-northwest and observed four organic-rich units with sharp upper contacts within the stratigraphy that can be correlated across the marsh using lithology and depth (Figs. 1 and 2a). South of the dike, core location elevations range from 2.0 to 2.3 m and north of the dike core locations range from 1.8 to 2.0 m (NAVD88).

The shallowest organic-rich unit was observed at every core location between 78-145 cm core depths, ranges from 5 cm thick in the northern section (*MD.18*) of the

locality to as much as 24 cm thick further south (*MD.08*), and varies from a muddy peat to a peat both across multiple core locations and also within the unit.

The second organic-rich unit has an abrupt upper contact between 170.5-213 cm core depths at seven core locations, is 4-12 cm thick, and varies from a rooted mud to a muddy peat between locations and within the unit. At *MD.06*, the second deepest buried organic rich-unit is at 170.5 cm core depth is sharp and separates a muddy peat from an overlying mud (Fig. 5b). The brown muddy peat unit is 6cm thick and capped by a grey mud that extends >20cm. CT images show a sharp ~3 mm contact with ~5mm of undulating relief and >6 cm of overlying mud that contains detrital organics and/or paleoburrow. The seemingly semi-vertical void that extends across the CT image is possibly a crack that occurred during sediment collection and/or shipping (Fig. 5b).

The sharp upper contact of the third deepest organic-rich unit was observed between 226-273 cm at nine core locations, is 4-33 cm thick, and varies from a rooted mud to a peat between locations and within the unit.. The CT scan of *MD.13* shows a sharp contact at 248 cm to have ~14mm of undulating relief and separates an 8 cm thick organic-rich unit, where the upper 3 cm is a light brown muddy peat and the lower 5 cm are a grey-brown rooted mud, from a >25 cm thick finely bedded grey mud.

The fourth organic-rich unit was observed in nine core locations, is 4-13 cm thick, and is a humified organic-rich unit with a sharp to moderately diffuse (~6 mm) upper contact. At *MD.05*, the sharp upper contact of the deepest buried organic-rich unit is at 308 cm depth, undulates over >15 mm, and separates a dark grey-black

organic-rich unit from an overlying grey mud (Fig. 5D). The organic rich unit is 12 cm thick and is overlain by a grey mud that extends >25 cm. X-ray analysis identifies that the overlying grey mud appears to have infiltrated into the underlying highly humified organic rich unit below (Fig. 5D).

Four organic-rich units were observed at five core locations while three organic-rich units were observed at seven core locations. Both second and third deepest buried organic-rich units display an increasingly organic content to the northeast towards the modern channel. McDaniel Creek archives the largest lateral extent of organic-rich units with sharp upper contacts throughout the estuary.

Jacoby Creek

Valentine (1992) and Pritchard (2004) studied the stratigraphy of the Jacoby Creek marsh and described two buried organic-rich units. Valentine (1992) described stratigraphy at five locations, four (three outcrops and one core) north of Jacoby Creek and one outcrop to the south. Pritchard (2004) described stratigraphy at three core locations north of Jacoby Creek and nine core locations to the south. Similar to previous investigations (Valentine, 1992; Pritchard, 2004), we observed one subsidence sequence close to the mouth of Jacoby Creek at *JC.6*. We extended stratigraphic mapping ~200-400m north from *JC.1* and observed three buried organic rich units (Figs. 1 and 2c).

Across a ten-core transect, three organic-rich units with sharp upper contacts were correlated based on depth in cores and lithology. Elevations of the core tops range from 1.95 to 2.39 m (NAVD88). At the northern and southern extents of the survey transect in cores *JC.6, 8,* and *7* only one buried organic-rich unit was observed.

Three buried organic-rich units were observed within 200 cm from the salt marsh surface at four core locations, *JC.2, 3, 5,* and *10*. The shallowest organic-rich unit was observed at 70-95 cm depths at eight core locations, has a sharp to abrupt upper contact, is 8-12 cm thick, and ranges from bold, well-developed peat to a muddy peat within the unit. The second deepest organic rich unit was observed at 120-140 cm depths at seven core locations, is 5-10 cm thick, and ranges from a peat to a muddy peat both within the unit and across multiple core locations. The deepest organic rich-unit was observed at 160-180 cm depths at five core locations, is a 4-8 cm thick highly-humified forest soil, has a sharp to gradational upper contact, and overlies pebbly-sand alluvial sediments.

At Jacoby Creek, we observed three buried organic rich units at four core locations, two buried organic-rich units at three locations, and one buried organic-rich unit at three core locations. Jacoby Creek core sites have the highest core top elevations, cover the smallest surface area, and have the most compact wetland stratigraphic section in northern Humboldt Bay.

Radiocarbon Ages

We used 20 radiocarbon ages of plant macrofossils to determine the timing of paleoenvironmental changes across the upper contacts of buried organic-rich units (Table 1). Whenever possible, we used identifiable plant material. Both minimum and maximum age samples were found above and below the three deepest buried organic-rich unit upper contacts and constrain the timing of those paleoenvironmental changes.

Although we obtained 23 radiocarbon ages, we exclude three dates where outlier analysis suggests that downward bioturbation and/or root penetration has

resulted in a younger age than stratigraphic position would suggest (sample *JC.14.02.D.100-101*), and detrital reworking and deposition has resulted in anomalous older dates than stratigraphic position suggests (*JC.14.02.D.103-104* and *JC.14.02.D.103-105*) (Fig. 2; Table 1). The calibrated ages range from modern to 1575–1707 cal years BP, indicating the sediments accumulated over the last two millennia (Table 1). We infer that the shallowest organic-rich unit burial occurred during the most recent 250 cal yrs BP (1700 CE) CSZ megathrust earthquake (Atwater 1987; Nelson 1992; Satake et al 2003; Atwater and Hemphill-Haley 2005), which is consistent with three maximum radiocarbon ages that range from 170-235 ^{14}C years.

Seven radiocarbon ages, five from core MR.14.02 and two from MR.14.05, provide a 1700-year chronology (Table 1). One maximum age (235±20) from the shallowest organic-rich unit falls within last ~300 yr radiocarbon calibration plateau and is consistent with the most recent CSZ 1700 CE earthquake. The age of a *D. spicata* rhizome derived from the second deepest buried organic-rich unit is consistent with previous paleoseismic dating results of the same unit, 476-511 cal. yr. BP (Valentine, 1992; Clarke and Carver 1992; Valentine , 2012). Previous investigations have suggested that the second deepest organic-rich unit could represent subsidence from a CSZ earthquake; however, we did not observe similar stratigraphy or radiocarbon age anywhere else within the marsh or across the estuary. Maximum ages from the third deepest organic rich unit are consistent at MR.14.02 and MR.14.05 (1000±15 and 990±20, respectively) and aid in correlation of stratigraphy across the marsh. The burial timing of the fourth organic-rich unit is constrained by a minimum age from MR.14.02 (1100±20) and a maximum age from MR.15.05 (1290±15).

Within the deepest organic-rich unit at MR.14.02, we dated roughly 25 *Atriplex* and *Potamogeton* seeds, which provide maximum age constraint (1690±20).

Eight radiocarbon ages, two from core MD.14.03, two from MD.14.06, three from MD.14.05, and one from MD.14.04, combine to provide a 1700-year chronology at McDaniel Creek (Table1). One maximum age (170±15) from the shallowest organic-rich unit falls within last ~300 yr radiocarbon calibration plateau and is consistent with the most recent CSZ 1700 CE earthquake. The timing of burial for the second organic-rich unit is constrained by two maximum ages (1040±15 and 990±15) and one minimum age (955±15). One maximum age (1480±15) for the third deepest organic-rich unit was taken from 15 cm below the upper contact of the unit (due to the availability of representative stratigraphy during the initial dating efforts). Two maximum ages (1750±15 and 1720±15) and a minimum age (1740±15) tightly constrain the timing of burial for the fourth deepest organic-rich unit.

Eight radiocarbon ages from core JC.14.02 provide a 1700-year chronology of three instances of environmental change (Table 1). One maximum age (195±15) from the shallowest organic-rich unit falls within last ~300 yr radiocarbon calibration plateau and is consistent with the most recent CSZ 1700 CE earthquake. Maximum ages were derived from the second and third buried organic-rich units (1280±20 and 1710±20, respectively). Two minimum ages, that may be detrital, were derived from plant macrofossils found within mud units directly overlying the two deeper buried organic-rich units (1130±20 and 1710±15, respectively).

Also at *JC.2*, we observed a ~7 cm thick slightly organic unit, which was ~5 cm beneath the shallowest organic-rich unit (DR2). Although we did not recognize a

lithological change from visual inspection in the field, a density contrast within the core was identified through CT analysis. Due to the similarity to a contact observed in two cores at Mad River Slough (*MR.2* and *MR.7*) we obtained three maximum ages on this slightly organic-rich unit (modern (post 1950 CE), 1240±20, and 1390+20). Either downward root penetration, bioturbation, or contamination of the core during extraction may explain the anomalously young modern age. The two older radiocarbon ages are stratigraphically inconsistent (Table 1) with the ages from the deeper two buried organic-rich units, possibly indicating the re-deposition of older material. Therefore, we hypothesize that contact C may have been eroded at Jacoby Creek sometime prior to the 250 yr BP earthquake. Because these three radiocarbon ages are inconsistent with ages of the rest of the core and are not in stratigraphic order and we do not include them within the composite stratigraphy used in the development of Bayesian age models.

Correlation of Stratigraphy Among the Study Sites

The age results provide context for stratigraphic correlations both within the marsh as well as across the estuary. Based on depth and radiocarbon age overlap, we correlate three buried organic-rich unit upper contacts A, D and E across the three marsh sites, contact C across two marsh sites, and Contact B was only observed at one marsh. In total, we observed five *mud-over-peat* and/or *mud-over-forest soil* contacts at northern Humboldt Bay.

Contact A

Contact A is directly above the shallowest, most distinct, and most wide-spread buried organic-rich unit observed at northern Humboldt Bay. Contact A was observed

at every core location at 75.5-93.5 cm depth at Jacoby Creek, 109-121 cm depth at McDaniel Creek, and at 103-142 at Mad River Slough. Three maximum radiocarbon ages, one from each marsh, of an in-growth position rhizome and two herbaceous stems ≤10mm below the contact, range from 170-235 ^{14}C years, corroborate stratigraphic correlation across the estuary. Contact A has radiocarbon ages consistent with previous research at Cascadia, which infers that the contact dates from the 250 cal yr BP (CE 1700) earthquake. For the remainder of the paper, we will refer to Contact A as the contact that formed at the time of the CE 1700 earthquake.

Contact B

Contact B has the most limited lateral extent within the estuary as it was observed in cores *MR.2* and MR.*7* at Mad River Slough which are less than 30m apart. At 161.5 and 166.5 cm core depth at *MR.2* and *MR.7*, the sharp upper contact of organic rich-unit has ~7mm of relief and is <10 cm below the base of shallowest organic-rich unit. The organic-rich unit is 2-4 cm thick and contains 0.25-0.5 cm thick intercalated clastic beds. (DR2). The overlying 8-10 cm thick mud unit, contains~0.25 cm thick intercalated slightly-rooted beds . One maximum age of an in-situ short-lived plant macrofossil found within 1 cm below contact B is 511–476 cal yrs BP, which does not overlap with any other radiocarbon age obtained in our investigation.

Contact C

Based on stratigraphic mapping and radiocarbon age overlap, contact C was observed at Mad River Slough and McDaniel Creek. Contact C was observed between 170.5 cm and 225 cm core depths across six core locations within Mad River Slough and seven core locations in McDaniel Creek. The age of contact C is bracketed by a

minimum age from a rhizome in growth position <15 mm above the contact at *MR.02* and four maximum radiocarbon ages of three rhizomes in growth position and a herbaceous stem each within <10 mm below the contact at *MR.02*, *MR.05, MD.03, and MD.06* (Table 1). The minimum sample age 798-926 cal. yr. BP over laps with the age range of the four maximum sample ages 802-956 cal. yr. BP (Table 1).

Contact D

Based on stratigraphic mapping and radiocarbon age overlap, contact D was observed at every marsh within the northern Humboldt Bay estuary. It was observed at 113-133 cm core depths at Jacoby Creek, 226-257 cm core depths at McDaniel Creek, and 234-302 cm depth at Mad River Slough. The burial timing of Contact D is constrained by two minimum ages and three maximum ages, one from each marsh. A *Grindelia spp.* stem <25 mm above the contact at *MR.02* and a rhizome in growth position <15mm from the contact at *JC.02* range in age 961-1166 cal yrs. BP. Three maximum age samples of a rhizome in growth position, rhizome fragments, and stem fragments were each found within 15 mm below the contacts and range in age 1181-1399 cal. yrs. BP.

Contact E

Based on stratigraphic mapping and radiocarbon age overlap, contact E was observed at every marsh within the northern Humboldt Bay estuary. Contact E was observed at 163-203 cm core depths at Jacoby Creek, 250-380 cm core depth McDaniel Creek, and 295-303 cm core depth at Mad River Slough. The burial timing of contact E is constrained by two minimum ages and four maximum ages of plant microfossils. Minimum ages of wood fragments from *JC.02* and a herbaceous stem at

MD.05, both <30 mm above the contacts, have an age range of 1561-1707 cal. yr. BP. The minimum at *MD.05* (1575-1707 cal. yr. BP) is older than three of the four maximum ages. The four maximum ages on two rhizomes in growth position, one rhizome or stem, and ~25 *atiplex* and *potamogeton* seeds <20 mm below the contact have a combined age range of 1558-1708 cal. yr. BP.

Radiocarbon Age Modeling for Timing of Abrupt Subsidence

We compiled the 20 calibrated age results in order to construct a composite stratigraphy across the study sites. Ages were assigned to appropriate depth intervals relative to the upper contact depth of buried organic-rich units that we observed to have widespread evidence of coseismic subsidence; contacts C, D, and E. We do not model contact B because of a lack of both correlative stratigraphy and radiocarbon age synchroneity beyond a dissected section of marsh. We do not model contact A due to the limitations of radiocarbon imposed by a plateau in the calibration curve post CE 1650 (Reimer et al., 2013). The assumption that this subsidence sequence represents the CSZ 1700 CE megathrust earthquake is consistent with the tsunami modeling of Satake et al. (2003), tree ring ages from Nelson et al., (1995), and our radiocarbon ages. Although we do not model the age distributions of contacts A or B, we do include the ages within the composite stratigraphic column. Contacts C and E, have similar maximum and minimum ^{14}C age ranges, respectively 167 and 147 cal yrs. Contact D had the largest range ^{14}C age distribution of 438 cal yrs due to an older maximum age which was found ~15 cm below the mapped upper contact. The estuary-wide composite stratigraphy was used in the construction of the Bayesian age models.

Bayesian age-depth modeling has been used by many RSL investigations that seek to refine the timing of past changes in RSL and decrease the error envelopes of sediment accumulation histories (Garret et al., 2013; Enkin et al., 2013; Witter et al., 2015; Dura et al., 2017). Model choice is a vital component of reducing timing uncertainties and the consistency of accumulation rates should be considered (Wright et al., 2017). For example, if deposition is seasonal, steady, and predictable, like a lake bottom, then OxCal U_Sequence command would be a good age model option because deposition is assumed to be uniform. However, if a sedimentation rate is variable then models that can account for randomness in deposition can be more suitable e.g., Bchron or OxCal P_Sequence. In contrast, if only an order is known, a more conservative model command is OxCal sequence could be appropriate, which only defines an order for events and groups of events. In regard to the ability to capture known accumulation variability, within their confidence intervals OxCal and Bchron outperform other age modeling programs (Wright et al., 2017).

Here we employ a sequence command OxCal model as a simple Bayesian age model using stratigraphic position to order ages as well as a more complicated Bchron Bayesian age model to develop paleoseismic chronologies at northern Humboldt Bay. Although a composite stratigraphic approach combines ages from locations with likely different erosional histories between cores, there are consistencies between the modeled age probability density functions for the three modeled contact ages between the two Bayesian age models (Figure 3; Table 3). In general, OxCal Sequence produces broader age probability density functions and Bchron generates tighter age

ranges that are slightly older and contain more prominent peaks of age probability density function timing of organic-rich unit burial (Fig. 3).

Due to the precision of our radiocarbon data set, even the more conservative OxCal Sequence age probability density functions provide tighter age distributions than those of several regional age distributions for plate-boundary rupture evidence (Fig.4). For Contact C, OxCal Sequence modeled an age distribution of 815-924 cal yrs BP and Bchron modeled an age distribution of 850-966 cal yrs BP (Fig. 3 and Table 2). For Contact D, OxCal Sequence method generated an age distribution of 1,004-1,233cal yr BP and Bchron modeled an age distribution of 1,158-1,246cal yrs BP (Fig. 3 and Table 2). For contact E, OxCal Sequence method generates an age distribution of 1,554-1,667 cal yr BP and Bchron modeled an age distribution of 1,620-1,709 cal yrs BP (Fig. 3 and Table 2).

BURIED ORGANIC-RICH UNIT UPPER CONTACTS: contact lithology, foraminiferal analyses, regional correlation, and origin

Based on stratigraphic mapping we observed up to five *mud-over-peat* and *mud-over-forest soil* contacts at northern Humboldt Bay. To evaluate if buried organic-rich units (contacts A, B, C, D, and E) are evidence of vertical deformation during past great CSZ earthquakes we consider six criteria proposed by Hemphill-Haley (1995) and Nelson et al, (1996). These criteria include suddenness of submergence, lasting submergence, amount of submergence, lateral extent of stratigraphic contacts, amount of subsidence, coincidence of tsunami deposit, and regional synchroneity of submergence by employing stratigraphic mapping, lithostratigraphic analysis, fossil foraminiferal analysis, and radiocarbon age estimates

that correlate with other plate boundary earthquake records in southern Cascadia (Table 4; Fig. 4). We do not discuss the coincidence of tsunami deposit criterion because we found no evidence for a tsunami deposit above buried organic-rich units. The ~20-25 m high, Lanphere-Ma-le'l Dunes, have likely protected northern Humboldt Bay from tsunami inundation (Fig. 1c; Vick, 1988; Pickart and Hesp, 2019).

We selected representative sediment cores for foraminiferal analyses from McDaniel Creek because it archives the largest lateral extent of contacts A, C, D, and E. Further, we analyzed contact B from Mad River Slough due to the absence of this contact at McDaniel Creek. Sudden and lasting foraminiferal community assemblage changes were found across four abrupt contacts; A, C, D, and E. A minimal change in fossil foraminiferal assemblages were observed across contact B, within the organic-rich unit and the overlying clastic mud, therefore we did not apply the BTF to the fossil data (DR 1). According to the BTF results, contact A and contact D record a similar amount of subsidence, contact C archives the smallest amount of subsidence, and contact E records the highest magnitude of subsidence. Pairwise comparison of modern and fossil foraminiferal assemblages were well below the 20th percentile threshold, indicating that all fossil assemblages had modern analogs.

Contact A (250 cal yrs BP, 1700 CE)

Contact A is directly above the shallowest, most distinct, and most wide-spread buried organic-rich unit observed at northern Humboldt Bay. Contact A was observed at every core location at 75.5-93.5 cm depth at Jacoby Creek, 109-121 cm depth at McDaniel Creek, and at 103-142 at Mad River Slough. Three maximum radiocarbon

ages, one from each marsh, of an in-growth position rhizome and two herbaceous stems ≤10mm below the contact, range from 170-235 ^{14}C years, corroborate stratigraphic correlation across the estuary. Contact A has radiocarbon ages consistent with previous research at Cascadia, which infers that the contact dates from the 250 cal yr BP (CE 1700) earthquake. For the remainder of the paper, we will refer to Contact A as the contact that formed at the time of the CE 1700 earthquake.

At *MD.03*, the shallowest buried organic-rich unit abrupt upper contact is at 115 cm core depth (Fig. 5a). The organic-rich brown peat unit is 8 cm thick and capped by a grey mud that extends >25cm. The CT scan of *MD..03* shows an abrupt 1-2 mm contact with ~5 mm of relief and fine bedding within the overlying mud unit from 97-115 cm core depth overlying indicated by alternating yellow and orange layers (Fig. 5) that represent differing densities of sediment.

Foraminifera in the brown peat unit dominantly consist of *B. pseudomacrescens* (27-54%), *T. inflata* (7-39%), and *J. macrescens* (5-33%), which is consistent with a peat soil forming near MHHW. Samples in the mud overlying the peat unit show an increase in the abundance of *M. fusca* (5 to 14%), *Reophax spp.* (0.05-3%), *Ammobaculites spp.* (0-1.4%), and *J. macrescens* (25 to 54%) and a decrease in the abundance of *B. pseudomacrescens* (12 to 29%) and *T. inflata* (16 to 27%). The presence of *Ammobaculites spp*., *Reophax spp*., and increase of *M. fusca* is consistent with sediments accumulating near MTL (Fig. 5; Kemp et al., 2018). For the subsidence estimate we used the reconstructed RSL elevations from intervals above and below the *mud-over-peat* contact. The fossil foraminifera BTF reconstruction suggests 0.83±0.44m of subsidence which is consistent with a previous broad

subsidence estimate based on diatom analysis at Jacoby Creek of 0-1.64 m (Pritchard, 2004) and also extends the latitudinal range of foraminifera-based transfer function estimates for the 1700 earthquake (Wang et al., 2013). Our new estimate is consistent with the "preferred" model of Wang et al., (2013).

Based on young ^{14}C ages that lie within the radiocarbon plateau, shallow depth, wide-spread correlation across the northern Humboldt Bay estuary, lasting and sudden submergence of 0.88 m, and its identification for ~300 km across southern Cascadia (Fig. 4 and Table 4), we determine that the shallowest organic-rich unit was covered by tidal mud during the most recent 250 cal yrs BP (1700 CE) CSZ megathrust earthquake.

Contact B (511 – 476 cal yrs BP)

Contact B has the most limited lateral extent within the estuary as it was only observed in cores *MR.2* and MR.*7* at Mad River Slough. At 169 cm core depth at *MR.2*, the sharp upper contact of organic rich-unit is the 6-8 cm below the shallowest organic-rich unit, has ~7mm of relief. Below 169 cm core depth the organic-rich unit is 2-4 cm thick (DR2). Above the 169 cm cored depth a slightly-rooted mud unit extends for 7cm. One maximum age of an in-situ short-lived plant macrofossil is 511–476 cal yrs BP, which does not overlap with any other radiocarbon age obtained in our investigation.

We found no distinct change in foraminiferal assemblages across contact B. Within the organic-rich unit fossil assemblages dominantly range from of *B. pseudomacrescens* (51-38%) and *J. macrescens* (23-32%), *T. inflata* (16-20%) and *M. fusca* (0-1%), which is consistent with a peat soil forming near MHHW. Although

samples in the mud overlying the peat unit show a slight increase in the abundance of *M. fusca* (4 to 6%) and *Reophax spp.* (0 to 3%), and decrease of *T. inflata* (3 to 26%), there are also moderate to high abundances of *B. pseudomacrescens* (40 to 44%) and *J. macrescens* (25 to 33%), which is consistent with sediment forming between mean high water (MHW) and MHHW (DR 3?). Foraminiferal abundances in the 2cm of mud overlying the peat were extremely low (<30 individuals) suggesting that the assemblage may not be in-situ (Kemp et al., 2018).

Based on a lack of lateral extent of the contact, lack of radiocarbon age overlap within the estuary or with plate-boundary earthquake evidence age distributions regionally, and minimal fossil foraminiferal assemblage change, we do not apply the BTF to the fossil foraminifera assemblage data from contact B and we infer that it does not represent coseismic subsidence induced from megathrust rupture. We infer that this organic-rich unit is the base of the organic-rich below contact A and that the mud that separates these organic rich units could be a local hydrographic event; a likely candidate cause is an overtopping of the Mad River levee that is 6 km to the north-northeast.

Contact C (815-924 cal yrs BP)

Based on stratigraphic mapping and radiocarbon age overlap, contact C was observed at Mad River Slough and McDaniel Creek. The age of contact C is bracketed by a minimum age from a rhizome in growth position <15 mm above the contact and four maximum radiocarbon ages of three rhizomes in growth position and an herbaceous stem <10 mm below the contact (Table 1). Using these minimum and

maximum ages, OxCal Sequence modeled an age distribution of 815-924 cal yrs BP and Bchron modeled an age distribution of 850-966 cal yrs BP (Fig. 3 and Table 2).

The second deepest subsidence contact at 170.5 cm core depth at *MD.06* is sharp and separates a muddy peat from an overlying mud (Fig. 5b). The brown muddy peat unit is 6cm thick and capped by a grey mud that extends >20cm. CT images show a sharp ~3 mm contact with ~5mm of undulating relief and >6 cm of overlying mud that contains either detrital organics or is a paleoburrow. The seemingly semi-vertical void that extends across the CT image is possibly a crack that occurred during sediment collection and/or shipping (Fig. 5b).

Foraminifera in the light brown muddy peat unit dominantly consist of *B. pseudomacrescens* (12-40%) and *T. inflata* (24-36%), which is consistent with a peat soil forming near MHHW. Samples in the grey mud overlying the peat unit show an increase in the abundance of *M. fusca* (21 to 33%) and *J. macrescens* (27 to 37%) and a decrease in the abundance of *B. pseudomacrescens* (4 to 9%), which is consistent with sediments accumulating below but in close proximity to MHW. For the subsidence estimate we used the reconstructed RSL elevations from the first unmixed centimeter intervals above and below the *mud-over-peat* contact, which are 1 cm apart. The fossil foraminifera BTF reconstruction shows 0.39±0.33 m of subsidence.

Although the OxCal Sequence generated age distribution for contact C overlaps with age distributions of plate-boundary evidence at Talbot Creek, Bradley Lake, Eel River and the timing of turbidite T3 there is a lack of correlation with evidence at Coquille River, Sixes River, Lagoon Creek, and southern Humboldt Bay (Fig. 4). At Lagoon Creek, no tsunami deposit is found with an age distribution that

overlaps with contact C (Abramson, 1998; Garrison-Laney, 1998). This may be explained by coastal foredune heights that were sufficiently high to present a barrier to tsunami inundation. A potential explanation may be that the age of tsunami deposit W is derived from detrital material and may not represent a close maximum age. Both southern Humboldt Bay (Patton, 2004) and Sixes River (Kelsey et al., 2002) sites contain an undated buried organic-rich unit that was described below the inferred CSZ 1700 buried organic-rich unit and above a deeper and older buried organic-rich unit. Therefore, the undated buried organic-rich unit at southern Humboldt Bay and Sixes River could potentially contain a correlative age distribution with contact C at northern Humboldt Bay.

There are at least three potential explanations why there is a lack of correlation with contact C and evidence at Coquille River (Witter et al., 2003): 1) no earthquake occurrence; 2) formation threshold, where slip on the megathrust was insufficient to cause enough vertical deformation to be recorded by the salt marsh; and 3) preservation threshold, where the coastal system had not fully recovered/reset from the previous earthquake rupture (Benson et al., 2001), ~1170-1370 cal yr BP. Preservation threshold seems unlikely because there was >200 years between the previously documented earthquake and our inferred timing for contact C (Witter et al., 2003). There are correlative age distributions further north at Talbot Creek (Fig. 4), southern Washington, and Vancouver Island (Nelson et al., 2006) and also to the south at Eel River (Fig. 4). However, at Talbot Creek, Milker et al., (2016) report little to no subsidence across their correlative contact B. Given northern Humboldt Bay contact C also records the least amount of subsidence over the four most recent earthquake

cycles, this may support the inference that insufficient coseismic deformation at the Coquille River during the earthquake that caused the formation of contact C.

Based on stratigraphic and age correlations within northern Humboldt Bay, lasting and sudden submergence of 0.39±0.33 m, and age distribution overlap with plate boundary earthquake evidence and/or tsunami deposits at Talbot Creek, Bradley Lake, Eel River and offshore turbidite T3, we infer that contact C is derived from coseismic subsidence induced by a plate-boundary earthquake.

Contact D (1004-1233 cal yrs BP)

Based on stratigraphic mapping and radiocarbon age overlap, contact D was observed at every marsh within the northern Humboldt Bay estuary. Two minimum ages, one a detrital *Grindelia* spp. stem <25 mm above the contact and a rhizome in growth position <15mm from the contact, and three maximum ages on a rhizome in growth position, rhizome fragments and stem fragments <15 mm below the contact, constrain the timing of burial. Using these minimum and maximum ages, OxCal Sequence method generated an age distribution of 1,004-1,233cal yr BP and Bchron modeled an age distribution of 1,158-1,246cal yrs BP (Fig. 3 and Table 2).

The third deepest subsidence contact at 248 cm core depth at *MD.13* is sharp and separates a muddy peat from an overlying mud. The CT scan of *MD.13* shows the contact to have ~14mm of undulating relief. The organic-rich unit is 8 cm thick, where the upper 3 cm is a light brown muddy peat and the lower 5 cm are a grey-brown rooted mud. The organic-rich unit is overlain by a grey mud that extends >25cm.

Foraminifera in the organic-rich unit dominantly consist of *B. pseudomacrescens* (3-48%), *T. inflata* (9-71%), and *J. macrescens* (22-52%), which is

consistent with a peat soil forming near MHHW. Although samples in the grey mud overlying the peat unit are also dominated by *J. macrescens* (27-38%), *T. inflata* (15-19%), and *B. pseudomacrescens* (12-18%) the assemblages show a marked increase in the abundance of *M. fusca* (14 to 17%) and contain *Ammobaculites* spp. (~1%) and *Reophax* spp. (~1%), which are typically associated with sediments accumulating closer to MTL (Kemp et al., 2018). For the subsidence estimate we use the reconstructed RSL elevations that are 2 cm apart and are the first unmixed centimeter intervals above and below the *mud-over-peat* contact. The fossil foraminifera BTF reconstruction shows 0.99±0.44 m of subsidence across contact D.

The OxCal Sequence model generated age distribution for contact D overlaps with age distributions for evidence of plate-boundary earthquakes at Eel River, Lagoon Creek, Bradley Lake, Coquille River, Talbot Creek, and the T3a turbidite. There is no correlation with southern Humboldt Bay and Sixes River (Fig. 4). Although southern Humboldt Bay (Patton, 2004) and Sixes River (Kelsey et al., 2003) locations each contain an undated buried organic-rich unit that could potentially correlate with either contact C or D at northern Humboldt Bay, the undated units cannot correlate to both. Similar to the arguments made for lack of evidence for at Coquille River during the timing of burial for contact C, there are at least three potential explanations for the lack of stratgraphic evidence for plate-boundary earthquake during the earthquake that caused the burial of contact D; 1) no earthquake occurrence, 2) formation threshold, and 3) preservation threshold. The first explanation seems unlikely because there are correlative ages of stratigraphic evidence for plate-boundary rupture to the north, e.g., Talbot Creek and Coquille River, and to

the south at Eel River as well as corresponding age distributions for tsunami deposits at Bradley Lake and Lagoon Creek. Moreover, Goldfinger et al (2012), suggest that the earthquake that caused T3a turbidite extended for 444 km and was a southern Cascadia rupture, which encompasses basins offshore of all sites in Fig 4.

Based on age correlations within northern Humboldt Bay, lasting and sudden submergence of 0.99±0.44 m, and age distribution overlap of plate boundary earthquake evidence and/or tsunami deposits at Talbot Creek, Coquille River, Lagoon Creek, Eel River and offshore turbidite T3a, we infer that contact C is derived from coseismic subsidence induced by a plate-boundary earthquake.

Contact E (1554-1667 cal yrs BP)

Based on stratigraphic mapping and radiocarbon age overlap, contact E was observed at every marsh within the northern Humboldt Bay estuary. The age of contact E is constrained by two minimum ages, of detrital wood fragments and a herbaceous stem (likely detrital) <30 mm above the contact, and four maximum ages on two rhizomes in growth position, one rhizome or stem, and ~25 atiplex and potamogeton seeds <20 mm below the contact. Using these minimum and maximum ages, OxCal Sequence method generates an age distribution of 1,554-1,667 cal yr BP and Bchron modeled an age distribution of 1,620-1,709 cal yrs BP (Fig. 3 and Table 2).

The deepest subsidence contact at 308 cm depth at *MD.05* (Fig. 5d) is a sharp, undulating (>15 mm) contact that separates a dark grey-black organic-rich unit from an overlying grey mud (Fig. 5D). X-ray analysis identifies that the overlying grey mud appears to have infiltrated into the underlying highly humified organic rich unit below

(Fig. 5D). The organic rich unit is 12 cm thick and is overlain by a grey mud that extends >25 cm.

The foraminifera assemblages of the humified organic rich unit have decreasing abundances, from 200 to <30, with distance below (4cm) the contact and are dominated by *M. fusca* (48-52%), *T. inflata* (35-38%) and contain low abundances of *Reophax* spp. (<1%); such an assemblage is typically indicative of an environment that formed below MHW. However, while foraminifera abundances above the deepest organic rich unit are consistent with other analyzed intervals (>200 individuals) the decreasing abundances of foraminifera with distance from the upper contact of the organic-rich unit is consistent with mixing (e.g., Engelhart et al., 2013; Milker et al., 2015). Based on visual appearance in photo and X-ray imagery, decreasing foraminiferal abundances, and similarity to foraminiferal assemblages within the overlying clastic mud unit we interpret that foraminifera assemblage found within the organic-rich unit is not in-situ or indicative of the depositional environment. Moreover, Engelhart et al., (2015) report diatom analysis of core *JC.14.02A* at Jacoby Creek that suggests the organic rich unit formed as a dry upland surface and not salt marsh. Therefore, considering the diatom data at *JC.14.02A,* correlation of radiocarbon ages, and a lack of in-situ fossil foraminiferal assemblages, we conclude that the fourth deepest organic-rich unit represents a depositional environment that formed above the highest occurrence of foraminifera. Foraminifera in the grey mud above the organic-rich unit are dominated by *M. fusca* (60-65%) and *T. inflata* (25-31%), while *Ammobaculites* spp. and *Reophax* spp. are both present at ~1%, signifying an assemblage that formed are around MTL. Based first interval that

contains in-situ fossil foraminifera above the organic-rich unit, we subtract the reconstructed RSL elevation for this interval, as predicted by the BTF, from the elevation of the highest occurrence of foraminifera in northern Humboldt Bay which is 2.5 m (NAVD 88). This results in a limiting estimate for subsidence of ≥ 1.09 m.

Seven of the eight onshore sites (Fig. 4) record evidence for a plate-boundary earthquake and the offshore turbidite T5 ages overlap with the age distribution for contact E. There is a notable absence of age correspondence at Sixes River with the age distribution for contact D. However, Kelsey et al., (2005) dated two fragments of woody detritus, which were found within soil 3 at Sixes River, and propose the possibility that the calibrated radiocarbon age distribution of 1940-2130 is potentially several hundred years older than the timing of burial for the organic rich unit. There are abundant corresponding age distributions for contact E both offshore, throughout southern Cascadia (Fig. 4), and further north along the Cascadia margin including central Oregon and southern Washington (Shennan et al., 1996; Nelson et al., 1996b; 1998; Nelson et al., 2004; Atwater et al, 2004: Graehl et al., 2014).

Based on age correlations across northern Humboldt Bay, lasting and sudden submergence of >1.09? m, and age distribution overlap of regional plate boundary earthquake evidence, tsunami deposits, and offshore turbidite T5, we infer that contact E is derived from coseismic subsidence induced by a plate-boundary earthquake.

CONCLUSION

High-precision chronostratigraphic methods and quantitative RSL reconstructions utilized within this investigation refine our understanding of the paleoseismic history at northern Humboldt Bay. Wetland stratigraphy at three tidal

marshes within northern Humboldt Bay show four distinct buried organic-rich units (contacts A, C, D, and E) and one less distinct buried organic-rich unit (contact B). We use stratigraphic, chronologic, fossil foraminifera analyses, and regional timing comparisons to evidence of plate boundary earthquakes at other paleoseismic sites to infer that contacts A, C, D, and E record subsidence during past CSZ plate boundary earthquakes. Data for contact B, found only at Mad River Slough, are insufficient to infer whether it records a great earthquake. It may have formed through local non-seismic hydrographic processes associated with the slough. Multiple minimum and maximum limiting ages of short-lived plant macrofossils, found above and below subsidence contacts and the construction of Bayesian age models provide the tightest age distributions for stratigraphic evidence of plate boundary earthquakes along the southern Cascadia coastline, which are: 815-924 cal yr BP (~870 cal yrs BP), 1,004-1,233 cal yrs BP (~1,125cal yrs BP), and 1,554-1667 cal yrs BP (~1,600 cal yr BP). At northern Humboldt Bay, stratigraphic evidence for four plate boundary earthquakes corresponds with stratigraphic evidence from eight proximal coastal paleoseismic locations (43.5°-40.5° N). We reconstruct RSL elevations by applying a foraminiferal BTF to fossil data from representative stratigraphic sequences collected at McDaniel Creek marsh that span the past four CSZ earthquakes. The coseismic subsidence estimates are 0.90 ±0.46m for the 1700 CE earthquake, 0.39±0.33 m for the ~870 cal yrs BP earthquake, 0.99±0.44 m ~1,125 cal yrs BP earthquake, and ≥0.86 m for the ~1,600 cal yrs BP earthquake, which is a minimum because the paleoenvironment prior to the earthquake likely formed above the upper limit of foraminiferal habitation.

The lithostratigraphic, chronostratigraphic, and quantitative microfossil RSL reconstruction research approaches utilized by this investigation set a precision standard for future paleoseismic investigations in Cascadia. Similar methods should be applied in future studies directed towards the development a comprehensive paleogeodetic database and an improved understanding of CSZ plate boundary earthquake characteristics. Our results highlight the need for additional precise coseismic subsidence estimates and paleoseismic chronologies from southern Cascadia such as at Eel River (~40.65° N), southern Humboldt Bay (~40.7° N), and Sand Mine Marsh (~41.74° N).

REFERENCES

Abramson, H.F., 1998. *Evidence for tsunamis and earthquakes during the last 3500 years from Lagoon Creek, a coastal freshwater marsh, northern California* (M.S. thesis, Humboldt State University).

Adams, J., 1990. Paleoseismicity of the Cascadia subduction zone: Evidence from turbidites off the Oregon-Washington margin. *Tectonics*, *9*(4), pp.569-583.

Atwater, B.F., 1987. Evidence for great Holocene earthquakes along the outer coast of Washington State. *Science*, *236*(4804), pp.942-944.

Atwater, B.F., 1992. Geologic evidence for earthquakes during the past 2000 years along the Copalis River, southern coastal Washington. *Journal of Geophysical Research: Solid Earth*, *97*(B2), pp.1901-1919.

Atwater, B.F. and Hemphill-Haley, E., 1997. *Recurrence intervals for great earthquakes of the past 3,500 years at northeastern Willapa Bay, Washington* (No. 1576). USGPO; Information Services [distributor].

Atwater, B.F., Tuttle, M.P., Schweig, E.S., Rubin, C.M., Yamaguchi, D.K. and Hemphill-Haley, E., 2003. Earthquake recurrence inferred from paleoseismology. *Developments in Quaternary Sciences*, *1*, pp.331-350.

Benson, B.E., Atwater, B.F., Yamaguchi, D.K., Amidon, L.J., Brown, S.L., and Lewis, R.C., 2001, Renewal of Tidal Forests in Washington State after a Subduction Earthquake in A.D. 1700: Quaternary Research, v. 56, p. 139–147, doi: 10.1006/qres.2001.2251.

Bronk Ramsey, C., 2008. Radiocarbon dating: Revolutions in Understanding. *Archaeometry*, *50*(2), pp.249-275.

Cahill, N., Kemp, A.C., Horton, B.P. and Parnell, A.C., 2016. A Bayesian hierarchical model for reconstructing relative sea level: from raw data to rates of change. *Climate of the Past*, *12*(2), pp.525-542.

Clarke, S.H. and Carver, G.A., 1992. Late Holocene tectonics and paleoseismicity, southern Cascadia subduction zone. *Science*, *255*(5041), pp.188-192.

Darienzo, M.E. and Peterson, C.D., 1990. Episodic tectonic subsidence of late Holocene salt marshes, northern Oregon central Cascadia margin. *Tectonics*, *9*(1), pp.1-22.

Darienzo, M.E., Peterson, C.D. and Clough, C., 1994. Stratigraphic evidence for great subduction-zone earthquakes at four estuaries in northern Oregon, USA. *Journal of Coastal Research*, pp.850-876.

Davies, M.H., Mix, A.C., Stoner, J.S., Addison, J.A., Jaeger, J., Finney, B. and Wiest, J., 2011. The deglacial transition on the southeastern Alaska Margin: Meltwater input, sea level rise, marine productivity, and sedimentary anoxia. *Paleoceanography and Paleoclimatology*, *26*(2).

de Rijk, S., 1995. Salinity control on the distribution of salt marsh foraminifera (Great Marshes, Massachusetts). *The Journal of Foraminiferal Research*, *25*(2), pp.156-166.

Dura, T., Horton, B.P., Cisternas, M., Ely, L.L., Hong, I., Nelson, A.R., Wesson, R.L., Pilarczyk, J.E., Parnell, A.C. and Nikitina, D., 2017. Subduction zone slip variability during the last millennium, south-central Chile. *Quaternary Science Reviews*, *175*, pp.112-137.

Engelhart, S.E., Horton, B.P., Nelson, A.R., Hawkes, A.D., Witter, R.C., Wang, K., Wang, P.L. and Vane, C.H., 2013. Testing the use of microfossils to reconstruct great earthquakes at Cascadia. *Geology*, *41*(10), pp.1067-1070.

Engelhart, S.E., Horton, B.P., Vane, C.H., Nelson, A.R., Witter, R.C., Brody, S.R. and Hawkes, A.D., 2013. Modern foraminifera, δ 13 C, and bulk geochemistry of central Oregon tidal marshes and their application in paleoseismology. *Palaeogeography, Palaeoclimatology, Palaeoecology*, *377*, pp.13-27.

Engelhart, S.E., Hemphill-Haley, E., Kelsey, H.M., and Padgett, J.S. *Refined Estimates of Coseismic Subsidence along the Southern Cascadia Subduction Zone in Northern Humboldt Bay (Arcata Bay): Collaborative Research with University of Rhode Island and Humboldt State University*. No. G14AP00128 and G14AP00129. U.S. Geological Survey

Enkin, R.J., Dallimore, A., Baker, J., Southon, J.R. and Ivanochko, T., 2013. A new high-resolution radiocarbon Bayesian age model of the Holocene and Late Pleistocene from core MD02-2494 and others, Effingham Inlet, British Columbia, Canada; with an application to the paleoseismic event chronology of the Cascadia Subduction Zone. *Canadian Journal of Earth Sciences*, *50*(7), pp.746-760.

Fatela, F. and Taborda, R., 2002. Confidence limits of species proportions in microfossil assemblages. *Marine Micropaleontology*, *45*(2), pp.169-174.

Garrett, E., Shennan, I., Woodroffe, S.A., Cisternas, M., Hocking, E.P. and Gulliver, P., 2015. Reconstructing paleoseismic deformation, 2: 1000 years of great

earthquakes at Chucalén, south central Chile. *Quaternary Science Reviews*, *113*, pp.112-122.

Garrison-Laney, C.E., 1998. *Diatom evidence for tsunami inundation from Lagoon Creek, a coastal freshwater pond, Del Norte County, California* (Doctoral dissertation, Humboldt State University).

Graehl, N.A., Kelsey, H.M., Witter, R.C., Hemphill-Haley, E. and Engelhart, S.E., 2015. Stratigraphic and microfossil evidence for a 4500-year history of Cascadia subduction zone earthquakes and tsunamis at Yaquina River estuary, Oregon, USA. *Bulletin*, *127*(1-2), pp.211-226.

Guilbault, J.P., Clague, J.J. and Lapointe, M., 1995. Amount of subsidence during a late Holocene earthquake—evidence from fossil tidal marsh foraminifera at Vancouver Island, west coast of Canada. *Palaeogeography, Palaeoclimatology, Palaeoecology*, *118*(1), pp.49-71.

Guilbault, J.P., Clague, J.J. and Lapointe, M., 1996. Foraminiferal evidence for the amount of coseismic subsidence during a late Holocene earthquake on Vancouver Island, west coast of Canada. *Quaternary Science Reviews*, *15*(8), pp.913-937.

Hawkes, A.D., Horton, B.P., Nelson, A.R. and Hill, D.F., 2010. The application of intertidal foraminifera to reconstruct coastal subsidence during the giant Cascadia earthquake of AD 1700 in Oregon, USA. *Quaternary International*, *221*(1), pp.116-140.

Hawkes, A.D., Horton, B.P., Nelson, A.R., Vane, C.H. and Sawai, Y., 2011. Coastal subsidence in Oregon, USA, during the giant Cascadia earthquake of AD 1700. *Quaternary Science Reviews*, *30*(3), pp.364-376.

Hemphill-Haley, E., 1995. Diatom evidence for earthquake-induced subsidence and tsunami 300 yr ago in southern coastal Washington. *Geological Society of America Bulletin*, *107*(3), pp.367-378.

Holden, P.B., Birks, H.J.B., Brooks, S.J., Bush, M.B., Hwang, G.M., Matthews-Bird, F., Valencia, B.G. and Van Woesik, R., 2017. BUMPER v1. 0: a Bayesian user-friendly model for palaeo-environmental reconstruction.

Horton, B.P. and Edwards, R.J., 2005. The application of local and regional transfer functions to the reconstruction of Holocene sea levels, north Norfolk, England. *The Holocene*, *15*(2), pp.216-228.

Horton, B. P., & Edwards, R. J., 2006. Quantifying Holocene Sea Level Change Using Intertidal Foraminifera: Lessons from the British Isles. Cushman Foundation for Foraminiferal Research Special Publication, 40, 97.

Kelsey, H.M., Witter, R.C. and Hemphill-Haley, E., 1998. Response of a small Oregon estuary to coseismic subsidence and postseismic uplift in the past 300 years. *Geology*, *26*(3), pp.231-234.

Kelsey, H.M., Witter, R.C. and Hemphill-Haley, E., 2002. Plate-boundary earthquakes and tsunamis of the past 5500 yr, Sixes River estuary, southern Oregon. *Geological Society of America Bulletin*, *114*(3), pp.298-314.

Kelsey, H. M., Nelson, A. R. Witter, R. C., and Hemphill-Haley, E. 2005, Tsunami history of an Oregon coastal lake reveals a 4,600 year record of great earthquakes on the Cascadia subduction zone, Geological Society of America Bulletin, 117, 1009-1032.

Kelsey, H.M., Engelhart, S.E., Pilarczyk, J.E., Horton, B.P., Rubin, C.M., Daryono, M.R., Ismail, N., Hawkes, A.D., Bernhardt, C.E. and Cahill, N., 2015. Accommodation space, relative sea level, and the archiving of paleo-earthquakes along subduction zones. *Geology*, *43*(8), pp.675-678.

Kemp, A.C., Nelson, A.R. and Horton, B.P., 2013. Radiocarbon dating of plant macrofossils from tidal-marsh sediment. *in:* Shroder, J. F., (ed.) Treatise on Geomorphology, 14, 370-388, Academic Press, San Diego.

Kemp, A.C., Cahill, N., Engelhart, S.E., Hawkes, A.D. and Wang, K., 2018. Revising Estimates of Spatially Variable Subsidence during the AD 1700 Cascadia Earthquake Using a Bayesian Foraminiferal Transfer Function. *Bulletin of the Seismological Society of America*, *108*(2), pp.654-673.

Li, W.H., 1992. *Evidence for the late Holocene coseismic subsidence in the Lower Eel River valley, Humboldt county, Northern California: An application of foraminiferal zonation to indicate tectonic submergence* (Doctoral dissertation, Humboldt State University).

Milker, Y., Horton, B.P., Vane, C.H., Engelhart, S.E., Nelson, A.R., Witter, R.C., Khan, N.S. and Bridgeland, W.T., 2015. Annual and seasonal distribution of intertidal foraminifera and stable carbon isotope geochemistry, Bandon Marsh, Oregon, USA. *The Journal of Foraminiferal Research*, *45*(2), pp.146-155.

Milker, Y., Nelson, A.R., Horton, B.P., Engelhart, S.E., Bradley, L-A., and Witter, R.C., 2016. Differences in coastal subsidence in southern Oregon (USA) during at least six prehistoric megathrust earthquakes. *Quaternary Science Reviews*.

Nelson, A.R., 1992. Discordant 14C ages from buried tidal-marsh soils in the Cascadia subduction zone, southern Oregon coast. *Quaternary Research*, *38*(1), pp.74-90.

Nelson, A.R., Shennan, I. and Long, A.J., 1996a. Identifying coseismic subsidence in tidal-wetland stratigraphic sequences at the Cascadia subduction zone of western North America. *Journal of Geophysical Research: Solid Earth*, *101*(B3), pp.6115-6135.

Nelson, A.R., Jennings, A.E. and Kashima, K., 1996b. An earthquake history derived from stratigraphic and microfossil evidence of relative sea-level change at Coos Bay, southern coastal Oregon. *Geological Society of America Bulletin*, *108*(2), pp.141-154.

Nelson, A.R., Sawai, Y., Jennings, A.E., Bradley, L.A., Gerson, L., Sherrod, B.L., Sabean, J. and Horton, B.P., 2008. Great-earthquake paleogeodesy and tsunamis of the past 2000 years at Alsea Bay, central Oregon coast, USA. *Quaternary Science Reviews*, *27*(7), pp.747-768.

Nelson, A.R., Ota, Y., Umitsu, M., Kashima, K. and Matsushima, Y., 1998. Seismic or hydrodynamic control of rapid late-Holocene sea-level rises in southern coastal Oregon, USA?. *The Holocene*, *8*(3), pp.287-299.

Nelson, A.R., Asquith, A.C. and Grant, W.C., 2004. Great earthquakes and tsunamis of the past 2000 years at the Salmon River estuary, central Oregon coast, USA. *Bulletin of the Seismological Society of America*, *94*(4), pp.1276-1292.

Patton, J., 2004, Late Holocene coseismic subsidence and coincident tsunamis, southern Cascadia subduction zone, Hookton Slough, Humboldt Bay, California. M.S. thesis, Humboldt State University, 76p.

Pickart, A.J. and Hesp, P.A., 2019. Spatio-temporal geomorphological and ecological evolution of a transgressive dunefield system, Northern California, USA. *Global and planetary change*, *172*, pp.88-103.

Pritchard, C. J., 2004. *Late Holocene relative sea-level changes, Arcata Bay, California: Evaluation of freshwater syncline movement using coseismically buried soil horizons*. M.S. thesis, Humboldt State University, Department of Geology.

Rothwell, R.G. and Rack, F.R., 2006. New techniques in sediment core analysis: an introduction. *Geological Society, London, Special Publications*, *267*(1), pp.1-29.

Schlosser, S., and A. Eicher. 2012. The Humboldt Bay and Eel River Estuary Benthic Habitat Project. California Sea Grant Publication T-075. 246 p.

Scott, D.B. and Medioli, F.S., 1980. Living vs. total foraminiferal populations: their relative usefulness in paleoecology. *Journal of Paleontology*, pp.814-831.

Shennan, I., Long, A.J., Rutherford, M.M., Green, F.M., Innes, J.B., Lloyd, J.M., Zong, Y. and Walker, K.J., 1996. Tidal marsh stratigraphy, sea-level change and large earthquakes, I: a 5000 year record in Washington, USA. *Quaternary Science Reviews*, *15*(10), pp.1023-1059.

Troels-Smith, J., 1955. Karakterisering af lose jordarter. Characterization of unconsolidated sediments.

van de Plassche, O., 1979, Sea-level research in the provinces of south Holland, Netherlands: Proceedings of the "1978 international symposium of coastal evolution in the Quaternary", Sao Paulo, Brazil, p. 534-551.

Valentine, D.W., 1992. *Late Holocene stratigraphy, Humboldt Bay, California: evidence for late Holocene paleoseismicity of the southern Cascadia subduction zone*. M.S. thesis, Humboldt State University.

Valentine, D.W., Keller, E.A., Carver, G., Li, W.H., Manhart, C. and Simms, A.R., 2012. Paleoseismicity of the southern end of the Cascadia subduction zone, northwestern California. *Bulletin of the Seismological Society of America*, *102*(3), pp.1059-1078.

Vick, G.S., 1988. *Late Holocene paleoseismicity and relative sea level changes of the Mad River Slough, northern Humboldt Bay, California*. M.S. thesis, Humboldt State University.

Wang, P.L., Engelhart, S.E., Wang, K., Hawkes, A.D., Horton, B.P., Nelson, A.R. and Witter, R.C., 2013. Heterogeneous rupture in the great Cascadia earthquake of 1700 inferred from coastal subsidence estimates. *Journal of Geophysical Research: Solid Earth*, *118*(5), pp.2460-2473.

Table 1. Summary of northern Humboldt Bay radiocarbon ages.

Calibrated Age (2σ cal yrs BP)	Analytical Age (1σ 14C yrs BP)	Lab Number	13C (‰)	Site Identifier	Depth (cm)	Description of Dated Material	Type	Contact
				Mad River:				
307 - 1	235±20	OS-117742	-24.84	MR.14.02.B	140.5-141.5	Herbaceous stem	Maximum	A
511 - 476	420±15	OS-117743	-13.89	MR.14.02.B	161.5-162.5	Distichlis rhizome	Maximum	B
956 - 802	990±20	OS-117744	-11.39	MR.14.02.B	225.5-226	2 Distichlis rhizomes	Maximum	C
956 - 912	1000±15	OS-117822	-26.65	MR.14.05.B	188.5-189	Herbaceous stem	Maximum	C
1057 - 961	1100±20	OS-119965	-24.8	MR.14.02.A	273-273.5	Detrital grindelia stem	Minimum	D
1280 - 1183	1290±15	OS-119965	-25.69	MR.14.05.C	246-247	Rhizome	Maximum	D
1690 - 1545	1690±20	OS-118743	-25.57	MR.14.02.A	297.50-298.25	~25 seeds (atriplex and potamogeton)	Maximum	E
				McDaniel Slough:				
283 - 1	170±15	OS-119960	-24.32	MD.14.03.C	117-118	Herbaceous stem	Maximum	A
926 - 798	955±15	OS-119963	-25.64	MD.14.06.C	168.5-169.5	Rhizome	Minimum	C
951 - 804	990±15	OS-117738	-26.03	MD.14.06.C	169.5-170.5	2 rhizomes	Maximum	C
965 - 929	1040±15	OS-117739	-26.82	MD.14.03.C	212.5-213.5	Rhizome	Maximum	C
1399 - 1328	1480±15	OS-119962	-27.84	MD.14.05.A	276-277	Rhizome and stem fragments	Maximum	D
1707 - 1575	1740±15	OS-119961	-27.06	MD.14.05.B1	306.5-307.5	Herbaceous stem (detrital?)	Minimum	E
1695 - 1565	1720±15	OS-117740	-28.02	MD.14.05.B1	308-309	2 rhizomes	Maximum	E
1708 - 1614	1750±15	OS-117741	-15.26	MD.14.04.B	379.5-380.5	Distichlis rhizome	Maximum	E
				Jacoby Creek:				
289 - 1	195±15	OS-117608	-13.5	JC.14.02.C	81-82cm	Distichlis rhizome	Maximum	A
1263 - 1082	1240±20	OS-123307	-12.82	JC.14.02.D	104-105	Herbaceous stem (detrital?)	N/A	N/A
1333 - 1285	1390+20	OS-124863	-24.62	JC.14.02.D	103-105	Potamogeton seed casings (detrital?)	N/A	N/A
Modern	>Modern	OS-125075	-16.36	JC.14.02.B	100-101	Herbaceous stem (detrital?)	N/A	N/A
1166 - 968	1130±20	OS-119878	-26.64	JC.14.02.D	130-130.5	Rhizome	Minimum	D
1277 - 1181	1280±20	OS-117609	-27.65	JC.14.02.C	125.5-126	Rhizome fragments	Maximum	D
1692 - 1561	1710±15	OS-119959	-28.43	JC.14.02.C	167.5-168	Wood fragment (detrital)	Minimum	E
1694 - 1558	1710±20	OS-117610	-27.4	JC.14.02.C	170-171.5	Rhizome or stem	Maximum	E

Table 2. Summary of Bayesian age models

Organic-rich contact	OxCal 4.2 calibrated age range (yr BP at 2σ)	Bchron calibrated age range (yr BP at 2σ)
A	CSZ 1700 CE*	
C	815-924	850-966
D	1,004-1,233	1,158-1,246
E	1,554-1667	1,620-1,709

* (Atwater 1987; Nelson 1992; Satake et al 2003; Atwater and Hemphill-Haley 2005)

Table 3. Summary of subsidence estimates

Buried organic-rich unit	Core site	Depth of contact (cm)	Subsidence estimate (m)
A	MD.3	115	0.88±0.44
C	MD.6	170	0.39±0.33
D	MD.13	222	0.99±0.44
E	MD.5	307	≥0.86

Table 4. Buried organic rich unit attributes consistent with subduction earthquake origin

Buried organic-rich unit	Sharp (<3mm) contact between buried organic-rich unit and overlying mud	Long-lasting relative sea-level rise (overlying mud >10cm thick)	Fine to very fine sand layer immediately overlies organic-rich unit	Foraminifera assemblages consistent with abrupt relative sea-level rise accompanying organic-rich unit burial	The buried organic-rich unit is laterally extensive, e.g., observed across estuary	Calibrated age range (2σ) of buried organic-rich unit is chronologically consistent with regional record of Cascadia subduction zone earthquakes
A	+	+	-	+	+	+
B	+	-	-	-	-	-
C	+	+	-	+	-	+
D	+	+	-	+	+	+
E	+	+	-	+	+	+

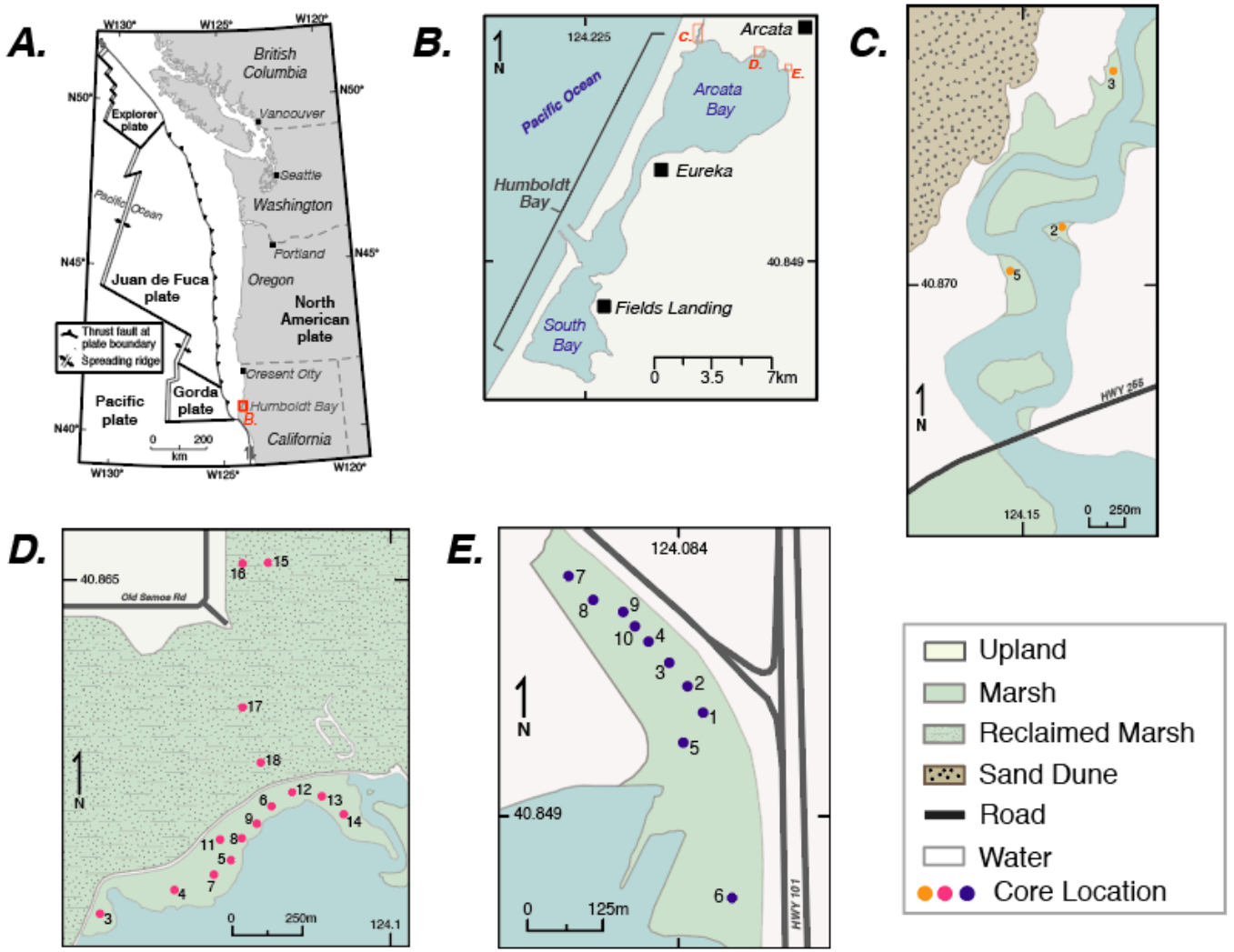

Figure 1.

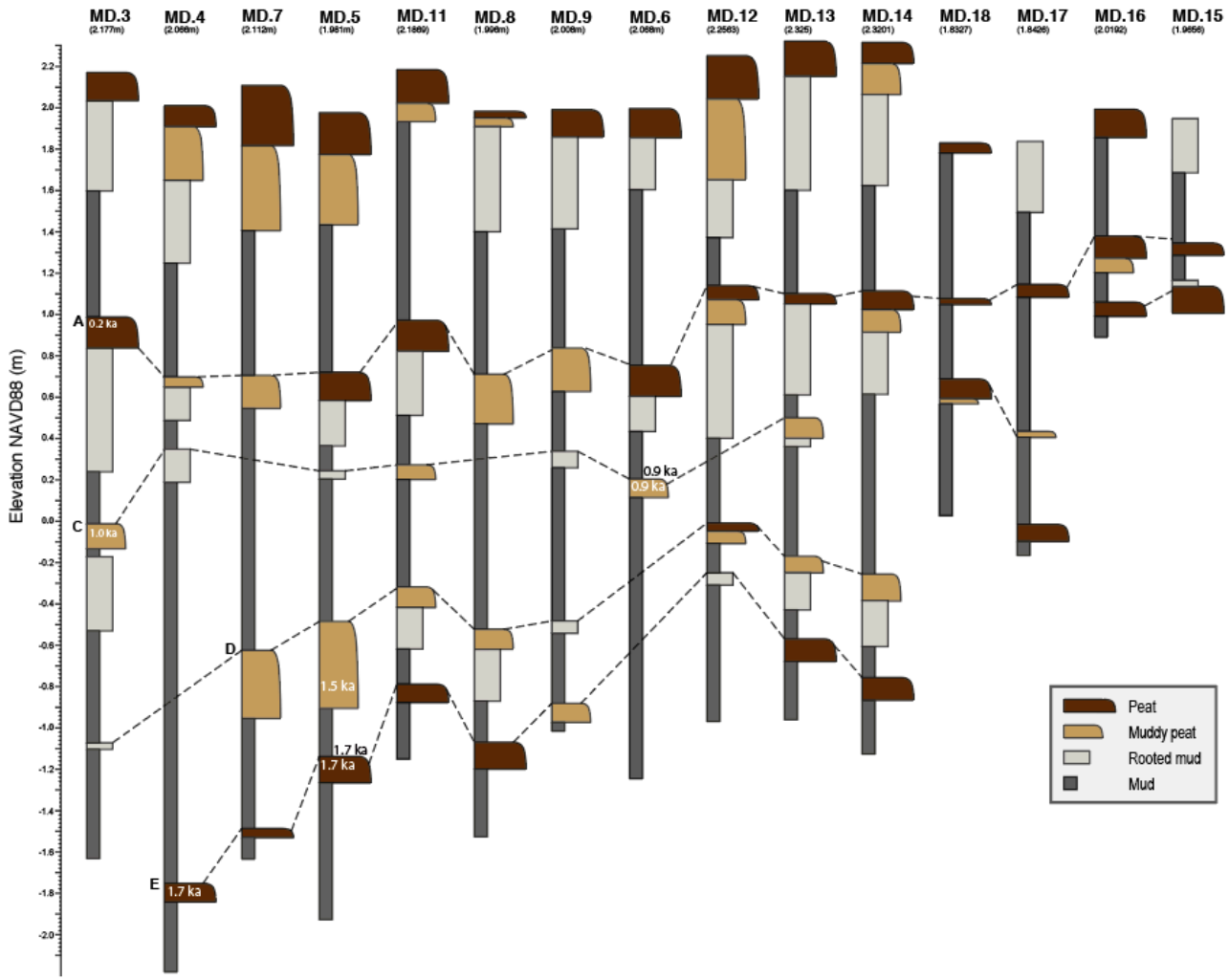

Figure 2.

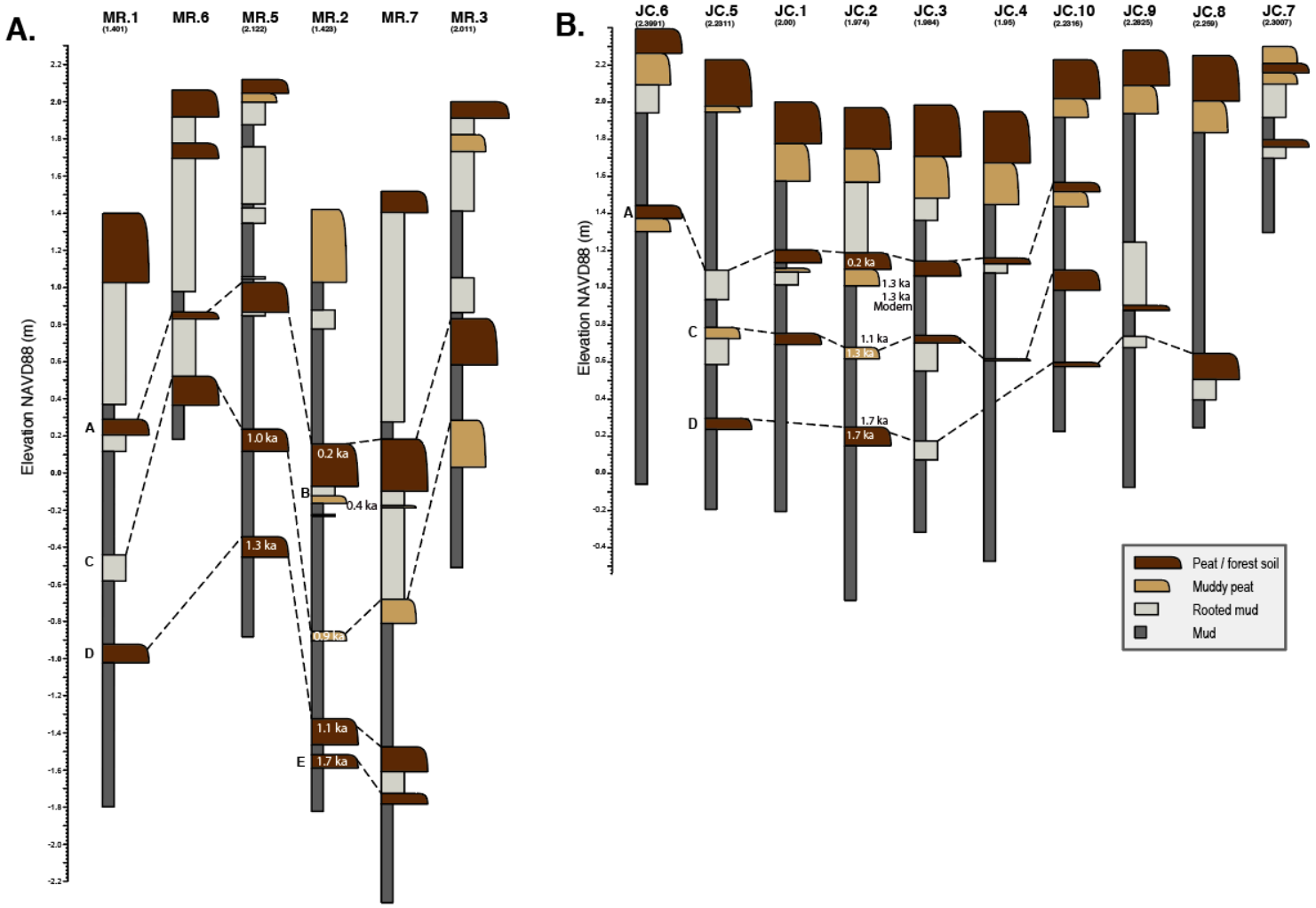

Figure 3.

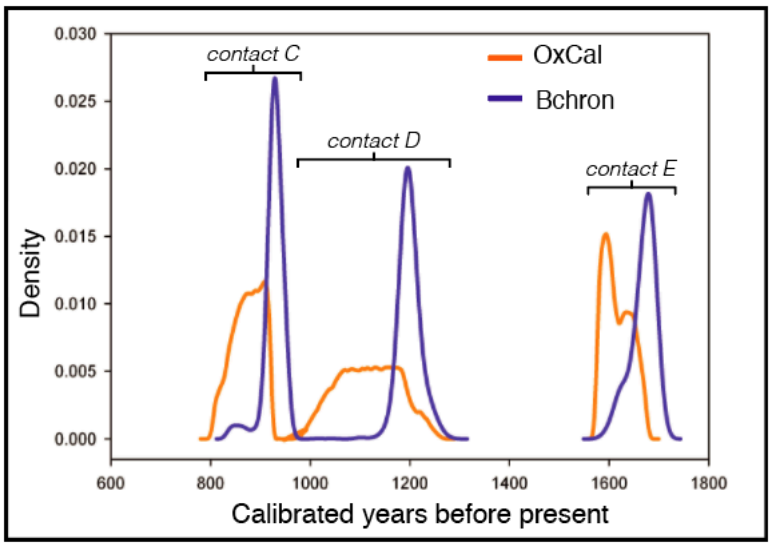

Figure 4.

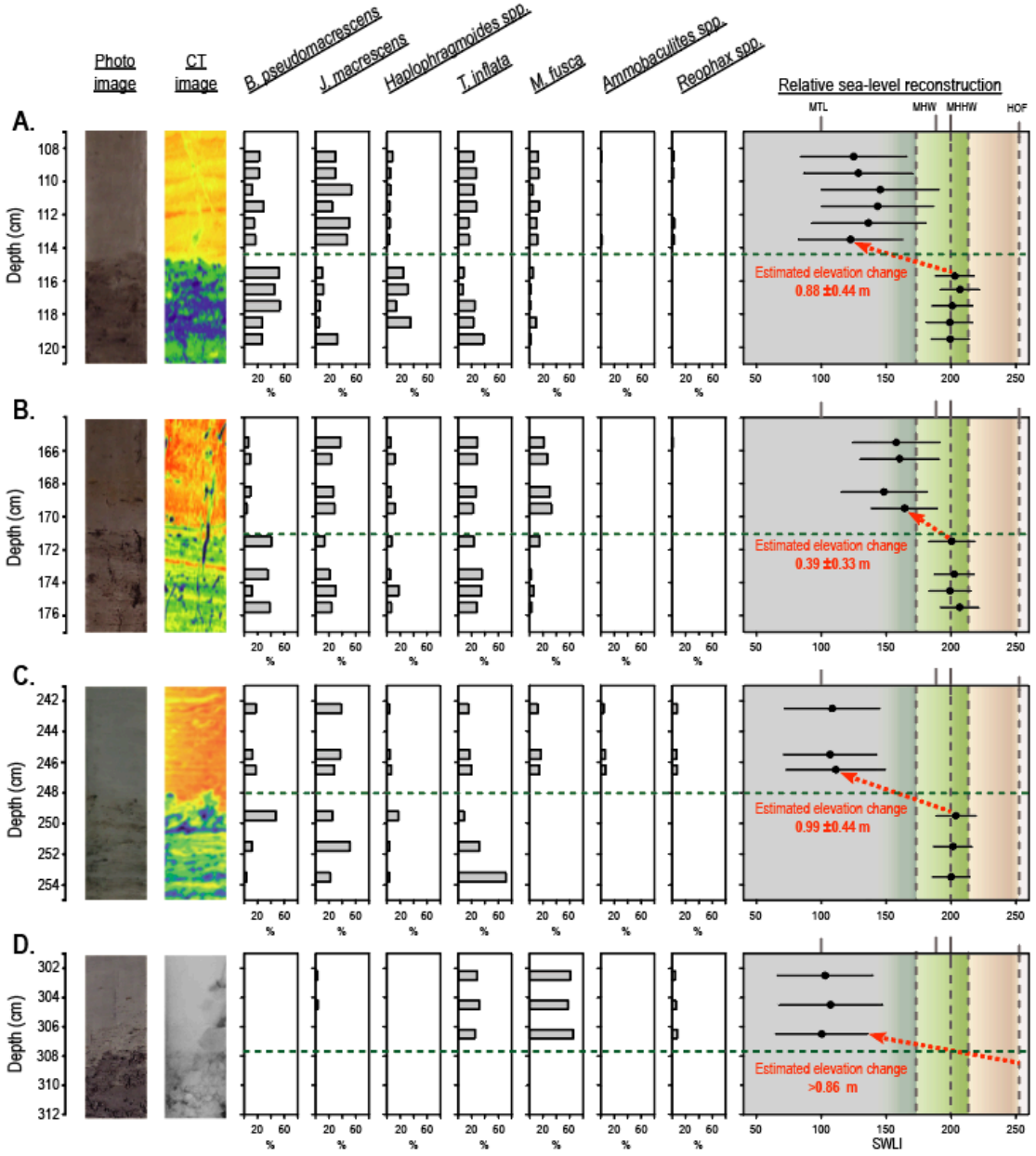

Figure 5.

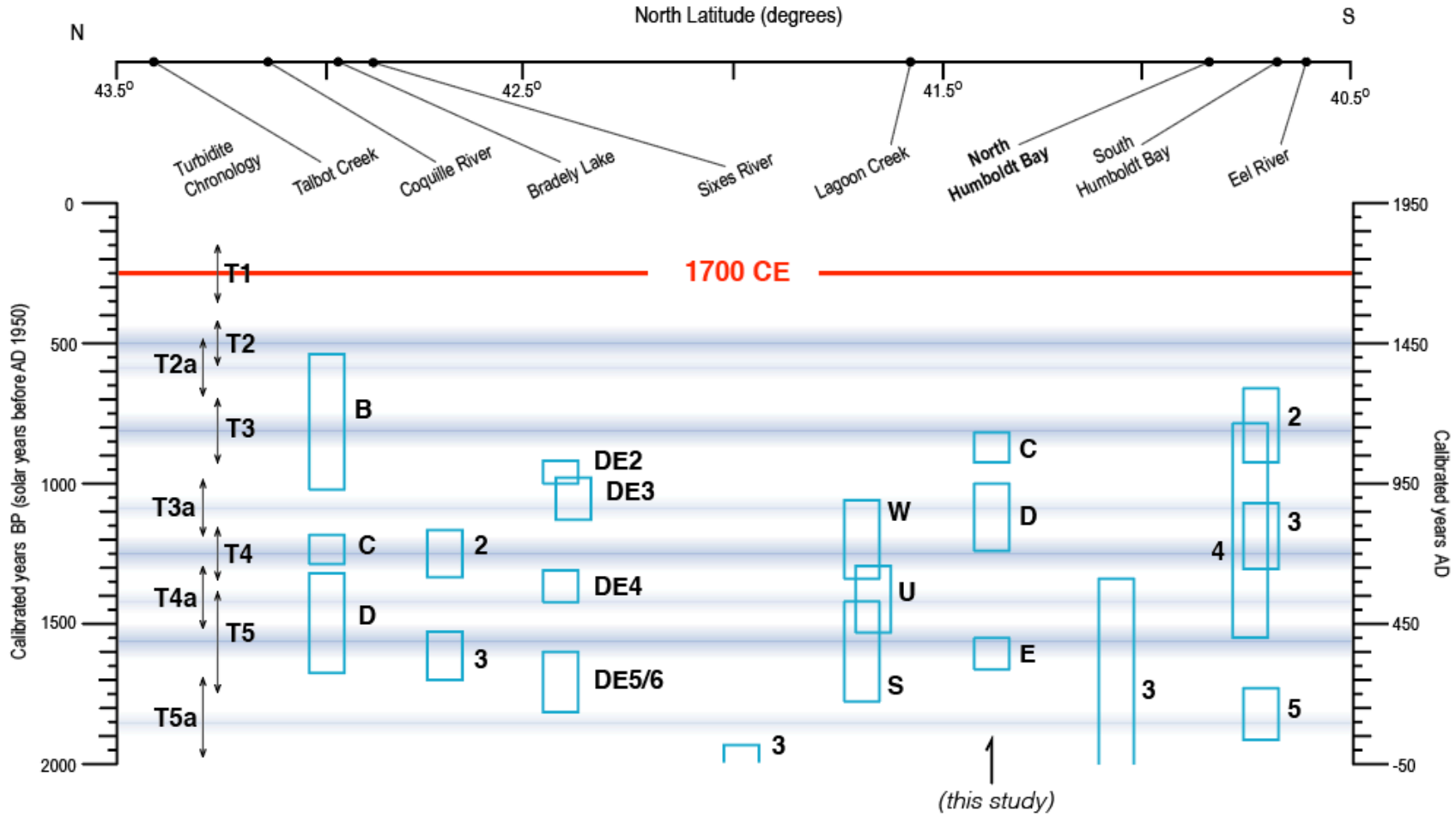

Figure 6.

CHAPTER 2

Variability of coseismic subsidence estimates from sites in northern Humboldt Bay, California (USA)

J. Scott Padgett[1], Simon E. Engelhart[1], Harvey M. Kelsey[2], Robert C. Witter[3], Niamh Cahill[4] and Brian Savage[1]

[1]Department of Geosciences, University of Rhode Island, Kingston, Rhode Island 02881, USA
[2]Department of Geology, Humboldt State University, Arcata, California 95524, USA
[3]U.S. Geological Survey, Alaska Science Center, 4210 University Drive, Anchorage, Alaska 99508, USA
[4] Department of Mathematics and Statistics, Maynooth University, Kildare, Ireland

This chapter/manuscript is prepared for submission to the journal *Marine Micropaleontology*.

ABSTRACT

We extend application of the quantitative microfossil approach for reconstructing coseismic subsidence to the southern Cascadia margin. We use these data to evaluate within-site and within-bay depositional variability and subsequent effects on coseismic subsidence estimates from megathrust earthquakes and test the reproducibility of a validated foraminiferal-based Bayesian transfer function at northern Humboldt Bay, California (~44.8°N, -124.2°W). We examine three abrupt *mud-over-peat* (coseismic subsidence) contacts along a 6-km transect at Jacoby Creek, McDaniel Creek and Mad River Slough. Our quantitative reconstructions of relative sea-level rise across each contact using a foraminiferal transfer function give subsidence estimates with errors of ±0.26-0.52 m. To assess the reproducibility of our estimates, we analyzed 20 sediment cores containing the three mud-over-peat contacts; nine examples of the 1700 CE earthquake (average of 0.63 ±0.36 m subsidence), five examples of the ~870 cal yrs BP earthquake (average of 0.3 ±0.35 m), and six examples of the ~1,125 cal yrs BP earthquake (average of 0.7±0.39 m).

For site average reconstructions, inter-site variability (mid-point to mid-point) ranged from a maximum of 0.47 m between McDaniel Creek (0.80 ± 0.41 m) and Mad River Slough (0.33 ± 0.25 m) for the 1700 CE earthquake, to a minimum of 0.06 m between McDaniel Creek (0.43 ± 0.34 m) and Mad River Slough (0.37 ± 0.36 m) for the 870 cal yrs BP earthquake. Intra-site variability of coseismic subsidence estimates ranges from a maximum of 0.59 m for the 1700 CE earthquake at McDaniel Creek to a minimum of 0.0 m for the 1,125 cal yrs BP earthquake at Mad River Slough. Of the three earthquakes, the 1700 CE earthquake had the highest variability in coseismic

subsidence estimates. At Mad River Slough, marsh-wide mixed foraminiferal assemblages in the mud above the 1700 CE subsidence contact suggests influence of a second-order processes (e.g., erosion, liquefaction, slumping, and sediment availability). This conclusion is also supported by CT imagery that documents high variability in sediment density within these cores above the 1700 CE contact that is not seen at other sites. Based on our results, we recommend a minimum of two, to ideally three, quantitative microfossil RSL reconstructions across the same stratigraphic sequence to provide increased confidence in the estimates.

1. INTRODUCTION

Stratigraphy consisting of abrupt *mud-over-peat* and *mud-over-forest soil* contacts are the most common signature of coastal coseismic subsidence associated with megathrust deformation in temperate environments (Atwater, 1987; Combellick, 1991; Nelson 1992; Shennan et al., 1996, 1999; Sawai, 2001, 2002; Cisternas et al., 2005). Early coastal paleogeodetic research revolutionized our understanding of subduction zone hazards by identifying and mapping wetland stratigraphy consistent with megathrust rupture and estimating coseismic vertical deformation across subsidence contacts based on qualitative and semi-quantitative elevation assignments of paleo-depositional environments (Plafker, 1969; Atwater, 1992; Nelson 1992, 1996; Darienzo et al., 1994; Shennan et al., 1996; Atwater and Hemphill-Haley, 1997). However, subsequent refinement of relative sea-level (RSL) reconstructions and coseismic subsidence estimates using quantitative methods can now help better understand the complexities of past megathrust rupture such as segmentation and

variability of rupture magnitude (Guilbault et al., 1995, 1996; Hamilton and Shennan, 2005; Hawkes et al., 2010, 2011; Wang et al., 2013; Garrett et al., 2015; Milker et al., 2015, 2016; Shennan et al., 2016; Dura et al., 2017; Kemp et al., 2018). Along the coasts of the Cascadia margin, fully-quantitative RSL reconstructions (transfer functions) based on fossil foraminiferal assemblages yield precise (<±0.3m) estimates of coseismic subsidence (Guilbault et al., 1995, 1996; Nelson et al., 2008; Hawkes et al., 2010, 2011; Engelhart et al., 2013a, Wang et al., 2013; Milker et al., 2016, Kemp et al, 2018). Although, the accuracy of Cascadia foraminiferal transfer functions has been validated in experiments where known elevation changes have occurred (Engelhart et al., 2013; Kemp et al., 2018), uncertainties remain in regard to the variability of paleoseismic stratigraphy of the same earthquake sequence and the appropriate spatial range (geospatial extent) of a coseismic subsidence estimate (i.e., ~1-10's km^2). For example, was there local erosion of the pre-earthquake surface, compaction, or liquefaction of underlying sediments? Was there physical or biological mixing above and/or below subsidence contacts? How long did it take for sedimentation to resume after coseismic subsidence?

Preservation of coseismic land-level changes recorded in coastal stratigraphy is the combined result of first and second order processes (Atwater et al., 1987; Nelson et al., 1996; Zong et al., 2003; Milker et al., 2016; Shennan et al., 2016). Beyond continuous RSL rise, megathrust-induced surface deformation is the primary factor driving stratigraphic preservation of wide-spread, rapid, and lasting changes in RSL and is likely uniform over 1-5 km^2 distances. Whereas secondary factors such as erosion, liquefaction, slumping, and sediment availability, may not be consistent over

0-1 km^2 distances and could cause variability in coastal coseismic stratigraphy. On small scales (1-10cm), within a single marsh, stratigraphic irregularities across a subsidence contact are common, e.g., contact thickness and contact relief (Nelson et al., 1996; Atwater and Hemphill-Haley, 1997; Milker et al., 2016). After extensive mapping of wetland stratigraphy, coastal paleogeodetic investigations avoid subtle stratigraphic irregularities and select the most-representative stratigraphic section for microfossil analyses and derivation of a coseismic subsidence estimate. This estimate is then often assumed to be representative over an entire estuary (Guilbault et al., 1995; 1996; Nelson et al., 1996; Shennan et al., 1996; Hawkes et al., 2010; 2011; Engelhart et al., 2013a; Wang et al., 2013). On a margin-wide scale, across multiple estuaries, foraminiferal-based transfer function investigations of the CSZ 1700 CE earthquake have shown that vertical deformation was non-uniform along the margin (e.g., Hawkes et al., 2011; Wang et al., 2013; Kemp et al., 2018). Therefore, small-scale contact stratigraphic and biostratigraphic preservation irregularities may have important implications for paleoseismic interpretations.

It is promising that comparisons of foraminiferal-based transfer function subsidence estimates derived from tidal-marsh cores 2-43 m apart demonstrated that estimates are reproducible in Oregon (Milker et al., 2016). In Alaska, Shennan and Hamilton, (2006), demonstrated that diatom transfer function subsidence estimates are reproducible within the same marsh over 200-2500 m apart and conclude reconstructions across the same stratigraphic contact will improve confidence in an assigned average estimate. However, the variability of the coseismic subsidence estimates was not a focal point of the investigation. To our knowledge, no work has

focused on assessing the reproducibility of microfossil-based transfer-function derived coseismic deformation estimates over distances of 1-6 km across multiple tidal marshes in the same estuarine system. This is important as these are spatial scales where second order influences on stratigraphic preservation of coseismic land-level changes may not be uniform. In order to evaluate site-specific, estuary-wide, and regional systematic differences, it is necessary to identify the extent of stratigraphic and biostratigraphic variability.

Therefore, in this paper we test the reproducibility of coseismic subsidence estimates using an existing Bayesian foraminiferal transfer function (BTF; Kemp et al., 2018) at northern Humboldt Bay, California (~44.8°N, -124.2°W) to assess within-site and within-estuary variability. We examine three abrupt mud-over-peat (coseismic subsidence) contacts along a 6-km transect from Jacoby Creek, McDaniel Creek, and Mad River Slough (Fig. 1; Padgett et al., in prep). To assess the reproducibility of our estimates, we analyzed 20 sediment cores containing the three mud-over-peat contacts; nine examples of the 250 cal yrs BP contact, five examples of the ~870 cal yrs BP contact, and six examples of the ~1125 cal yrs BP contact. Based on our results, we recommend using an average of 2-3 reconstructions to ensure confidence in estimates of coseismic subsidence. Where possible, these should be drawn from multiple marshes within the estuary.

2. STUDY AREA

With no major rivers discharging into it, northern Humboldt Bay is a depositional center for Holocene tidal and marsh sediment (Vick, 1988; Clarke and

Carver, 1992; Valentine, 1992). Barnhart et al., (1992) estimate a yearly sediment input to be 7.6x10 m^3 of very fine to fine sand, silt and clay. Humboldt Bay substrate is dominantly composed of silt and clay but coarser-grained sediments are found proximate to the bay entrance and within tidal channel troughs (Thompson, 1971; Borgeld and Stevens, 2004). Most sediment delivered to Humboldt Bay is derived from the mouth of the bay and is likely sourced from storm events and sediment plumes from the Eel River ~12 km to the south (Thompson, 1971; Borgeld and Stevens, 2007). Several fringe salt-marsh environments have formed along the periphery and proximate to small drainages but also on dissected islands (Eicher, 1987; Vick, 1988 Clarke and Carver, 1992; Valentine, 1992; Pritchard, 2004). These coastal lowlands are protected from the Pacific Ocean by ~20-25 m high Lanphere-Ma-le'l Dunes (Fig. 1c; Vick, 1988; Pickart and Hesp, 2019). A NOAA tide gauge station at the mouth of Mad River Slough documents a 2.36 m semi-diurnal tide range (Mean Highest High Water, MHHW – Mean Lowest Low Water, MLLW). High marshes form at elevations around mean highest high water (MHHW) and low marshes form at elevations around mean high water (MHW; Pritchard, 2004).

Observations within northern Humboldt Bay are consistent with typical Cascadia tidal wetland floral and faunal distributions (Pritchard, 2004; Hawkes et al., 2010; Kemp et al., 2018). Benthic foraminiferal communities differ along an intertidal gradient such that higher marsh environments, around MHHW, are often dominated by *Trochaminita spp.*, *Haplophragmoides spp.*, *Balticammina pseudomacrescens*, *Trochammina inflata*, and *Jadammina macrescens*. Whereas at elevations from ~MHW down to mean tide level (MTL), increasing percentages of *Miliammina fusca*,

Ammobaculites spp., *Reophax spp.,* and calcareous foraminifera species are reported (Guilbault et al., 1995, 1996; Nelson et al., 2008; Hawkes, 2010, 2011; Engelhart et al., 2013a, 2013b; Milker et al., 2015, 2016; Kemp et al., 2018). Kemp et al., (2018) show that these intertidal benthic foraminiferal communities are comparable along the west coast of North America from at least ~35.5 -50° N. In high marsh environments floral communities include *Castilleja exserta*, *Distichlis spicata*, *Grindelia spp*., *Jaumea carnosa, Spartina densiflora*, and *Triglochin maritimum* (Eicher, 1987; Schlosser and Eicher, 2012). Floral communities of middle and lower marsh environments include *Distichlis spicata*, *Salicornia virginica*, *Spartina densiflora*, and *Triglochin maritimum* (Eicher, 1987; Schlosser and Eicher, 2012).

3. METHODS

In this study we focus on wetland stratigraphy at Jacoby Creek , McDaniel Creek, and Mad River Slough marshes at northern Humboldt Bay, California. Throughout the northern Humboldt Bay estuary, Padgett et al., (*in-prep*), mapped abrupt (<2mm) to sharp (<10mm) *mud-over-peat* and *mud-over-forest soil* contacts. Based on depth in cores, radiocarbon age distributions, fossil foraminiferal analysis, and regional plate boundary age distribution comparisons, Padgett et al., (*in-prep*), observed four stratigraphic sequences consistent with coseismic subsidence caused by megathrust-earthquake rupture. We selected 20 representative sediment cores segments (50 cm length) of stratigraphic sequences that document the past three megathrust earthquakes, as discussed in Padgett et al. (in prep), for foraminiferal analysis.

Our research approach is three-fold; 1) lithostratigraphic analysis (describe subsurface contact stratigraphy), 2) relative sea-level reconstructions (estimate paleoenvironmental elevation changes using fossil foraminiferal data and an existing BTF; Kemp et al., 2018), and 3) intra- (one site) and inter-site (multiple sites) reproducibility assessment (identify within-site and within-bay stratigraphic, biostratigraphic, and coseismic subsidence estimate variability).

3.1 Lithostratigraphic analysis

3.1.1 Stratigraphic description and sampling

Based on stratigraphic mapping across three sites, over a >6 km transect (Fig. 1b), at northern Humboldt Bay we selected 20 representative stratigraphic sections that span three earthquake induced subsidence contacts from Mad River Slough (8), McDaniel Creek (7), and Jacoby Creek (5). Sharp (<10mm) to abrupt (<2mm) *mud-over-peat* and *mud-over-forest soil* contacts were mapped primarily using a 30 mm wide gouge core up to ~4 m depth below the ground surface. Sediment cores were collected with either an Eijkelkamp peat sampler or a 60 mm gouge core, depending on substrate, for biostratigraphic analyses. We preferentially chose to sample with the Eijkelkamp peat sampler because the design of the equipment allows for the collection of an uncontaminated sample because it captures material directly adjacent to the primary stress direction of the coring apparatus. However, in a number of cases the nature of the sediment material was too stiff to operate this sampler type. In such examples the 60 mm gouge was used for sediment core sample collection.

Wetland stratigraphy consists of clastic mud and interbedded organic-rich units. A clastic “mud” refers to a lithology of a grey to olive massive to finely (1-

3mm) bedded silts and clays. An "organic-rich unit" refers to a dark salt-marsh peat or a forest soil. Grain size, sedimentary structures, contacts, thickness, and facies changes were described in the field using general stratigraphic methods in combination with the Troels-Smith (1955) method for describing organic-rich sediment. Stratigraphic unit descriptions employed in this investigation include peat, muddy peat, peaty mud, and mud. Organic percentages for peat, muddy peat, and peaty mud are 100%-75%, 75%-50%, and 50%-25%, respectively. Silt and clay units that consist of <25% organics by volume are described as "mud".

3.1.2 Stratigraphic Imaging

Contact sharpness and through-core continuity are not always clear from optical inspection. Therefore, we followed recent paleoseismic studies (e.g., Goldfinger et al., 2012; Patton et al., 2013; Briggs et al., 2014; Milker et al., 2016) and obtained high-resolution imagery in order to analyze fossil core density contrasts. Computerized tomography (CT) scans were conducted at Rhode Island South County Hospital and Oregon State University College of Veterinary Medicine, following methodologies outlined in Rothwell and Rack (2006) and Davies et al. (2011). At South County Hospital, CT analysis was performed using a 32 Slice GE Light speed Scanner with technical factors set at 120 kVp and 200-400 mA and a pitch of 0.969:1. At Oregon State University, CT analysis was performed using a Toshiba Aquilion 64 Slice and the scans were collected at 120 kVp and 200 mA and a pitch of 0.5s (100 mAs). For visualization purposes, the resulting images were processed with a "bone" algorithm to generate coronal images every mm across the core. We also collected X-radiation (X-ray) images, which were taken with a Shimadzu UD150B-40 and imaged

with a Fuji FCR XL-2 at the University of Rhode Island Health Center to illuminate density differences within the collected fossil sediment cores for further inspections of density contrasts and where CT imagery was unavailable. Sediment core density images were joined into composite imagery using Horos and Adobe software.

3.1.3 Surveying to sea-level datum

Sample elevations for each core were acquired using a Leica GS15 real-time kinematic global positioning system (RTK-GPS) utilizing a separate base and rover. Data collected by the RTK-GPS base were post-processed using OPUS to obtain North American Vertical Datum 1988 (NAVD88) orthometric elevations. To establish elevations with respect to a tidal datum, we took RTK-GPS measurements of tidal benchmarks associated with the temporary tide gauge installation (12/01/1978 to 03/31/1979) at Mad River Slough (NOAA ID: 9418865).

3.2 Relative sea-level reconstructions

3.2.1 Foraminifera

We followed standard sample preparation and analysis (e.g. Scott and Medioli, 1982; de Rijk, 1995; Horton and Edwards, 2006). Fossil foraminifera were concentrated by sieving 1 cm intervals of sediment (~3cm^3), from collected cores, over 500- and 63-micron sieves and retaining the material between those size fractions. The 500-micron sieve was checked for larger foraminifera before material was discarded. Fossil samples were analyzed until at least 200 dead foraminifera were identified, or until the entire sample was enumerated (Fatela and Taborda, 2002). Such count numbers are likely conservative given the low diversity of salt-marsh foraminiferal assemblages (Kemp et al., submitted). Following Kemp et al., (2018),

only samples with >30 foraminifera were used in the production of quantitative RSL reconstructions because low abundances may reflect a non in-situ assemblage and/or may not be representative of the depositional environment. Foraminifera were identified following taxonomy based on Hawkes et al., (2010) and Milker et al., (2015). Additionally, we combine *Haplophragmoides spp* and *Ammobaculites spp.* following Kemp et al., (2018).

3.2.2 Bayesian Transfer Function

Estimates of coastal vertical deformation during megathrust earthquakes can be derived from microfossil analyses of wetland stratigraphic sequences. Along the coast of Cascadia, foraminiferal-based transfer functions provide high-precision RSL reconstructions by statistically relating fossil assemblages to modern intertidal distributions (Guilbault et al., 1995; 1996; Nelson et al., 2008, Hawkes et al., 2010; 2011; Engelhart et al., 2013b; Wang et al., 2013; Milker et al., 2016; Kemp et al., 2018). Kemp et al., (2018) developed a BTF that incorporates an extended West Coast modern foraminifera training set, allows for flexible species-response curves, and can formally incorporate prior information from additional proxies, e.g., other microfossil groups, $\delta^{13}C$, or stratigraphic context, which combine to produce high-precision RSL reconstructions and extends applicability of the methodology (Cahill et al., 2016; Holden et al., 2017). We follow Kemp et al., (2018) and assign stratigraphic context as informative priors to RSL reconstructions. The stratigraphic context ranges from either clastic dominated tidal flat to low salt-marsh sediment, which accumulates at elevations between mean low water (MLW) and MHHW (20-200 SWLI), or organic-rich high salt marsh, which accumulates at elevations from MHW to the highest

occurrence of foraminifera (180-252 SWLI; Kemp et al., 2018). In order to evaluate goodness of fit between a fossil assemblage and a modern analog, we used the Bray-Curtis distance metric (Kemp and Telford, 2015: Kemp et al., 2018). Due to low species diversity, a threshold of less than the 20th percentile of the dissimilarity coefficient values is appropriate for salt-marsh foraminifera modern and fossil assemblage pairings (Kemp and Telford, 2015).

3.3 Reproducibility assessment

Typically at Cascadia, one coseismic subsidence estimate has been used to represent subsidence for an estuary (e.g., Hemphill-Haley 1995; Guilbault et al., 1996; Shennan et al., 1996; Sabean, 2004; Hawkes et al., 2011; Wang et al., 2013). However, if there was a scenario, e.g., erosion of the inundated surface, liquefaction, compaction, or delayed resumption of sedimentation that was anomalous to the rest of the marsh then that stratigraphy and fauna assemblages could be misleading and/or not representative. In order to test the possibility of a misrepresentation of coseismic subsidence and account for stratigraphic variability we compiled ≥2 RSL reconstructions per each earthquake stratigraphic sequence at three marsh locations. We compiled 20 coseismic subsidence estimates over the most recent three earthquake cycles at northern Humboldt Bay. We derive subsidence estimates using a BTF and take mean values per earthquake and per site across the estuary. By constructing multiple coseismic subsidence estimates for the same earthquake stratigraphy, we assess and identify the appropriate number of reconstructions necessary to confidently account for stratigraphic variability and characterize coseismic subsidence for the area

in question. We assign the term reproducible to coseismic subsidence estimates that overlap with other coseismic subsidence estimate ranges. Furthermore, for a particular earthquake stratigraphic sequence in question, if two or more coseismic subsidence estimates are reproducible then the estimate range is validated and we gain confidence in assigning an averaged estimate to the area.

4. RESULTS

4.1 Contact lithology, foraminiferal analyses and subsidence estimate

In hand-augured cores we observed, dark organic-rich units overlain in sharp contact to grey mud units. The organic-rich units contain relatively abundant plant macrofossils and in general, the older and deeper buried organic-rich units were increasingly humified. Clastic muds contained sparse plant macrofossils and were often massive and occasionally finely bedded. We did not observe any sand layers in-between an organic-rich unit and overlying mud across the estuary. By applying the BTF to fossil foraminiferal assemblages, we derived quantitative coseismic subsidence estimates from RSL reconstructions (Table1; Figs. 2-12). Below we describe the stratigraphic and biostratigraphic characteristics which influenced the RSL reconstructions of each core analyzed within this investigation.

4.1.1 Earthquake 1 - (250 cal yrs BP, 1700 CE)

We evaluated nine stratigraphic sections of the most recent earthquake at northern Humboldt Bay (Padgett et al., *in-prep*). Three stratigraphic sections were collected from each tidal marsh location.

4.1.1.1 Jacoby Creek

At *JC.02,* the upper contact of the shallowest earthquake-induced buried organic-rich unit is at 75.5 cm core depth (Fig. 2a). The picture and CT image of *JC.02* show an abrupt 1-2 mm contact with ~17 mm of relief where clastic mud has infiltrated ~20 mm below the contact. The organic-rich peat unit is 15 cm thick and grades from a dark brown peat to light brown rooted mud at the base. Foraminifera in the organic-rich unit dominantly consist of *B. pseudomacrescens* (20-58%), *T. inflata* (24-42%), and *J. macrescens* (17-40%), which is consistent with a high salt-marsh peat. Above the organic rich unit is a >25cm thick grey mud, which has very thin to thin (0.1–0.3 mm) thick laminations that start ~4cm above the lower contact and continue up section towards the base of the overlying modern peat surface soil; the laminations are indicated by alternating yellow and orange layers in the CT image. Although samples in the overlying grey mud unit are also dominated by *J. macrescens* (39-67%), *T. inflata* (10-33%), and *B. pseudomacrescens* (3-24%), the assemblages show an increase in the abundance of *M. fusca* (1-30%) and contain *Ammobaculites* spp. (<5%) and *Reophax* spp. (<7%), which are typically associated with sediments accumulating below MHW and closer to MTL (Kemp et al., 2018). For the subsidence estimate, we use the reconstructed RSL elevations that are 2 cm apart, which are the first full centimeter intervals above and below the contact that avoid the relief of the *mud-over-peat* contact. The fossil foraminifera BTF reconstruction shows 0.75±0.52 m of subsidence.

At *JC.06*, the upper contact of the shallowest earthquake-induced buried organic-rich unit is at 93.5 cm core depth (Fig. 2b). The picture and CT scan of *JC.02* show an abrupt 1-2 mm contact with ~7 mm of relief. the peat unit . The organic-rich

peat unit is 18 cm thick, slightly denser <1.0 cm below the upper contact, and grades from a dark brown peat to light brown rooted mud at the base. Foraminifera in the organic-rich unit dominantly consist of *B. pseudomacrescens* (22-35%), *T. inflata* (27-38%), and *J. macrescens* (14-23%), which is consistent with a high salt-marsh peat. Above the organic-rich unit is a >25cm thick grey mud unit with 1cm thick visible bed ~1cm above the lower contact. Foraminifera in the grey mud unit dominantly consist of *M. fusca* (45-53%), *T. inflata* (11-23%), and *J. macrescens* (16-23%) but also include *Ammobaculites* spp. (1-8%) and *Reophax* spp. (1-5%), which are typically associated with sediments accumulating below MHW and closer to MTL (Kemp et al., 2018). For the subsidence estimate, we use the reconstructed RSL elevations that are 2 cm apart, which are the first full centimeter intervals above and below the contact that avoid the relief of the *mud-over-peat* contact. The fossil foraminifera BTF reconstruction shows 1.00±0.40 m of subsidence.

At *JC.10*, the upper contact of the shallowest earthquake-induced buried organic-rich unit is at 79.5 cm core depth (Fig. 2c). The picture and CT scan of *JC.10* show an abrupt 1-2 mm contact with ~7 mm of relief and also reveal overlying mud infiltration into the underlying organic-rich unit with a sub-vertical orientation on the right-side of the sediment core. The organic-rich peat unit is 13 cm thick and grades from a brown-grey muddy peat to grey-brown peaty mud at the base. Overlying the organic-rich unit is a >25cm thick grey mud unit. Foraminifera in the organic-rich unit dominantly consist of *B. pseudomacrescens* (24-50%), *T. inflata* (24-34%), and *J. macrescens* (17-41%), which is consistent with a high salt-marsh peat. Even though foraminifera in the grey mud unit also dominantly consists of *T. inflata* (29-40%), *J.*

macrescens (24-32%), and *B. pseudomacrescens* (11-16%) it also includes *M. fusca* (8-11%), *Ammobaculites* spp. (4-5%) and *Reophax* spp. (1-5%) which are typically associated with sediments accumulating below MHW and closer to MTL (Kemp et al., 2018). For the subsidence estimate, we use the reconstructed RSL elevations that are 2 cm apart, which are the first full centimeter intervals above and below the contact that avoid the relief of the *mud-over-peat* contact. The fossil foraminifera BTF reconstruction shows 0.49±0.40 m of subsidence.

4.1.1.2 McDaniel Creek

At *MD.03*, the upper contact of the shallowest earthquake-induced buried organic-rich unit is ~horizontal at 115 cm core depth (Fig. 3a). The CT scan of *MD.03* shows an abrupt 1-2 mm contact with 5 mm of relief. The organic-rich unit is a 8 cm thick grey-brown peat. Foraminifera in the grey-brown peat unit dominantly consist of *B. pseudomacrescens* (27-54%), *T. inflata* (7-38%), and *J. macrescens* (5-33%), which is consistent with a high salt-marsh peat. Overlying the organic-rich unit is a >25 cm thick grey mud, which has very thin to thin (0.1–0.3 mm) laminations that start ~2cm above the lower contact; a burrow that extends from ~5 mm to 5 cm above the contacts the laminations are indicated by alternating yellow and orange layers in the CT image. Samples in the mud overlying the peat unit show an increase in the abundance of *M. fusca* (5 to 14%), *Reophax spp.* (0.05-3%), *Ammobaculites spp.* (0-1.4%), and *J. macrescens* (25 to 54%) and a decrease in the abundance of *B. pseudomacrescens* (12 to 29%) and *T. inflata* (16 to 27%). The presence of *Ammobaculites spp*., *Reophax spp*., and increase of *M. fusca* is consistent with sediments accumulating near MTL (Kemp et al., 2018). For the subsidence estimate,

we use the reconstructed RSL elevations that are 2 cm apart, which are the first full centimeter intervals above and below the contact that avoid the relief of the *mud-over-peat* contact. The fossil foraminifera BTF reconstruction suggests 0.90 ±0.44m of subsidence.

At *MD.*12, the upper contact of the shallowest earthquake-induced buried organic-rich unit is abrupt at 109 cm core depth (Fig. 3b). The picture and CT scan of *MD.12* show an abrupt 1-2 mm contact that undulates with ~8 mm of relief. The organic-rich peat unit is 18 cm thick and grades from a dark brown peat at the top to a grey brown rooted mud at the base. Foraminifera in the brown peat unit dominantly consist of *B. pseudomacrescens* (45-66%), *J. macrescens* (9-21%), and *T. inflata* (9-11%), which is consistent with a high salt-marsh peat. Overlying the organic-rich unit is a >25cm thick grey mud that has weak very-thin laminations and sporadic organics over 7cm above the lower contact, which are visible in the CT imagery (Fig. 3b). Foraminifera in the mud overlying the peat unit also dominantly consist of *T. inflata* (25-31%), and *J. macrescens* (23-28%), but show an marked increase in *M. fusca* (11 to 20%), *Reophax spp.* (2-6%), and *Ammobaculites spp.* (1-3%), which are typically associated with sediments accumulating below MHW and closer to MTL (Kemp et al., 2018). For the subsidence estimate, we use the reconstructed RSL elevations directly above and below the *mud-over-peat* contact. The fossil foraminifera BTF reconstruction suggests 0.49±0.40 m of subsidence.

At *MD.13*, the upper contact of the shallowest earthquake-induced buried organic-rich unit is abrupt at 121.5 cm core depth (Fig. 3c). The picture and CT image show an abrupt 1-2 mm contact with 17 mm of relief. The organic-rich brown muddy

peat unit is 10 cm thick and grades from a brown-grey muddy peat at the top to a grey brown rooted mud at the base. Foraminifera in the brown peat unit dominantly consist of *T. inflata* (33-44%), *J. macrescens* (15-25%), *M. fusca* (13 to 19%), and *Haplophragmoides spp*. (8-21%), which is consistent with a mid-high salt marsh peat. The overlying grey mud is >25cm thick and has infiltrated the right side of the sediment core. Foraminifera in the overlying grey mud also dominantly consist of *T. inflata* (29-44%), *J. macrescens* (17-29%), *M. fusca* (19 to 21%), and *Haplophragmoides spp*. (10-18%), but also contain a marked increase of *Reophax spp.* (3-6%), and *Ammobaculites spp.* (2-5%), which is consistent with sediment accumulating near MTL (Kemp et al., 2018).). For the subsidence estimate, we use the reconstructed RSL elevations that are 2 cm apart, which are the first full centimeter intervals above and below the contact that avoid the relief of the *mud-over-peat* contact. The fossil foraminifera BTF reconstruction suggests 1.04±0.42m of subsidence.

4.1.1.3 Mad River Slough

At *MR.05*, the upper contact of the shallowest earthquake-induced buried organic-rich unit is at 105.5 cm core depth (Fig. 4a). The picture and CT image show a sharp (3 mm) contact with ~12 mm of relief and a plant macro fossil (*M. triglochin)* in growth position spanning across the contact. The organic-rich peat unit is 18 cm thick and grades from a dark brown peat to a brown muddy peat at the base. Foraminifera in the brown peat unit dominantly consist of *B. pseudomacrescens* (34-62%), *Haplophragmoides spp.* (11-40%), and *T. inflata* (15-22%), which is consistent with a high salt-marsh peat. The overlying grey rooted mud extends >25cm and contains thin

laminations <15 cm above the contact. Foraminifera in the mud overlying the peat unit also dominantly consist of *M. fusca* (56 to 73%) which is consistent with an environment below MHW, but also show a marked increase in *M. petila.* (2-4%) that is typically found above MHHW (Kemp et al. 2018). For the subsidence estimate, we use the reconstructed RSL elevations that are 3 cm apart, which are the first full centimeter intervals above and below the contact that avoid the relief of the *mud-over-peat* contact. The fossil foraminifera BTF reconstruction suggests 0.36±0.26 m of subsidence.

At *MR.03,* the upper contact of the shallowest earthquake-induced buried organic-rich unit is at 103 cm core depth (Fig. 4b). The picture and X-ray image of *MR.03* show a sharp (3 mm) contact with ~7 mm of relief. The organic-rich peat unit is 24 cm thick, which grades from a dark brown peat to a brown muddy peat at the base. Foraminifera in the brown peat unit dominantly consist of *B. pseudomacrescens* (33-64%), and *Haplophragmoides spp.* (18-47%), which is consistent with a high salt-marsh peat. The overlying grey rooted mud extends >25cm with thin organic-rich laminations throughout. However within the lower 3 cm of the mud unit the laminations have 5-7 mm of relief. Foraminifera in the mud unit dominantly consist of *J. macrescens* (24-37%) and show a marked increase in *M. fusca* (6-34%), which is consistent with an environment below MHW. For the subsidence estimate, we use the reconstructed RSL elevations that are 3 cm apart, which are the first full centimeter intervals above and below the contact that avoid the relief of the *mud-over-peat* contact. The fossil foraminifera BTF reconstruction suggests 0.36±0.24 m of subsidence.

At *MR.02*, the upper contact of the shallowest earthquake-induced buried organic-rich unit is at ~142 cm core depth (Fig. 4c). The picture and CT image show a horizontal 2 mm contact with 3 mm of relief and also reveal a 1 cm thick grey mud with sharp upper and lower contacts ~1.5 cm below the contact. The organic-rich peat unit is 23 cm thick grades from a dark brown peat to a brown rooted mud at the base. Foraminifera in the brown peat unit dominantly consist of *B. pseudomacrescens* (66-78%) and *J. macrescens* (8-21%), which is consistent with a high salt-marsh peat. The grey mud unit is a >25cm thick with and sporadic organics over 6 cm above the lower contact, which are visible in the CT imagery (Fig. 3b). Foraminifera in the mud unit also dominantly consist of *J. macrescens* (12-56%) and also show a marked increase in *M. fusca* (7-55%), which is consistent with an environment below MHW. However, within the first two reconstructed mud unit intervals above the contact, *B. pseudomacrescens* are present at 34 and 15 % respectively. For the subsidence estimate, we use the reconstructed RSL elevations that are 2 cm apart, which are the first full centimeter intervals above and below the contact that avoid the relief of the *mud-over-peat* contact. The fossil foraminifera BTF reconstruction suggests 0.28±0.26 m of subsidence.

4.1.2 Earthquake 2 - (815-924 cal yrs BP)

We evaluated five stratigraphic sections of the second most recent earthquake at northern Humboldt Bay (Padgett et al., *in-prep*). Three stratigraphic sections were collected from Mad River Slough and two stratigraphic sections were collected from McDaniel Creek. Earthquake 2 was not observed at Jacoby Creek (Padgett et al., *in-prep*).

4.1.2.1 McDaniel Creek

At *MD.06*, the upper contact of the second earthquake-induced buried organic-rich unit is at 170.5 cm core depth (Fig. 5a). The picture and X-ray image show a sharp ~3 mm horizontal contact. The organic-rich unit is 14 cm thick and contains thin l organic-rich lamentations that form a grey-brown peat. Foraminifera in the light brown-grey muddy peat unit dominantly consist of *B. pseudomacrescens* (12-40%), *J. macrescens* (13-30%), and *T. inflata* (24-36%), which is consistent with a high salt-marsh peat. The overlying grey mud is >25cm thick. Foraminifera within the mud unit show an increase in the abundance of *M. fusca* (21-33%) and *J. macrescens* (27-37%) and a decrease in the abundance of *B. pseudomacrescens* (4-9%), which is consistent with sediments accumulating below MHW. For the subsidence estimate, we use the reconstructed RSL elevations that are 1 cm apart, which are the first full centimeter intervals above and below the contact that avoid the relief of the *mud-over-peat* contact. The fossil foraminifera BTF reconstruction shows 0.39±0.33 m of subsidence.

At *MD.03*, upper contact of the second earthquake-induced buried organic-rich unit is at 211 cm core depth (Fig. 5b). The picture and X-ray images show a sharp ~3 mm horizontal contact. The light brown-grey rooted mud unit is 10 cm thick and contains thin l organic-rich lamentations that form a grey-brown peat. Foraminifera in the grey brown rooted mud unit dominantly consist of *T. inflata* (36-53%), and *J. macrescens* (31-53%), which is consistent with a high salt-marsh peat. The overlying mud unit is >25 cm thick and contains very thin to thin laminations in the lower 10 cm of the unit. Foraminifera within the grey mud dominantly consist of *M. fusca* (27-45%), *J. macrescens* (13-54%), and *T. inflata* (12-39%), which is consistent with

sediments accumulating below MHW. For the subsidence estimate, we use the reconstructed RSL elevations that are 1 cm apart, which are the first full centimeter intervals above and below the contact that avoid the relief of the *mud-over-peat* contact. The fossil foraminifera BTF reconstruction shows 0.46±0.35 m of subsidence.

4.1.2.2 Mad River Slough

At *MR.02*, the upper contact of the second earthquake-induced buried organic rich unit is at 220.5 cm core depth (Fig. 6a). The photo and X-ray image show a ~1 cm mud lens 5 mm below the upper contact of the peat unit. The brown peat unit is 26 cm thick and grades from a brown peat at the upper 9 cm of the unit to a brown-grey rooted mud at the base. Foraminifera in the light brown peat unit consist of *J. macrescens* (22-64%), *T. inflata* (21-29%), *Haplophragmoides spp.* (6-22%), and *B. pseudomacrescens* (1-21%), which is consistent with a high salt-marsh peat. However, the foraminiferal assemblage at 221.5 cm is directly below the upper contact of the peat unit contains *M. fusca* at 6% and is the lowest RSL reconstruction of all organic-rich unit reconstructions within the investigation, 192 SWLI. Below the contact and within the peat unit, foraminifera assemblages do not differ within the 1 cm mud lens compared to the assemblages above and below. The overlying grey rooted mud extends >25cm with thin organic-rich laminations throughout except for the lower 3 cm, which is denser than the rest of the overlying unit. Foraminifera in the grey mud dominantly consist of *M. fusca* (32-57%), and *J. macrescens* (23-50%), which is consistent with sediment accumulating below MHW (Kempt et al., 2018). For the subsidence estimate we used the reconstructed RSL elevations from the directly above

and below the *mud-over-peat* contact. The fossil foraminifera BTF reconstruction shows 0.51±0.30 m of subsidence.

At *MR*.03, the upper contact of second earthquake-induced buried organic-rich unit is at 149 cm core depth (Fig. 6b). The picture and X-ray images show a ~0.3 cm thick organic lens 1 cm above the sharp, ~3 mm horizontal contact. The buried organic-rich unit is a 35 cm thick light brown peat. Foraminifera in the brown peat unit dominantly consist of *J. macrescens* (21-46%), *T. inflata* (40-53%) but also contain *M. fusca* (6-17%) which is consistent with a mid-high salt marsh peat. The overlying light brown-grey rooted mud is >25cm thick and contains organic-rich beds 1-4 cm thick. Foraminifera light brown-grey rooted mud overlying the peat unit also dominantly consist of *T. inflata* (39-70%), *J. macrescens* (23-50%), and *M. fusca* (6-15%), which is consistent with sediment accumulating near MHW. For the subsidence estimate we used the reconstructed RSL elevations from the directly above and below the *mud-over-peat* contact. The fossil foraminifera BTF reconstruction shows 0.26±0.25 m of subsidence, which is the lowest estimate of subsidence observed within this investigation.

At MR.05, the upper contact of second earthquake-induced buried organic-rich unit is at 188 cm core depth (Fig. 6c). The picture and X-ray image and show a ~0.75 cm thick mud lens 1.5 cm below the sharp, 3 mm, upper contact of the peat unit. The organic-rich unit is a 35 cm thick brown peat that grades from a brown peat with mud laminations to with the upper 6 cm to a rooted brown-grey mud at the base. Foraminifera in the brown peat unit consist of *J. macrescens* (15-48%), *T. inflata* (15-44%), and *B. pseudomacrescens* (3-56%), which is consistent with a high salt marsh

peat. The overlying light brown-grey rooted mud is >25cm thick and contains organic-rich beds 1-4 cm thick. Foraminifera light brown-grey rooted mud dominantly consist of *J. macrescens* (28-67%), and *M. fusca* (6-61%), which is consistent with sediments accumulating below MHW (Kemp et al., 2018). For the subsidence estimate we used the reconstructed RSL elevations from the directly above and below the *mud-over-peat* contact. The fossil foraminifera BTF reconstruction shows 0.33±0.26 m of subsidence.

4.1.3 Earthquake 3 - (1004-1233 cal yrs BP)

We evaluated six stratigraphic sections, two from each marsh site, of the third most recent earthquake at northern Humboldt Bay (Padgett et al., *in-prep*).

4.1.3.1 Jacoby Creek

At JC.02, the upper contact of the second earthquake-induced buried organic-rich unit is at 131 cm core depth (Fig 7a) and has radiocarbon ages that are consistent with the third most recent megathrust earthquake at northern Humboldt Bay (Padgett et al., in-prep). The picture and CT imagery display sharp a 3mm contact that undulates over ~12 mm. There are disconnected organics <1cm of the contact. The organic-rich unit 11 cm thick and grades from dark brown peat within 3 cm below the upper contact to a greyish brown muddy peat at the base. Foraminifera in the light brown peat unit consist of *B. pseudomacrescens* (48-69%), *T. inflata* (15-23%), and *J. macrescens* (10-21%), which is consistent with a high salt marsh peat. The overlying grey mud is >25 cm thick. Within the mud unit, the CT image reveal 2 to 9 mm thick organic laminations with an increasing dip bedding plan, ≥3.5 cm of relief, up sequence over ~20 cm over the base of the mud unit. Foraminifera within the grey

mud unit dominantly consist of *J. macrescens* (70-61%), and *T. inflata* (12-26%), but also contain *M. fusca* (3-27%), which is consistent with sediments accumulating below MHHW. For the subsidence estimate, we use the reconstructed RSL elevations that are 1 cm apart, which are the first full centimeter intervals above and below the contact that avoid the relief of the *mud-over-peat* contact. The fossil foraminifera BTF reconstruction shows 0.48±0.42 m of subsidence.

At JC.10, the upper contact of the second earthquake-induced buried organic-rich is at 124.5 cm core depth and has radiocarbon ages that are consistent with the third most recent megathrust earthquake at northern Humboldt Bay (Fig 7b; Padgett et al., in-prep). The photo and CT image show a sharp contact with 3 mm of relief. The organic-rich unit is a 10 cm thick and grades from 8 cm thick dark brown peat to a 2 cm thick grey brown muddy peat from top to base. Foraminifera in the dark brown peat unit consist of *B. pseudomacrescens* (39-65%), *T. inflata* (17-27%), and *J. macrescens* (6-24%), which is consistent with a high salt marsh peat. Foraminiferal in the overlying grey mud unit dominantly consist of *J. macrescens* (30-46%), and *T. inflata* (20-33%), and *M. fusca* (10-30%), but also contain *Reophax spp.* (0-9%) and *Ammobaculites spp.* (0-5%), which is consistent with sediments accumulating near MTL (Kemp et al., 2018). For the subsidence estimate, we use the reconstructed RSL elevations that are 2 cm apart, which are the first full centimeter intervals above and below the contact that avoid the relief of the *mud-over-peat* contact. The fossil foraminifera BTF reconstruction shows 0.94±0.44 m of subsidence.

4.1.3.2 McDaniel Creek

At *MD.13,* the upper contact of third earthquake-induced buried organic rich unit is at 248 cm core depth (Fig 8a) and has radiocarbon ages that are consistent with the third most recent megathrust earthquake at northern Humboldt Bay. The photo and CT scan show a sharp, 3mm, contact with ~14mm of undulating relief. The organic-rich unit is a 8 cm thick, where the upper 3 cm is a light brown muddy peat and the lower 5 cm are a grey-brown rooted mud. Foraminifera in the organic-rich unit dominantly consist of *B. pseudomacrescens* (3-48%), *T. inflata* (9-71%), and *J. macrescens* (22-52%), which is consistent with a high salt marsh peat. The organic-rich unit is overlain by a grey mud that extends >25cm. Although foraminifera in the grey mud unit are also dominated by *J. macrescens* (27-38%), *T. inflata* (15-19%), and *B. pseudomacrescens* (12-18%), the assemblages show a marked increase in the abundance of *M. fusca* (14 to 17%) and contain *Ammobaculites* spp. (~1%) and *Reophax* spp. (~1%), which are typically associated with sediments accumulating closer to MTL (Kemp et al., 2018). For the subsidence estimate, we use the reconstructed RSL elevations that are 3 cm apart, which are the first full centimeter intervals above and below the contact that avoid the relief of the *mud-over-peat* contact. The fossil foraminifera BTF reconstruction shows 0.99 ±0.44 m of subsidence across contact D.

At MD.12, the upper contact of the third earthquake-induced buried organic-rich unit is at 221.5 cm core depth (Fig. 8b) and has radiocarbon ages that are consistent with the third most recent megathrust earthquake at northern Humboldt Bay. The picture and CT imagery display an abrupt, 1-2 mm, and undulatory contact with 4 mm of relief. The organic rich unit is 7 cm thick and grades from a dark brown

peat to a grey brown muddy peat. The Ct imagery show a burrow that vertically infiltrated ~3-4 cm through the organic-rich unit. Foraminifera in the organic-rich unit consist of *B. pseudomacrescens* (55-64%), *T. inflata* (15-20%), and *J. macrescens* (11-18%), which is consistent with a high salt marsh peat. Although foraminifera in the grey mud unit are also dominated by *J. macrescens* (22-39%), *B. pseudomacrescens* (7-27%), and *T. inflata* (15-25%), the assemblages show a marked increase in the abundance of *M. fusca* (16 to 19%), *Reophax* spp. (2-9%), and contain *Ammobaculites* spp. (<2%) and which are associated with sediments accumulating closer to MTL (Kemp et al., 2018). For the subsidence estimate, we use the reconstructed RSL elevations that are 2 cm apart, which are the first full centimeter intervals above and below the contact that avoid the relief of the *mud-over-peat* contact. The fossil foraminifera BTF reconstruction shows 0.59±0.38 m of subsidence across contact D.

4.1.3.3 Mad River Slough

At *MR.05*, the upper contact of the third earthquake-induced buried organic-rich unit is at (Fig. 9a). The photo and CT imagery show an abrupt, 1 mm, horizontal contact. The organic-rich unit is 16 cm thick and grades from a dark brown peat over 12 cm into a 4 cm grey brown muddy peat from top to base. Foraminifera in the light brown peat unit consist of *Haplophragmoides spp.* (11-67) and *B. pseudomacrescens* (3-62%), which is consistent with a high salt marsh peat. The overlying mud is >25cm and contains sporadic organics. The CT imagery reveal a 0.3 cm thick bed that is denser than the overlying sediments at the base of the mud unit. Assemblages in the grey mud overlying the peat unit dominantly consist of *M. fusca* (44-75%) and *J. macrescens* (13-30%), which is consistent with sediments accumulating close to MTL

(Kemp et al., 2018). For the subsidence estimate, we use the reconstructed RSL elevations that are 1 cm apart, which are the first full centimeter intervals above and below the contact that avoid the relief of the *mud-over-peat* contact. The fossil foraminifera BTF reconstruction shows 0.59±0.36 m of subsidence.

At *MR.02*, the upper contact of the third earthquake-induced buried organic-rich unit is at 246 cm core depth (Fig. 9b). The picture and CT imagery display a sharp, 3- 4 mm, undulating contact with 8 mm of relief. The organic rich unit is 19 cm thick and grades from a 12 cm thick dark brown peat to a 7 cm dark grey brown muddy peat from top to base. Foraminifera in the light brown peat unit consist of *Haplophragmoides spp.* (17-45), *J. macrescens* (10-44%), *B. pseudomacrescens* (7-41%), and *T. inflata* (9-29%), which is consistent with a high salt marsh peat. Foraminifera in the grey mud unit dominantly consist of *T. inflata* (27-88%) and *M. fusca* (4-53%), which is consistent with sediment accumulating in between MTL and MHW (Kemp et al., 2018). For the subsidence estimate, we use the reconstructed RSL elevations that are 1 cm apart, which are the first full centimeter intervals above and below the contact that avoid the relief of the *mud-over-peat* contact. The fossil foraminifera BTF reconstruction shows 0.59±0.32 m of subsidence.

5. DISCUSSION

We compiled a dataset that tests the range of stratigraphic and biostratigraphic variability across three marshes over ~6 km using fossil foraminiferal assemblages and sediment core density imagery in an attempt to identify and assess any second order processes within wetland stratigraphy that could affect past coseismic deformation

estimates. Our results suggest that for the same earthquake stratigraphic sequence there is variability in foraminiferal assemblages both within a single marsh and across marshes in an estuary. Second order processes can influence such variability and identifying stratigraphic and biostratigraphic irregularities is integral to deriving a representative subsidence estimate for a marsh and/or across an estuary. While our data does highlight instances of mixing (i.e., earthquake 1 at Mad River Slough) that produce inter-site variability within coseismic subsidence estimates, our major result is to expand upon Milker et al., (2016). We find that coseismic subsidence estimates derived from foraminiferal transfer functions are reproduceable from closely-spaced cores (< 45m) but that estimates can also be reproduced 100's - 1000's m apart and across multiple marshes within an estuary. Our findings are consistent with coastal paleoseismic fossil-diatom transfer function investigations (Shennan and Hamilton, 2006; Shennan et al., 2014). Therefore, as discussed in detail below, we conclude that as for diatoms, multiple spread-out replications of foraminiferal-based coseismic subsidence estimates should be used to provide increased confidence in the results.

Intra-site variability of coseismic subsidence estimates (midpoint to midpoint) ranges from a maximum of 0.59 m for the 1700 CE earthquake at McDaniel Creek to a minimum of 0.0 m for the 1125 cal yrs BP earthquake at Mad River Slough (Table 1; Figs 11, 12, and 13). The maximum intra-site variability of 0.59 m is derived from the same location (McDaniel Creek) and stratigraphic sequence (1700 CE) as the largest subsidence estimate reported across the estuary over three earthquake cycles, 1.04 ±0.42 m (Table 1; Fig. 11). Moreover, the maximum intra-site variability is more than half of the maximum subsidence estimate, which suggests that if the RSL

reconstructions were not repeated and averaged, across the same stratigraphic sequence, then a single reconstruction could potentially be either an over or under representation of coseismic subsidence. However, because the intra-site coseismic subsidence estimate ranges overlap with the intra-site average estimate range we conclude that the estimates are reproducible (Figs 11, 12, and 13). Our intra-site variability data are similar to Shennan and Hamilton, (2006) results at Girdwood (Alaska), which ranged from a minimum of 0.09 m to a maximum of 0.51 m using a diatom transfer function. Our data suggests that intra-site variability is driven by foraminiferal assemblages within the mud units overlying the earthquake contact.

For individual core reconstructions, inter-site variability ranges from a maximum of 0.76 m between *MD.13* (1.04 ±0.42 m) and *MR.02* (0.28 ±0.26 m) for the 1700 CE earthquake, to a minimum of 0.00 m between *MD.12* (0.59 ±0.38 m) to either *MR. 02* (0.59 ±0.32 m) or *MR.05* (0.59 ±0.36 m) for the 1125 cal yrs BP earthquake (Table 1). For site average reconstructions, inter-site variability ranged from a maximum of 0.47 m between McDaniel Creek (0.80 m) and Mad River Slough (0.33 m) for the 1700 CE contact, to a minimum of 0.06 m between McDaniel Creek (0.43 ± 0.34 m) and Mad River Slough (0.37 ± 0.36 m) for the 870 cal yrs BP earthquake. The major variability for both within and across sites was observed in the stratigraphy of the 1700 CE earthquake and, therefore, we focus on our 1700 CE earthquake results in this discussion.

5.1 Foraminiferal assemblages that may impact coseismic subsidence estimate variability

Several Cascadia fossil foraminifera-based paleogeodetic investigations have observed evidence of overlying mud infiltration into the pore space of underlying organic-rich units (e.g., Nelson et al., 1996b; Engelhart et al., 2013a; Milker et al., 2016), which results in a minimum estimate of coseismic subsidence. For example, at Osprey Marsh (Coquille River) Engelhart et al., (2013a) inferred infiltration of foraminiferal assemblages across CSZ 1700 CE subsidence contact from the presence of *M. fusca* at high percentages within the organic-rich unit ≥ 3 cm below the subsidence contact, which violates Walther's law, i.e., *M. fusca* is an intertidal foraminifera species that does not have an optimal level of occurrence at a high-marsh peat forming intertidal elevation within the modern west coast (US) dataset (Kemp et al., 2018). Similarly, Milker et al, (2016) attribute mud infiltration 2 cm below two subsidence contacts at Talbot Creek based on the high percentages of *M. fusca* within the buried peat units in core 1. Kemp et al., (2018) show that such mixed foraminiferal assemblages can be accounted for by using informative priors with the BTF using the foraminiferal assemblage data from the marsh transplant experiment of Engelhart et al., (2013a). However, an informative prior assignment cannot fully account for the variability observed at northern Humboldt Bay. This is because our biostratigraphic results indicate that the organic-rich units for all of our reconstructions contain foraminiferal assemblages consistent with a high-marsh peat that forms at elevations near MHHW (Figs 2-9). Our BTF results show less than 25 cm of variation between these elevation estimates of the organic rich units prior to coseismic subsidence across all sites and variation within ~5 cm on average elevation estimates per stratigraphic section. In contrast, our biostratigraphic results indicate that overlying mud units for

all of our reconstructions contain foraminiferal assemblages inform RSL reconstructions that lie in-a much larger range between MHW and MTL, respectively, 1.77 m and 1.03 m (NAVD88).

Foraminiferal assemblages within the overlying mud units are the primary driver of the magnitude of subsidence estimates. Percentages of *M. fusca*, *Reophax spp.* and *Ammobaculites spp.* are common in mud units because these species' optima are below MHW, where minerogenic sediments dominate the depositional environment (Guilbault et al., 1995; 1996; Nelson et al., 1996b; Shennan et al., 1996; Hawkes et al., 2010; 2011; Engelhart et al., 2013a, 2013b; Wang et al., 2013; Milker et al ., 2015; 2016; Kemp et al., 2018). At Jacoby Creek core *JC.06*, the mud unit overlying the 1700 CE contact contains a relatively-high percentage of *M. fusca* (53%) and low percentage of *T. inflata* (15%), which contribute towards a large subsidence estimate of 1.00 ±0.40 m. In contrast in core *JC.10* the mud unit overlying the 1700 CE contact contains a lower percentage of *M. fusca* (8%) and higher percentage of *T. inflata* (38%), which produces a lower subsidence of 0.49±0.40 m. The different percentages of *M. fusca* at two locations within ~125 m apart from each other suggests that at least one site could have been influenced by second order processes.

Species that only occur in low abundances may also influence RSL reconstructions and, therefore, coseismic subsidence estimates. For example, *Reophax spp.* and *Ammobaculites spp.* are especially informative to RSL reconstructions because they are typically found at elevations closer to MTL within the modern west coast dataset (Hawkes et al., 2011; Milker et al., 2016; Kemp et al., 2018). The biostratigraphy of the 1125 yrs BP contact at Jacoby Creek is an example of a

relatively high intra-site variability (0.46 m), which may be explained by differences in small fauna percentages of key species within mud units (Fig. 7). At *JC.02* and *JC.10* both organic-rich units contain similar foraminiferal assemblages which are consistent with a high-marsh peat. The foraminiferal assemblages in the overlying mud units also contain similar assemblages which are dominated by J. macrescens (22-60%), T. inflata (17-29%) and M. fusca (3-25%), except that *JC.10* contains both *Reophax spp.* (≤9%) and *Ammobaculites spp.* (≤5%), where at *JC.02* neither species are present, and as a result the *JC.10* RSL reconstruction suggests almost twice as much subsidence, 0.94±0.44 m compared to 0.48±0.41 m at *JC.02*.

Relatively low intra-site variability, 0.08 m, for the 1700 CE contact at Mad River Slough, may also be explained by foraminiferal assemblages within the mud units. For the 1700 CE earthquake, Mad River Slough has smaller subsidence estimates (0.33 ±0.25 m) than those from both Jacoby Creek (0.62 ±0.44) and McDaniel Creek (0.80 ±0.44 m; Table 1; Fig 10). Additionally, the foraminiferal assemblages of the overlying mud units at Mad River Slough are consistent within site but they are different from the foraminiferal assemblages found within the overlying mud units at Jacoby Creek and McDaniel Creek. At Mad River Slough, the foraminiferal assemblage within the overlying mud contains both high-marsh and low-marsh species at *MR.05*, which are dominated by *M. fusca* but also with *M. petilla*; two species that have optima that do not overlap (Kemp et al., 2018). The occurrence of a relatively high percentage of *M. fusca* and presence of M. *petilla* is unlikely (Kemp et al., 2018) and suggests a strong possibility of a mixed assemblage. The mixture of low-marsh species and high-marsh species within the overlying mud units

drive the RSL reconstructions and drive the very consistent but relatively-low subsidence estimates at Mad River Slough for the 1700 CE contact.

Milker et al., (2016) also found high marsh species in higher than expected proportions within mud units that overly the 1700 CE contact at Talbot Creek, Oregon. Milker et al., (2016) attributed the presence of the higher marsh species, *B. pseudomacrescens*, in the mud unit to the brackish conditions of Talbot Creek locality and inferred that the derived estimate of coseismic subsidence is likely a minimum estimate. However, Talbot Creek coring site is >6 km upstream from Coos Bay estuary and Mad Rive Slough core locations are <1 km upstream from northern Humboldt Bay. Moreover, there is a low range of variability in the organic-rich units across the estuary. i.e., reconstructed RSL elevations are consistently around MHHW over three earthquake cycles, it is unlikely that Mad River Slough experienced more brackish conditions in 1700 CE than other investigated marshes (Jacoby Creek and McDaniel Slough) in northern Humboldt Bay.

Further evidence that mixing may be responsible for these low but consistent estimates may be found in CT imagery (e.g., Milker et al., 2016). The CT imagery of the mud units overlying the 1700 CE contacts at Mad River Slough (Figs. 4, and 10) show relatively dense minerogenic units with less-dense sporadic organics and irregular bedding planes, which are quite different than the massive and finely-laminated mud units at Jacoby Creek and McDaniel Creek (Figs. 2, 3, 11, and 12). This suggests contrasting depositional processes and/or environmental settings. Jacoby Creek and McDaniel Creek marshes are at the mouths of small mountainous creeks with year-round continuous discharge that empty into open-bay environments along

the northeast fringes of northern Humboldt Bay. In contrast, the Mad River Slough watershed is much smaller, less steep, and has less discharge than McDaniel Creek and Jacoby Creek watersheds. Moreover, the Mad River Slough is a topographic low that became inundated ~≤1600 cal yr BP (Padgett et al., in-prep) and forms dissected marsh environment that is pinned to the north by the Mad River (perpendicular orientation), to the west by the Lanphere-Dune sequence, and to the east it drains a portion of a Holocene alluvial platform (the Arcata Bottoms). Earthquake induced landslide can cause rapid erosion in mountain forests which results in high rates of particulate carbon (POC) in the downstream reaches (Wang et al., 2016; Turowski et al., 2016). Discharge from small mountainous streams will likely transport the turbid and POC laden water away from the fluvial system and eventually offshore. Therefore, it is likely that marsh environments exposed to a consistent discharge from small mountainous creeks and open-bay tidal conditions would experience flushing of water more often than an environment with low discharge and a more restricted access to the open bay source.

Therefore, based on density imagery, mixed fauna compositions, and differing environmental setting we infer that the lower section of the mud units overlying the 1700 CE contact at Mad River Slough are not representative of processes that occurred throughout northern Humboldt Bay estuary. Subsequent removal of the Mad River Slough estimates from the 1700 CE estuary-wide the average calculation would change the average subsidence estimate from 0.63 ±0.36 m to 0.77 ±0.36. However, because the site highlights potential variability within stratigraphic records of coseismic deformation we conservatively do not eliminate the values from the average

calculation. This result highlights the possibility of stratigraphic variability across an estuary and emphasizes the necessity of spread-out replicated reconstructions across the same stratigraphic sequence in order to avoid a misrepresentation of coseismic deformation.

5.2 Sedimentary processes that may impact coseismic subsidence estimate variability

There are several second order sedimentary processes that could potentially effect coseismic deformation estimates derived microfossil-based quantitative RSL reconstructions from wetland stratigraphy, e.g., liquefaction, compaction, erosion, and post-earthquake sedimentation.

Post-seismic liquefaction in a salt marsh could affect the elevation of the salt marsh platform in two ways; 1) a surface elevation decrease due to the removal of the liquefied material underneath 2) a surface elevation increase due to the subaerial deposition of ejected liquefied material, i.e., sand boils or blow (Clague et al., 1992; Quigley et al., 2013). Cascadia earthquake induced liquefaction features have been documented along the Cascadia coastal margin at the Copalis River, lower Columbia River (Atwater, 1992; Atwater, 1994; Obermeier and Dickenson, 2000), and possibly also at the Fraser River Delta in southwest Canada (Clague et al., 1992), where sedimentary evidence of dykes and sills that have age relationships that were likely earthquake induced. The coastal localities with sedimentary liquefaction features have accumulated late Holocene sediments and organics that overlie loose, moderately dense and thick (10's – 100's) sand deposits (Clague et al., 1992). Such a geologic relationship is uncommon along the Cascadia margin and so many locations do not host stratigraphic evidence for CSZ late Holocene earthquake induced liquefaction

features. Within the stratigraphy described in northern Humboldt Bay, we did not observe any liquefaction features (Padgett et al., *in-prep*). Therefore, we suggest that liquefaction is an unlikely second order taphonomic process that may have affected our coseismic subsidence estimates.

Compaction of a wetland stratigraphic sequences may cause a lowering of a salt marsh surface environment (Kemp et al., 2009; Kemp et al., 2015; Brain, 2015; 2017). Although compaction of stratigraphy on the east coast of the United States (US) has been documented at several wetland sites (Brain, 2015; Kemp et al., 2015; Brain et al., 2017), it has not been studied along the active Cascadia Margin. Along the east coast of the US, Holocene wetland environments accumulate continuous peat sections, which are prone to compaction (Bloom, 1964; Allen, 2000; Brian et al., 2017). For a high-resolution sea-level reconstruction of a continuous peat record stratigraphic compaction would result in an increase in the rate of sea-level rise on a sea-level curve through time. Along the Cascadia Margin, many wetland locations host a record of past relative sea-level changes over the late Holocene that is dominantly composed of minerogenic sediments that have potential to compact (Brain et al., 2011). Compaction of the material underlying Holocene coastal wetland stratigraphy is also possible. However, in much of Cascadia, the material underlying late Holocene coastal wetland stratigraphy is much older and should have already compacted because it has likely experienced 10+ earthquake cycles (e.g., Goldfinger et al., 2012). Therefore, compaction could potentially influence a coseismic subsidence estimate along the Cascadia margin and susceptibility increases if the salt marsh overlays an unconsolidated beach or dune sequence. However, such a site

environment setting would be fairly unique and is not the setting at most Cascadia coastal paleoseismic sites.

Erosion is a second order sedimentary process that could distort microfossil RSL reconstruction. Erosive processes could either remove organic material from the salt marsh surface, which would result in a RSL reconstruction that may not be the actual elevation of the organic-rich unit prior to earthquake deformation (Nelson et a., 1996). During tsunami inundation, some erosion may be expected (Srinvasalu et al., 2007; Switzer et al., 2008). However, at northern Humboldt Bay we did not observe tsunami deposits (Vick, 1988; Clarke and Carver, 1992). Therefore, it is unlikely that northern Humboldt Bay salt marshes experienced inundation velocities that would be necessary to significantly erode a salt-marsh peat soil. While stratigraphic mapping and radiocarbon age dating correlation results suggest that erosion may be responsible for an organic-rich unit missing at Jacoby Creek (Padgett et al., *in-prep*), this erosion is likely the result of a migrating stream channel and not coseismic inundation. Because erosion is the removal of material from a depositional setting, it is difficult to assess the amount of erosion that has taken place by investigating archived stratigraphy.

Wetland paleogeodetic investigations cannot resolve the time duration of "suddenness' of the resumption of sedimentation and so, coseismic subsidence estimates may inherently contain post seismic deformation (e.g., Nelson et al., 1996; Atwater et al., 2001; Witter et al., 2003; Wang et al., 2013).Spatial gaps in sedimentation across a marsh can occur during channel levee over topping related to the extent of a deposit, which can explain differences in foraminiferal assemblages

found in cores closely spaced, <10's m. Both local (1-2 km^2) and estuary-wide (~5-6 km) rapid sedimentation can impact post seismic stratigraphy, biostratigraphy, and subsequent interpretations of such (Atwater et al., 2001; Wang et al., 2013; Horton et al., 2017). Therefore, in order to avoid local sedimentation differences, spread-out and multiple microfossil group RSL reconstructions across the same stratigraphic sequence will likely improve confidence in a coseismic subsidence estimates. Even if post seismic sedimentation resumed immediately after an earthquake, further complications can arise due to the microfossil response time for re-habitation. For example, foraminiferal response time to re-habitation at a reclaimed marsh was observed to be 11 months at Ni-les'tun marsh, Oregon (Horton et al., 2017), which was coincident with the deposition of ~1cm of clastic material. In contrast, diatom re-habitation response time was observed to be 2 weeks (Horton et al., 2017). Therefore, different microfossils could under- or over-estimate coseismic deformation (Horton et al., 2017) depending on the post-seismic land motion. Although the timing of the year of an earthquake could influence microfossil assemblages above subsidence contacts, fauna response times are likely consistent across an marsh and estuary and are, therefore, unlikely to explain either intra- or intra-site coseismic subsidence variability here..

5.3 Identifying a sufficient number of reconstructions

To test the reproducibility of our coseismic subsidence estimates, we analyzed 5-9 different core sections across three subsidence contacts at northern Humboldt Bay (Table 1). A challenge for assessing the reliability of the estimates is that unlike the transplant experiment (e.g., Hamilton and Shennan, 2005; Engelhart et al. 2013) we do not the know the "correct" answer. To address this we average all inter-site coseismic

subsidence estimates and errors across the estuary for each earthquake stratigraphic sequence and assign that earthquake-averaged subsidence estimate error as the representative subsidence value. By taking the mean based on all possible combinations of subsidence estimates, we can identify how many RSL reconstruction samples are necessary to likely account for the stratigraphic variability and produce a result consistent with the averaged coseismic subsidence estimate across an estuarine system (Fig. 13).

Per earthquake sequence, all individual subsidence estimate error ranges overlap with the earthquake-averaged subsidence estimate error ranges (Figure 10). However, for the 1700 CE earthquake, the two largest estimate midpoints are outside of the averaged subsidence estimate error (Figure 13a). The 1700 CE earthquake subsidence estimates have a wider range of subsidence estimates than the 870 yrs BP and 1152 yrs BP subsidence estimates. For individual core subsidence estimate results, the CE 1700 CE earthquake show the maximum inter-site variability range of 0.76 m (between *MD.13*, 1.04 ±0.42 m, and *MR.02*, 0.28 ±0.26 m), while the 870 cal yrs BP and 1125 cal yrs BP earthquakes, show much lower variability ranges of 0.25 m and 0.40 m. For the most recent 1700 CE earthquake, nine RSL reconstructions average to a subsidence estimate of 0.63 ±0.36 m (Table 1, Figs. 2-4 and 13a) or 0.77 ± 0.43 m if the Mad River Slough samples are considered anomalous due to mixing. For the 870 cal yrs BP and 1125 cal yrs BP earthquake stratigraphic sequences, five and six RSL reconstructions average to 0.39 ±0.35 m and 0.7 ±0.39 m, respectively (Table 1, Figs. 5-9 and 13b,c). Within error ranges, the 870 yrs BP and 1125 yrs BP earthquake (five and six subsidence estimate midpoints, respectively) all fall within the earthquake-

averaged subsidence estimate errors. Similarly, Shennan et al., (2014) provide six subsidence estimates, derived from diatom transfer function analysis across the 1788 earthquake stratigraphy in Alaska, that also overlap with their earthquake average estimate.

Our data show that for 1700 CE earthquake all combinations of two subsidence estimates, one estimate midpoint is outside the earthquake averaged subsidence estimate error, which contrasts with all combinations of 2 subsidence estimates for the previous earthquakes, e.g., ~870 cal yrs BP (Fig 13b) and ~1125 cal yrs BP (Fig 10c). For each earthquake stratigraphic sequence, all combinations of three or more subsidence estimates give averages that lie within the averaged subsidence estimate produced from all reconstructions for that earthquake. The subsidence estimate variability for earthquakes 2 and 3 at northern Humboldt Bay and for the 1788 earthquake in Kalsin Bay, Kodiak Island, Alaska (Shennan et al., 2014), suggest that the variability found for the CSZ 1700 CE earthquake in northern Humboldt Bay is an outlier among wetland seismic deformation stratigraphy. Although, all combinations of four or RSL reconstructions will provide a more robust analysis, i.e., the inter-quartile range deceases with each additional reconstruction, it will not significantly decrease the averaged range of all subsidence estimate possible combinations. Therefore, producing a minimum of two, to ideally three, RSL reconstruction across the same stratigraphic sequence provides increased confidence in the estimate.

5.4 Implications for along strike

Due to a number of recent megathrust ruptures that have non uniform rupture distributions (e.g., 2004 M_w 9.2 Sumatra-Andaman, 2010 M_w 8.8 Maule, Chile, 2011

M_w 9.0 Tohoku-Oki, Japan) it is likely that past megathrust earthquakes also produced heterogeneous rupture scenarios (e.g., Shennan et al., 2016; Wang et al., 2013). Most of our knowledge of past megathrust rupture are derived from coastal stratigraphic evidence, therefore, it is critical to avoid mis-interpreting stratigraphic and biostratigraphic data. For example, within the CSZ paleogeodetic database there are low subsidence estimates adjacent to high subsidence estimates., e.g.., Netarts and Nehalem, as well as locations with very little subsidence (Alsea Bay; Hawkes et al., 2011; Wang et al., 2013; Kempt et al., 2018). A potential issue is that the range of estimates for a single earthquake at northern Humboldt Bay is similar to the range of estimates within the paleogeodetic database of the CSZ 1700 CE earthquake (Wang et al., 2013; Kempt et al., 2018).

Given the variability of transfer function subsidence estimates, does this suggest that low estimates at Netarts and Nehalem, for the 1700CE earthquake, could be anomalous coseismic subsidence estimates? This is highly unlikely because at each site there are two microfossil estimates with errors with overlap, even though one is non-transfer function estimate. At Netarts, a quantitative pollen and diatom RSL reconstructions suggest 0.4 ±0.3 m of subsidence (Shennan et al., 1998) is substantiated by a foraminifera reconstruction suggests 0.39 ±0.2 m subsidence (Kemp et al., 2018). At Alsea Bay, two fossil foraminiferal BTF estimates 0.13 ±0.21 and 0.16 ±0.21 m, which are based on separate foraminiferal analyses of Nelson et al., (2008) and Wang et al., (2013), respectively. Therefore, multiple microfossil reconstructions and subsidence estimates substantiates an assigned coseismic deformation estimate. However, prior to this investigation, Alsea and Netarts are

outliers within the paleogeodetic database because they were the only locations with more than one microfossil-based RSL reconstruction. Considering complicated features of heterogenous slip distributions, confidence would be gained if each of the constraints had at least two replicate RSL reconstructions.

6. CONCLUSION

Reconstructed RSL elevations and coseismic subsidence estimates were derived through applying a foraminiferal-based BTF to fossil data from stratigraphic sequences of the past three CSZ earthquakes across three marshes in northern Humboldt Bay, California. Second order process may have influenced the variability of the stratigraphic and biostratigraphic record of past great earthquakes at northern Humboldt Bay. Therefore, we compiled a large stratigraphic and biostratigraphic dataset that allowed for inter- and intra-site variability and replicability assessments of foraminiferal BTF coseismic subsidence estimates. We analyzed 20 sediment cores containing the three mud-over-peat contacts; nine for the 1700 CE contact (average of 0.63 ±0.36 m subsidence), five for the ~870 cal yrs BP contact (average of 0.39 ± 0.35 m), and six for the ~1125 cal yrs BP contact (average of 0.7 ± 0.39 m), which suggests that coseismic subsidence has varied over the three most recent earthquake cycles. Our new subsidence estimates generally agree with the relative magnitudes of coseismic subsidence provided from single estimates by Padgett et al. (*in-prep)*.

Our results suggest that there is stratigraphic and foraminiferal assemblage variability across marshes and across estuary for the same earthquake stratigraphic sequence. For example, intra-site variability of coseismic subsidence estimates reached a maximum of 0.59 m for the 1700 CE earthquake at McDaniel Creek.

Moreover, inter-site averaged coseismic subsidence variability reached a maximum of 0.47 m (midpoint to midpoint) between McDaniel Creek (0.80 ± 0.41 m) and Mad River Slough (0.33 ± 0.25 m) for the 1700 CE contact. Of the three earthquakes, the 1700 CE earthquake had the highest variability of coseismic subsidence estimates. At Mad River Slough, marsh-wide mixed foraminiferal assemblages above the 1700 CE subsidence contact suggest the influence of a second order sedimentation process such as the erosion and redeposition of high-marsh material in the days to weeks after the earthquake. However, aside from the 1700 CE earthquake at Mad River Slough, our findings suggest that large variability in BTF foraminifera subsidence estimates is uncommon within wetland stratigraphy in northern Humboldt Bay. Within error, all individual subsidence estimates overlap with the stratigraphic equivalent averaged subsidence estimate, both across a marsh and across an estuary.

Because we demonstrate that second order processes can influence the stratigraphic record, foraminiferal assemblages, and, therefore, subsidence estimates, identifying irregularities is integral to deriving and assigning a subsidence estimate for an estuary. Although second order processes influencing coseismic subsidence estimates are rare, highly variable, and difficult to assess within wetland stratigraphy, researchers can minimize the influence by reconstructing RSL changes over a minimum of two, to ideally three, spread-out stratigraphic sections of the same contact within the same marsh, and if possible across multiple marshes within an estuary.

7. REFERENCES

Atwater, B.F., 1987. Evidence for great Holocene earthquakes along the outer coast of Washington State. *Science*, *236*(4804), pp.942-944.

Atwater, B.F., 1992. Geologic evidence for earthquakes during the past 2000 years along the Copalis River, southern coastal Washington. *Journal of Geophysical Research: Solid Earth*, *97*(B2), pp.1901-1919.

Atwater, B.F., 1994. *Geology of Holocene liquefaction features along the lower Columbia River at Marsh, Brush, Price, Hunting, and Wallace Islands, Oregon and Washington* (No. 94-209). US Geological Survey.

Atwater, B.F. and Hemphill-Haley, E., 1997. *Recurrence intervals for great earthquakes of the past 3,500 years at northeastern Willapa Bay, Washington* (No. 1576). USGPO; Information Services [distributor].

Barnhart, R.A., Boyd, M.J. and Pequegnat, J.E., 1992. *The ecology of Humboldt Bay, California: an estuarine profile* (No. FWS-1). CALIFORNIA COOPERATIVE FISHERY RESEARCH UNIT ARCATA CA.

Borgeld, J. C., and A. W. Stevens (2004), Humboldt Bay, California: Surface Sediments 2000–2001, *Current Perspectives on the Physical and Biological Processes of Humboldt Bay*, 51.

Brain, M.J., 2015. Compaction. *Handbook of Sea-Level Research*, pp.452-469.

Brain, M.J., Long, A.J., Petley, D.N., Horton, B.P. and Allison, R.J., 2011. Compression behaviour of minerogenic low energy intertidal sediments. *Sedimentary Geology*, *233*(1-4), pp.28-41.

Brain, M.J., Kemp, A.C., Hawkes, A.D., Engelhart, S.E., Vane, C.H., Cahill, N., Hill, T.D., Donnelly, J.P. and Horton, B.P., 2017. Exploring mechanisms of compaction in salt-marsh sediments using Common Era relative sea-level reconstructions. *Quaternary Science Reviews*, *167*, pp.96-111.

Briggs, R.W., Engelhart, S.E., Nelson, A.R., Dura, T., Kemp, A.C., Haeussler, P.J., et al., 2014, Uplift and subsidence reveal a nonpersistent megathrust rupture boundary (Sitkinak Island, Alaska): Geophysical Research Letters, doi:10.1002/(ISSN)1944-8007.

Cahill, N., Kemp, A.C., Horton, B.P. and Parnell, A.C., 2016. A Bayesian hierarchical model for reconstructing relative sea level: from raw data to rates of change. *Climate of the Past*, *12*(2), pp.525-542.

Cisternas, M., Atwater, B.F., Torrejón, F., Sawai, Y., Machuca, G., Lagos, M., Eipert, A., Youlton, C., Salgado, I., Kamataki, T. and Shishikura, M., 2005. Predecessors of the giant 1960 Chile earthquake. *Nature*, *437*(7057), p.404.

Clarke, S.H. and Carver, G.A., 1992. Late Holocene tectonics and paleoseismicity, southern Cascadia subduction zone. *Science*, *255*(5041), pp.188-192.

Clague, J.J., Naesgaard, E. and Sy, A., 1992. Liquefaction features on the Fraser delta: evidence for prehistoric earthquakes?. *Canadian Journal of Earth Sciences*, *29*(8), pp.1734-1745.

Combellick, R.A., 1991. *Paleoseismicity of the Cook Inlet region, Alaska: Evidence from peat stratigraphy in Turnagain and Knik Arms* (No. 112). State of Alaska, Department of Natural Resources, Division of Geological & Geophysical Surveys.

Darienzo, M.E., Peterson, C.D. and Clough, C., 1994. Stratigraphic evidence for great subduction-zone earthquakes at four estuaries in northern Oregon, USA. *Journal of Coastal Research*, pp.850-876.

Davies, M.H., Mix, A.C., Stoner, J.S., Addison, J.A., Jaeger, J., Finney, B. and Wiest, J., 2011. The deglacial transition on the southeastern Alaska Margin: Meltwater input, sea level rise, marine productivity, and sedimentary anoxia. *Paleoceanography and Paleoclimatology*, *26*(2).

de Rijk, S., 1995. Salinity control on the distribution of salt marsh foraminifera (Great Marshes, Massachusetts). *The Journal of Foraminiferal Research*, *25*(2), pp.156-166.

Dura, T., Horton, B.P., Cisternas, M., Ely, L.L., Hong, I., Nelson, A.R., Wesson, R.L., Pilarczyk, J.E., Parnell, A.C. and Nikitina, D., 2017. Subduction zone slip variability during the last millennium, south-central Chile. *Quaternary Science Reviews*, *175*, pp.112-137.

Engelhart, S.E., Horton, B.P., Nelson, A.R., Hawkes, A.D., Witter, R.C., Wang, K., Wang, P.L. and Vane, C.H., 2013a. Testing the use of microfossils to reconstruct great earthquakes at Cascadia. *Geology*, *41*(10), pp.1067-1070.

Engelhart, S.E., Horton, B.P., Vane, C.H., Nelson, A.R., Witter, R.C., Brody, S.R. and Hawkes, A.D., 2013b. Modern foraminifera, δ 13 C, and bulk geochemistry of central Oregon tidal marshes and their application in paleoseismology. *Palaeogeography, Palaeoclimatology, Palaeoecology*, *377*, pp.13-27.

Engelhart, S.E., Hemphill-Haley, E., Kelsey, H.M., and Padgett, J.S., 2015. *Refined Estimates of Coseismic Subsidence along the Southern Cascadia Subduction Zone in Northern Humboldt Bay (Arcata Bay): Collaborative Research with*

University of Rhode Island and Humboldt State University. No. G14AP00128 and G14AP00129. U.S. Geological Survey

Eicher, A.L., 1987. *Salt marsh vascular plant distribution in relation to tidal elevation, Humboldt Bay, California*. M.S. thesis, Humboldt State University).

Fatela, F. and Taborda, R., 2002. Confidence limits of species proportions in microfossil assemblages. *Marine Micropaleontology*, *45*(2), pp.169-174.

Garrett, E., Shennan, I., Woodroffe, S.A., Cisternas, M., Hocking, E.P. and Gulliver, P., 2015. Reconstructing paleoseismic deformation, 2: 1000 years of great earthquakes at Chucalén, south central Chile. *Quaternary Science Reviews*, *113*, pp.112-122.

Goldfinger, C., Nelson, C.H., Morey, A., Johnson, J.E., Gutierrez-Pastor, J., Eriksson, A.T., Karabanov, E., Patton, J., Gracia, E., Enkin, R., Dallimore, A., Dunhill, G., Vallier, T., 2012, Turbidite event history: Methods and implications for Holocene paleoseismicity of the Cascadia subduction zone: USGS Professional Paper 1661-F, 184 pp.

Guilbault, J.P., Clague, J.J. and Lapointe, M., 1995. Amount of subsidence during a late Holocene earthquake—evidence from fossil tidal marsh foraminifera at Vancouver Island, west coast of Canada. *Palaeogeography, Palaeoclimatology, Palaeoecology*, *118*(1), pp.49-71.

Guilbault, J.P., Clague, J.J. and Lapointe, M., 1996. Foraminiferal evidence for the amount of coseismic subsidence during a late Holocene earthquake on Vancouver Island, west coast of Canada. *Quaternary Science Reviews*, *15*(8), pp.913-937.

Hamilton, S. and Shennan, I., 2005. Late Holocene relative sea-level changes and the earthquake deformation cycle around upper Cook Inlet, Alaska. *Quaternary Science Reviews*, *24*(12-13), pp.1479-1498.

Hawkes, A.D., Horton, B.P., Nelson, A.R. and Hill, D.F., 2010. The application of intertidal foraminifera to reconstruct coastal subsidence during the giant Cascadia earthquake of AD 1700 in Oregon, USA. *Quaternary International*, *221*(1), pp.116-140.

Hawkes, A.D., Horton, B.P., Nelson, A.R., Vane, C.H. and Sawai, Y., 2011. Coastal subsidence in Oregon, USA, during the giant Cascadia earthquake of AD 1700. *Quaternary Science Reviews*, *30*(3), pp.364-376.

Hemphill-Haley, E., 1995. Diatom evidence for earthquake-induced subsidence and tsunami 300 yr ago in southern coastal Washington. *Geological Society of America Bulletin*, *107*(3), pp.367-378.

Holden, P.B., Birks, H.J.B., Brooks, S.J., Bush, M.B., Hwang, G.M., Matthews-Bird, F., Valencia, B.G. and Van Woesik, R., 2017. BUMPER v1. 0: a Bayesian user-friendly model for palaeo-environmental reconstruction.

Horton, B.P., Milker, Y., Dura, T., Wang, K., Bridgeland, W.T., Brophy, L., Ewald, M., Khan, N.S., Engelhart, S.E., Nelson, A.R. and Witter, R.C., 2017. Microfossil measures of rapid sea-level rise: Timing of response of two microfossil groups to a sudden tidal-flooding experiment in Cascadia. *Geology*, *45*(6), pp.535-538.

Kemp, A.C., Horton, B.P., Culver, S.J., Corbett, D.R., van de Plassche, O., Gehrels, W.R., Douglas, B.C. and Parnell, A.C., 2009. Timing and magnitude of recent accelerated sea-level rise (North Carolina, United States). *Geology*, *37*(11), pp.1035-1038.

Kemp, A.C., Hawkes, A.D., Donnelly, J.P., Vane, C.H., Horton, B.P., Hill, T.D., Anisfeld, S.C., Parnell, A.C. and Cahill, N., 2015. Relative sea-level change in Connecticut (USA) during the last 2200 yrs. *Earth and Planetary Science Letters*, *428*, pp.217-229.

Kemp, A.C., and Telford, R.J. 2015. Transfer functions. *Handbook of Sea-Level Research.* I Shennan, A.J. Long and B.P. Horton (Editors), John Wiley and Sons, Chichester, United Kingdom, pp.470-99.

Kemp, A.C., Cahill, N., Engelhart, S.E., Hawkes, A.D. and Wang, K., 2018. Revising Estimates of Spatially Variable Subsidence during the AD 1700 Cascadia Earthquake Using a Bayesian Foraminiferal Transfer Function. *Bulletin of the Seismological Society of America*, *108*(2), pp.654-673.

Milker, Y., Horton, B.P., Vane, C.H., Engelhart, S.E., Nelson, A.R., Witter, R.C., Khan, N.S. and Bridgeland, W.T., 2015. Annual and seasonal distribution of intertidal foraminifera and stable carbon isotope geochemistry, Bandon Marsh, Oregon, USA. *The Journal of Foraminiferal Research*, *45*(2), pp.146-155.

Milker, Y., Nelson, A.R., Horton, B.P., Engelhart, S.E., Bradley, L-A., and Witter, R.C., 2016. Differences in coastal subsidence in southern Oregon (USA) during at least six prehistoric megathrust earthquakes. *Quaternary Science Reviews*.

Nelson, A.R., 1992. Discordant 14C ages from buried tidal-marsh soils in the Cascadia subduction zone, southern Oregon coast. *Quaternary Research*, *38*(1), pp.74-90.

Nelson, A.R., Shennan, I. and Long, A.J., 1996a. Identifying coseismic subsidence in tidal-wetland stratigraphic sequences at the Cascadia subduction zone of

western North America. *Journal of Geophysical Research: Solid Earth*, *101*(B3), pp.6115-6135.

Nelson, A.R., Jennings, A.E. and Kashima, K., 1996b. An earthquake history derived from stratigraphic and microfossil evidence of relative sea-level change at Coos Bay, southern coastal Oregon. *Geological Society of America Bulletin*, *108*(2), pp.141-154.

Nelson, A.R., Sawai, Y., Jennings, A.E., Bradley, L.A., Gerson, L., Sherrod, B.L., Sabean, J. and Horton, B.P., 2008. Great-earthquake paleogeodesy and tsunamis of the past 2000 years at Alsea Bay, central Oregon coast, USA. *Quaternary Science Reviews*, *27*(7), pp.747-768.

Obermeier, S.F. and Dickenson, S.E., 2000. Liquefaction evidence for the strength of ground motions resulting from late Holocene Cascadia subduction earthquakes, with emphasis on the event of 1700 AD. *Bulletin of the Seismological Society of America*, *90*(4), pp.876-896.

Patton, J.R., Romsos, C., Black, B., Morey, A.E., Djadjadihardja, Y. and Goldfinger, C., 2013. Seismoturbidite record as preserved at core sites at the Cascadia and Sumatra–Andaman subduction zones.

Pickart, A.J. and Hesp, P.A., 2019. Spatio-temporal geomorphological and ecological evolution of a transgressive dunefield system, Northern California, USA. *Global and planetary change*, *172*, pp.88-103.

Plafker, G., 1969. Tectonics of the March 27, 1964, Alaska earthquake.

Pritchard, C. J., 2004. *Late Holocene relative sea-level changes, Arcata Bay, California: Evaluation of freshwater syncline movement using coseismically buried soil horizons*. M.S. thesis, Humboldt State University, Department of Geology.

Rothwell, R.G. and Rack, F.R., 2006. New techniques in sediment core analysis: an introduction. *Geological Society, London, Special Publications*, *267*(1), pp.1-29.

Sabean, J. 2004, Application of foraminifera to detecting land level change associated with great earthquakes along the west coast of North America [unpublished M.S, thesis]: Department of Earth Sciences, Simon Fraser University, Vancouver, Canada, 85 pp.

Sawai, Y., 2001, Distribution of living and dead diatoms in tidal wetlands of northern Japan: relations to taphonomy: Palaeogeography, Palaeoclimatology, Palaeoecology, v. 173, p. 125-141.

Sawai, Y., Nasu, H., Yasuda, Y., 2002, Fluctuations in relative sea-level during the past 3000 yr in the Onneth estuary, Hokkaido, northern Japan: Journal of Quaternary Science, v. 17, no. 5-6, p. 607-622.

Schlosser, S., and A. Eicher. 2012. The Humboldt Bay and Eel River Estuary Benthic Habitat Project. California Sea Grant Publication T-075. 246 p.

Scott, D.B. and Medioli, F.S., 1980. Living vs. total foraminiferal populations: their relative usefulness in paleoecology. *Journal of Paleontology*, pp.814-831.

Shennan, I., Long, A.J., Rutherford, M.M., Green, F.M., Innes, J.B., Lloyd, J.M., Zong, Y. and Walker, K.J., 1996. Tidal marsh stratigraphy, sea-level change and large earthquakes, I: a 5000 year record in Washington, USA. *Quaternary Science Reviews*, *15*(10), pp.1023-1059.

Shennan, I., Scott, D.B., Rutherford, M. and Zong, Y., 1999. Microfossil analysis of sediments representing the 1964 earthquake, exposed at Girdwood Flats, Alaska, USA. *Quaternary International*, *60*(1), pp.55-73.

Shennan, I. and Hamilton, S., 2006. Coseismic and pre-seismic subsidence associated with great earthquakes in Alaska. *Quaternary Science Reviews*, *25*(1-2), pp.1-8.

Shennan, I., Barlow, N., Combellick, R., Pierre, K. and Stuart-Taylor, O., 2014. Late Holocene paleoseismology of a site in the region of maximum subsidence during the 1964 Mw 9.2 Alaska earthquake. *Journal of Quaternary Science*, *29*(4), pp.343-350.

Shennan, I., Garrett, E. and Barlow, N., 2016. Detection limits of tidal-wetland sequences to identify variable rupture modes of megathrust earthquakes. *Quaternary Science Reviews*, *150*, pp.1-30.

Srinivasalu, S., Thangadurai, N., Switzer, A.D., Mohan, V.R. and Ayyamperumal, T., 2007. Erosion and sedimentation in Kalpakkam (N Tamil Nadu, India) from the 26th December 2004 tsunami. *Marine Geology*, *240*(1-4), pp.65-75.

Switzer, A.D. and Jones, B.G., 2008. Large-scale washover sedimentation in a freshwater lagoon from the southeast Australian coast: sea-level change, tsunami or exceptionally large storm?. *The Holocene*, *18*(5), pp.787-803.

Thompson, R.W., 1971. Recent sediments of Humboldt Bay. *Eureka, California. Washington, DC: American Chemical Society, Petroleum Research Fund*.

Troels-Smith, J., 1955. Karakterisering af lose jordarter. Characterization of unconsolidated sediments.

Turowski, J.M., Hilton, R.G. and Sparkes, R., 2016. Decadal carbon discharge by a mountain stream is dominated by coarse organic matter. *Geology*, *44*(1), pp.27-30.

Valentine, D.W., 1992. *Late Holocene stratigraphy, Humboldt Bay, California: evidence for late Holocene paleoseismicity of the southern Cascadia subduction zone*. M.S. thesis, Humboldt State University.

Vick, G.S., 1988. *Late Holocene paleoseismicity and relative sea level changes of the Mad River Slough, northern Humboldt Bay, California*. M.S. thesis, Humboldt State University.

Wang, P.L., Engelhart, S.E., Wang, K., Hawkes, A.D., Horton, B.P., Nelson, A.R. and Witter, R.C., 2013. Heterogeneous rupture in the great Cascadia earthquake of 1700 inferred from coastal subsidence estimates. *Journal of Geophysical Research: Solid Earth*, *118*(5), pp.2460-2473.

Wang, J., Jin, Z., Hilton, R.G., Zhang, F., Li, G., Densmore, A.L., Gröcke, D.R., Xu, X. and West, A.J., 2016. Earthquake-triggered increase in biospheric carbon export from a mountain belt. *Geology*, *44*(6), pp.471-474.

Zong, Y., Shennan, I., Combellick, R.A., Hamilton, S.L. and Rutherford, M.M., 2003. Microfossil evidence for land movements associated with the AD 1964 Alaska earthquake. *The Holocene*, *13*(1), pp.7-20.

Table 1. Coseismic subsidence estimates northern Humboldt Bay estuary

Jacoby Creek	Subsidence estimate (m)	McDaniel Creek	Subsidence estimate (m)	Mad River Slough	Subsidence estimate (m)	Inter-site average (m)
			Earthquake 1 – 250 cal yr BP			
JC.02.D	0.75 ±0.52	MD.03.D	0.90 ±0.46	MR.05.C	0.36 ±0.26	
JC.06.B	1.00 ±0.40	MD.12.A	0.45 ±0.34	MR.03.D	0.36 ±0.24	
JC.10.A	0.49 ±0.40	MD.13.A	1.04 ±0.42	MR.02.C	0.28 ±0.26	**0.63 ±0.36**
Intra-site Average	**0.62 ±0.44**	Intra-site Average	**0.80 ±0.41**	Intra-site Average	**0.33 ±0.25**	
			Earthquake 2 – 870 cal yr BP			
N.D.	N.D.	MD.06.C	0.39 ±0.33	MR.02.C	0.51 ±0.30	
		MD.03.C	0.46±0.35	MR.03.C	0.26 ±0.24	
				MR.05.C	0.33 ±0.54	**0.39 ±0.35**
		Intra-site Average	**0.43±0.34**	Intra-site Average	**0.37 ±0.36**	
			Earthquake 3 – 1125 cal yr BP			
JC.02.D	0.48 ±0.42	MD.13.A	0.99 ±0.44	MR.05.C	0.59 ±0.32	
JC.10.A	0.94 ±0.44	MD.12.B	0.59 ±0.38	MR.02.C	0.59 ±0.36	**0.7 ±0.39**
Intra-site Average	**0.71 ±0.43**	Intra-site Average	**0.79 ±0.41**	Intra-site Average	**0.59 ±0.34**	

N.D. no data

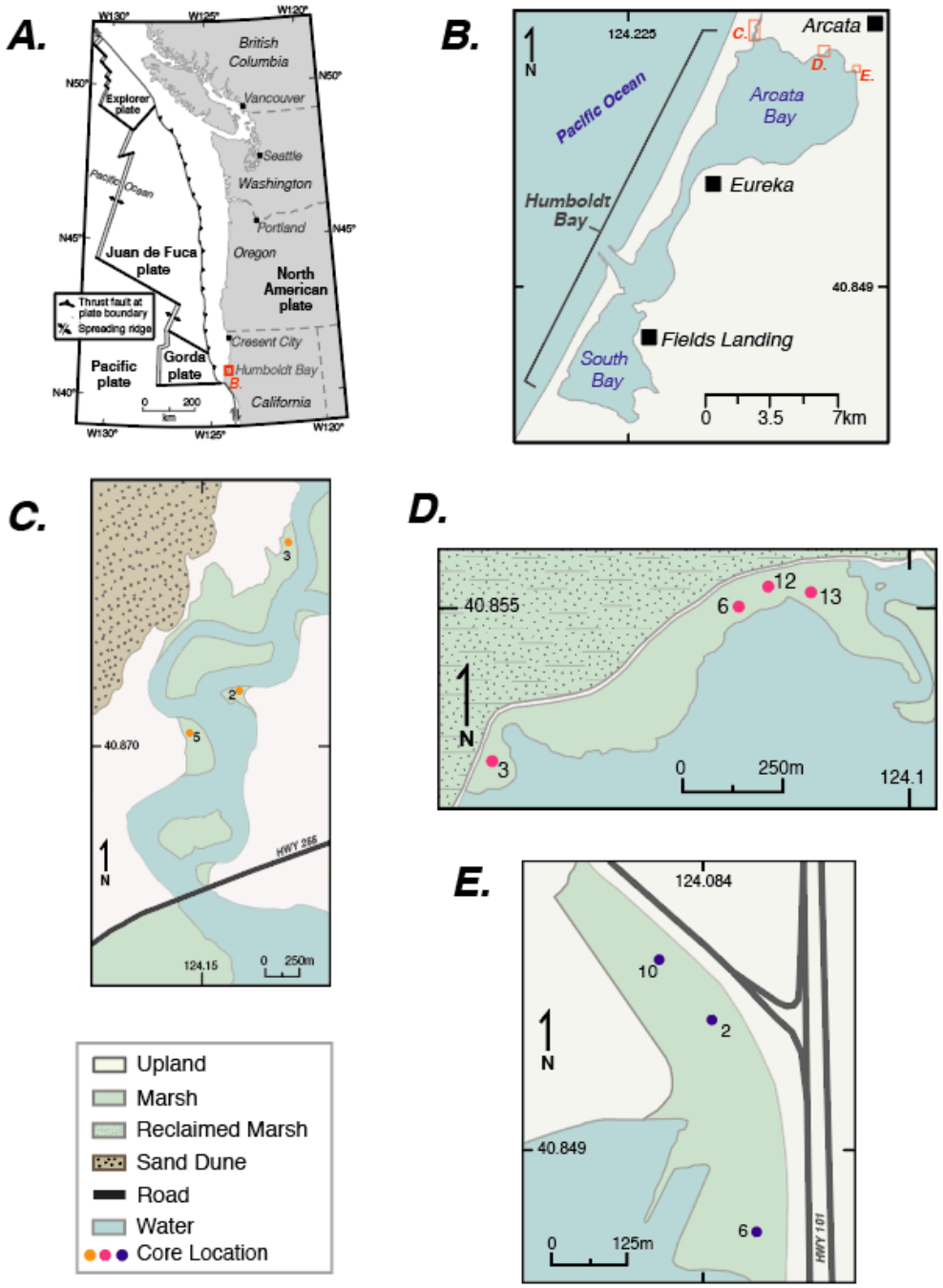

Figure 1.

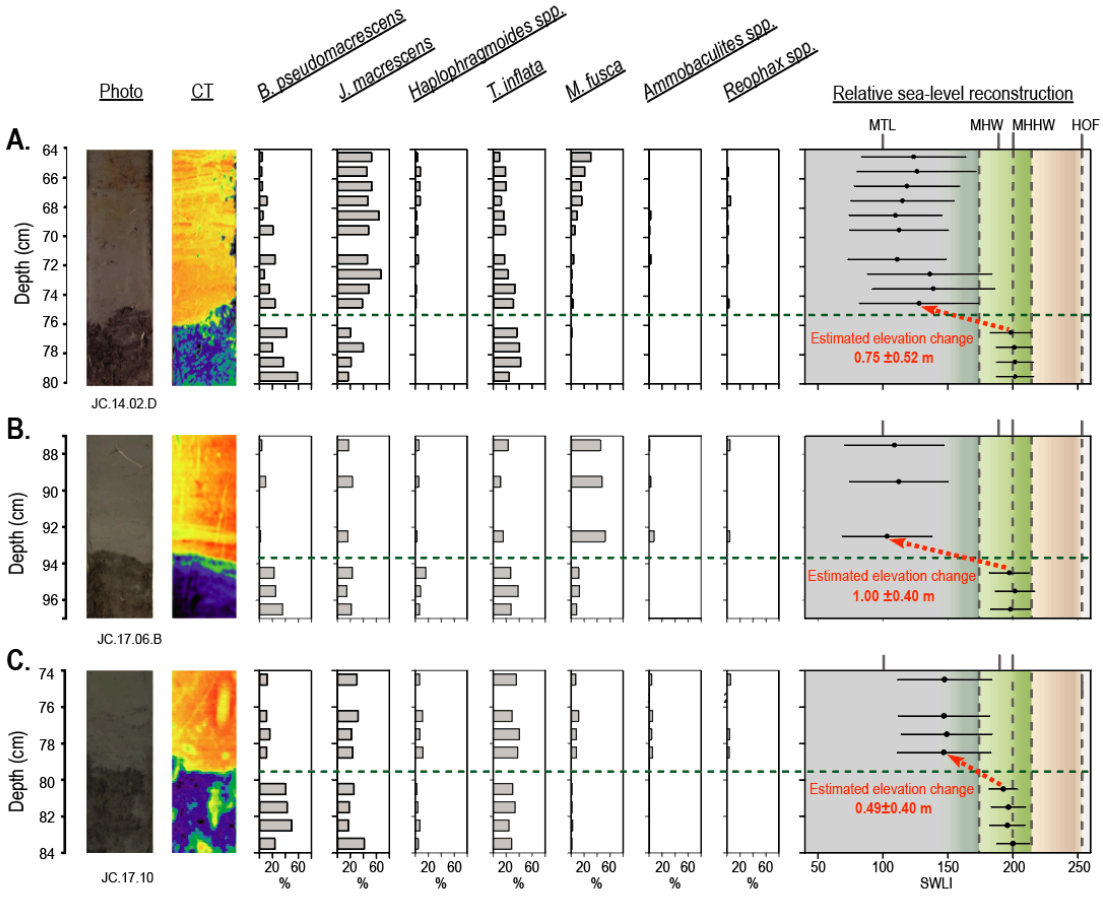

Figure 2.

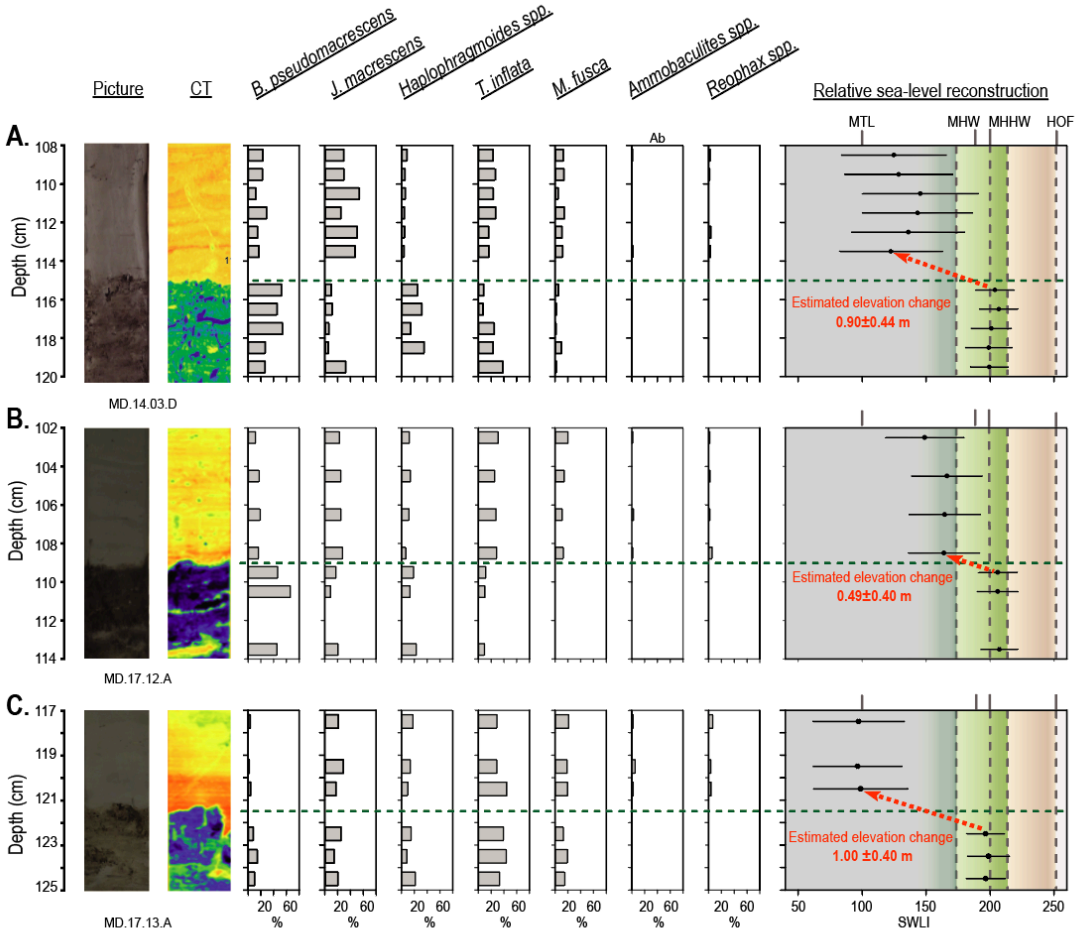

Figure 3.

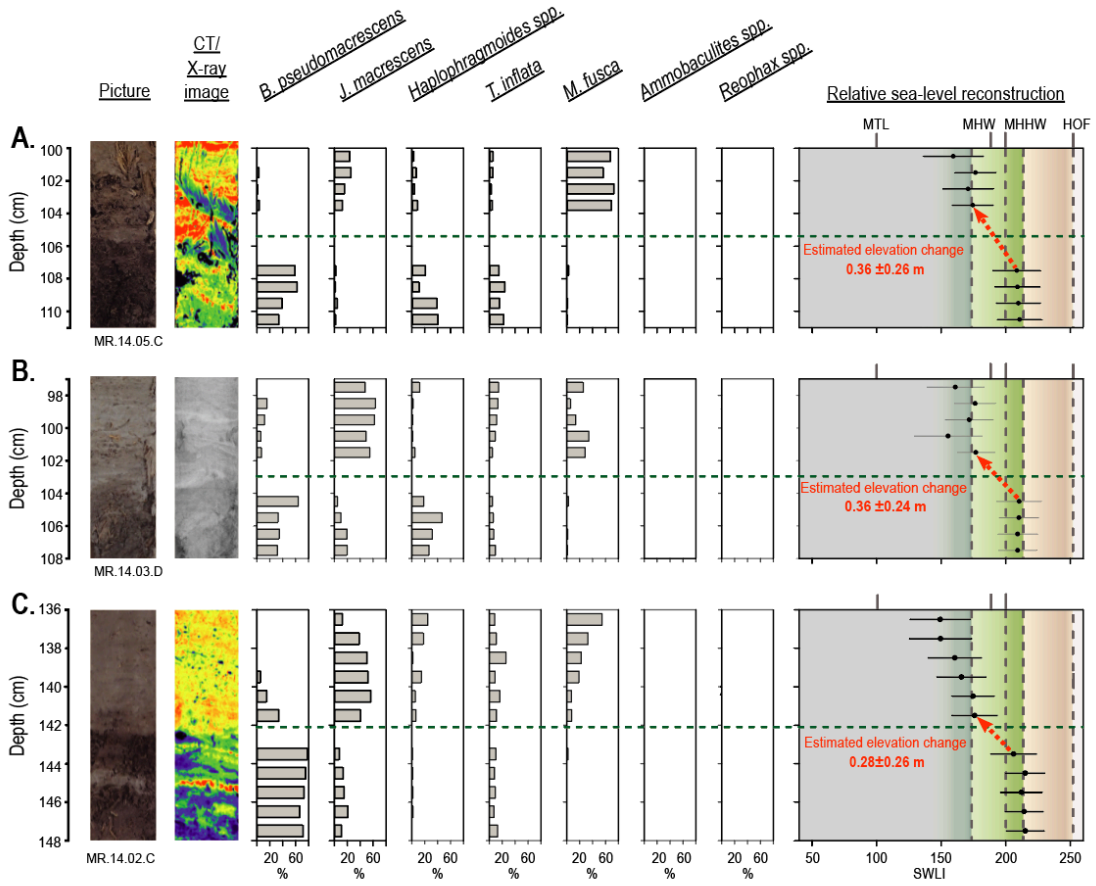

Figure 4.

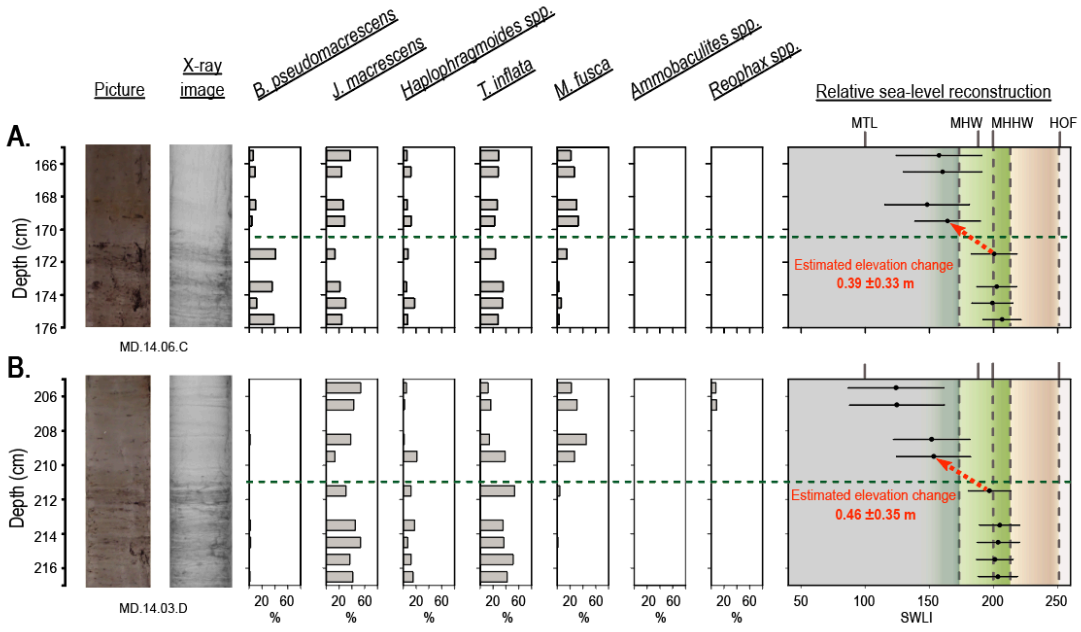

Figure 5.

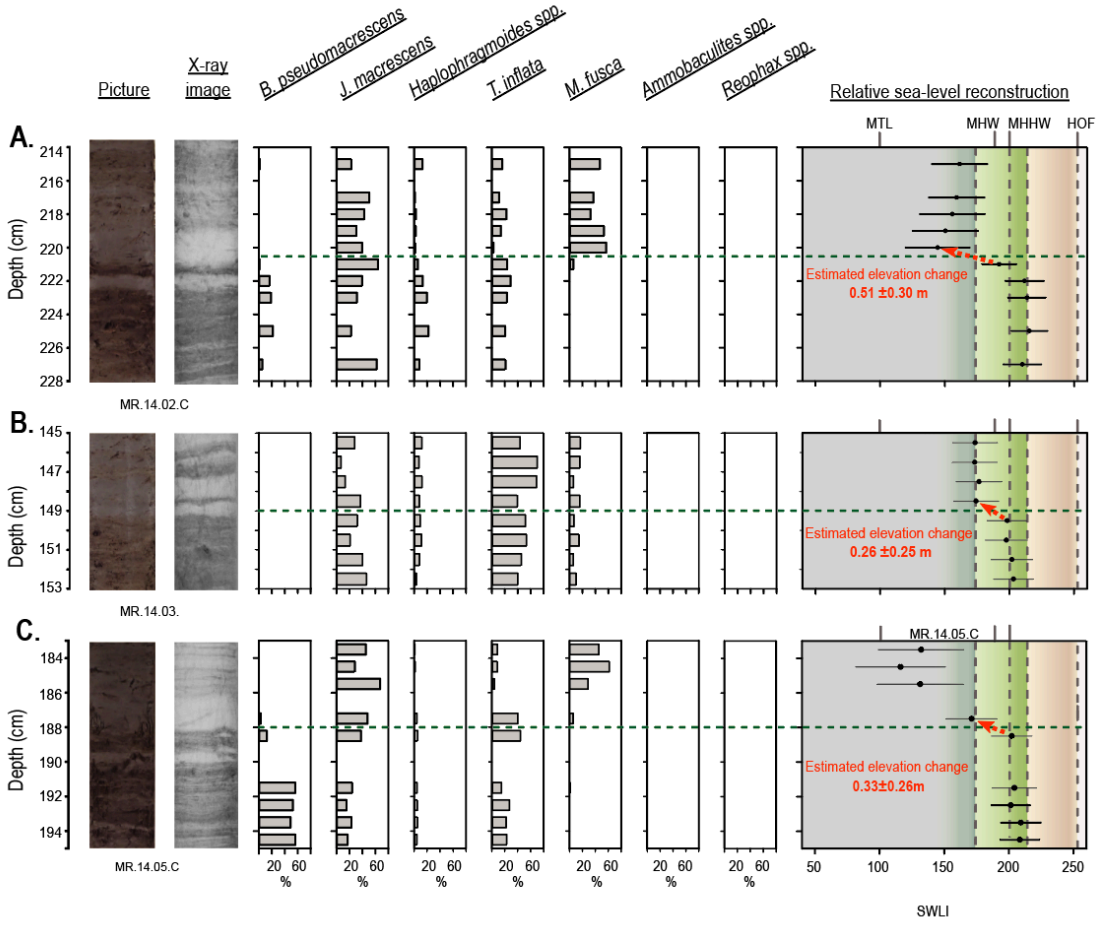

Figure 6.

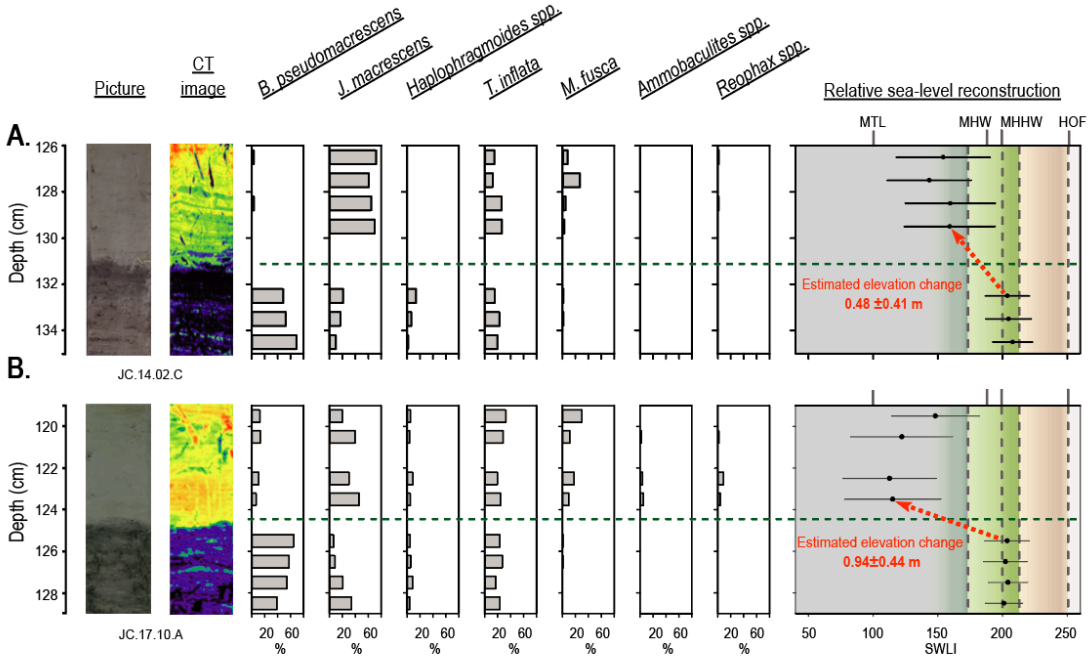

Figure 7.

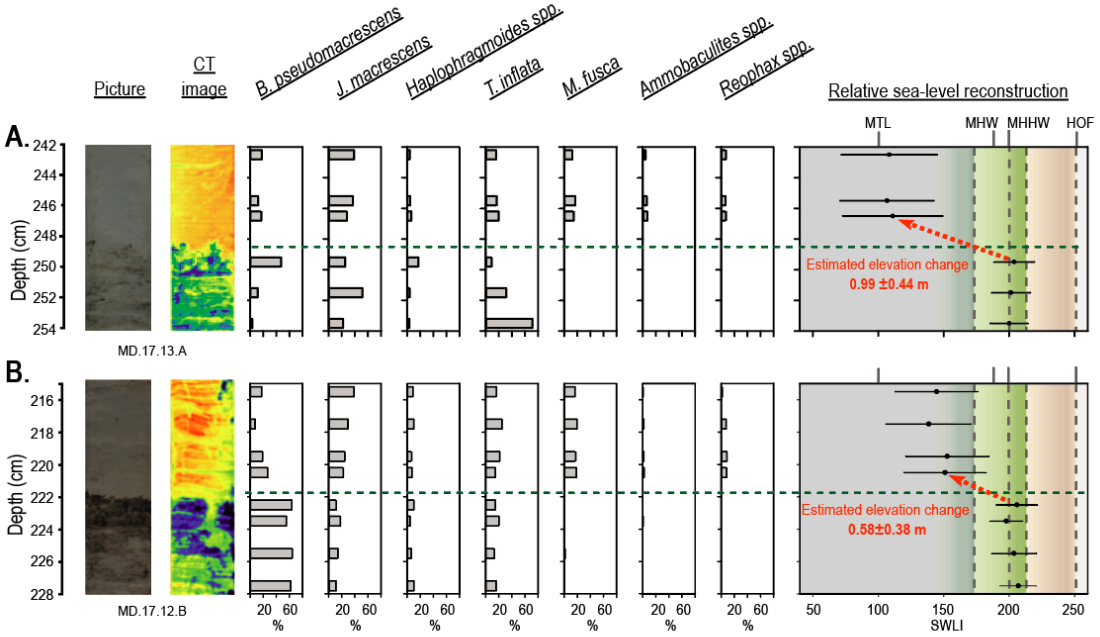

Figure 8.

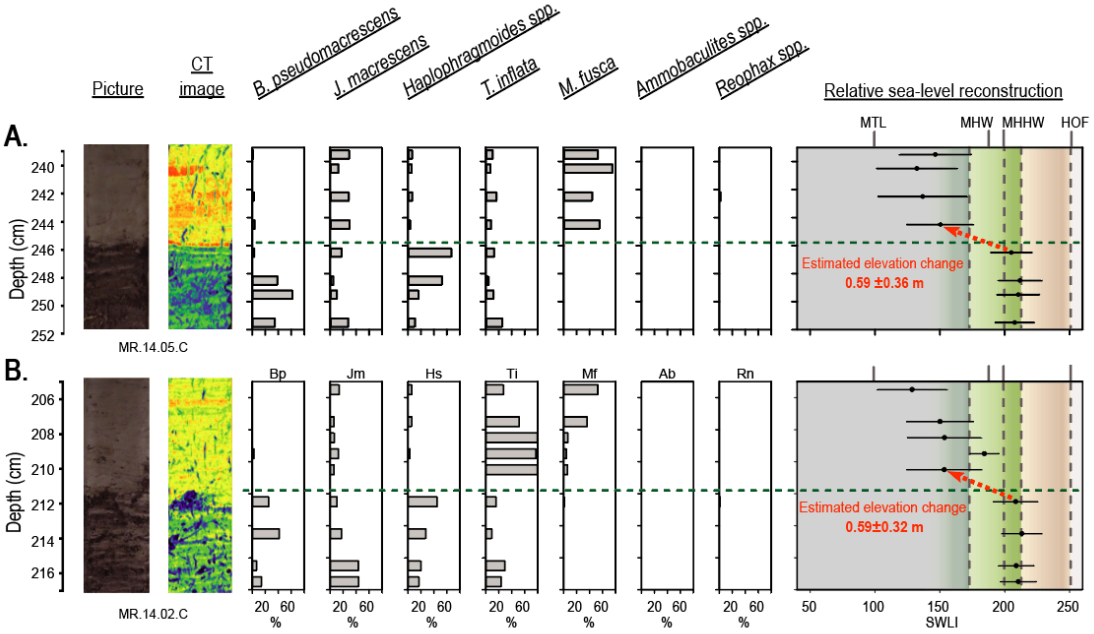

Figure 9.

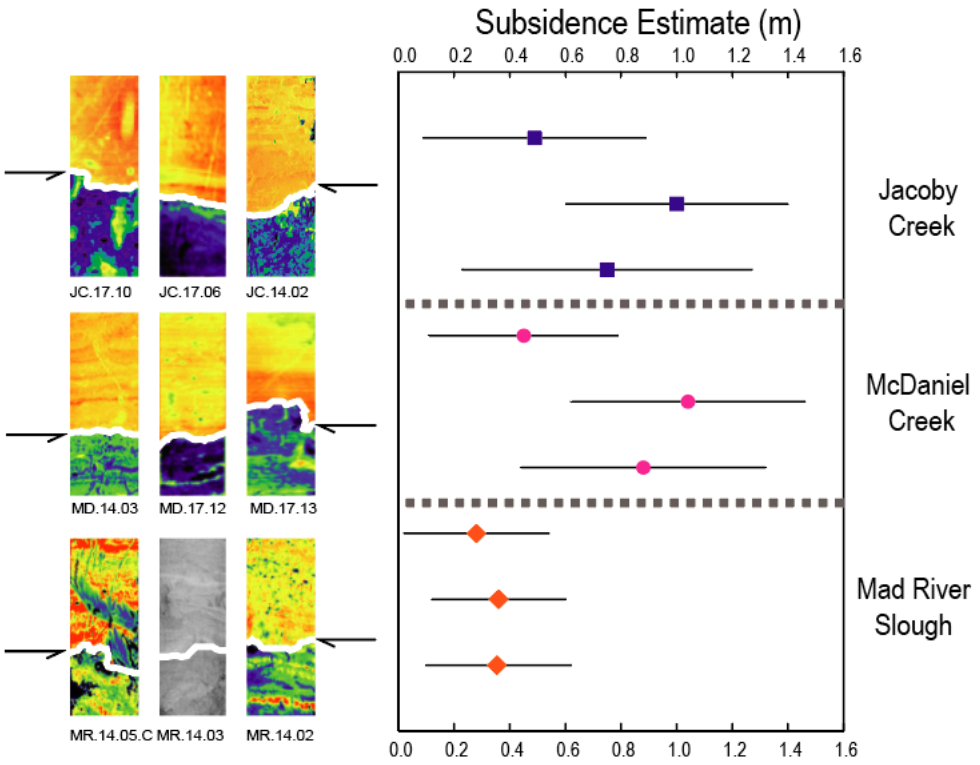

Figure 10.

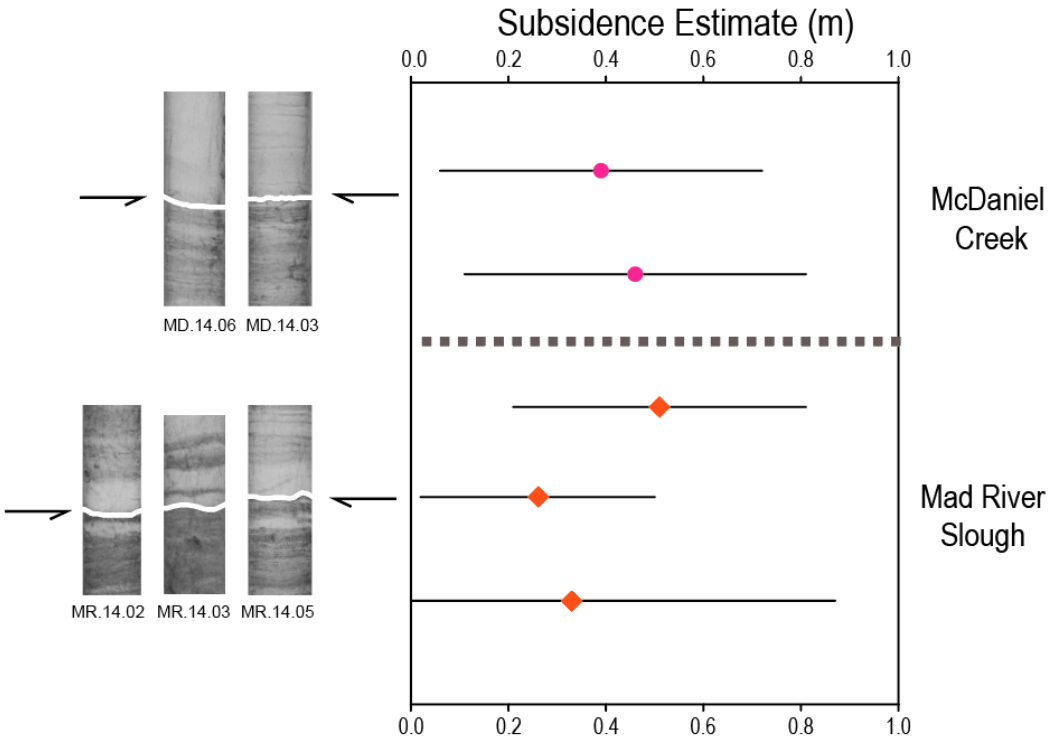

Figure 11.

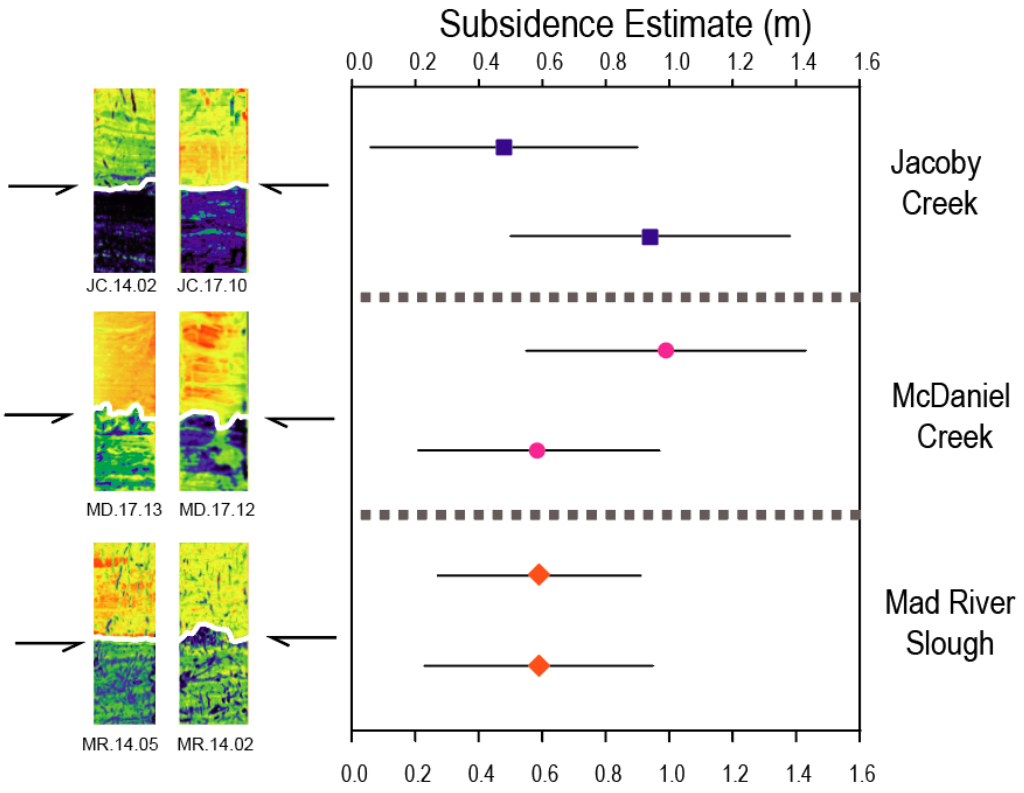

Figure 12.

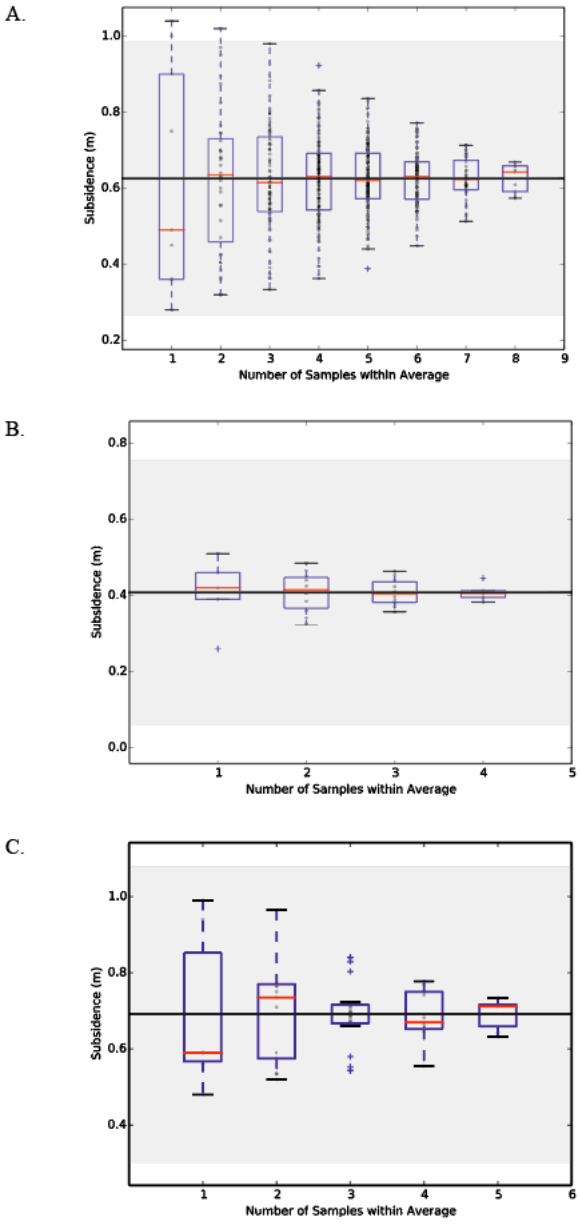

Figure 13.

CHAPTER 3

Expanding the Cascadia 1700 CE paleogeodetic database with subsidence estimates from southwest Washington and the implications for an elastic dislocation model

J. Scott Padgett[1], Simon Engelhart[1], Matthew C.R. Sypus[2], Kelin Wang[2,3], Andrea D. Hawkes[4], Niamh Cahill[5], Robert C. Witter[6], Alan Nelson[7], Isabel Hong[8], Benjamin Horton[8,9,10], and Harvey Kelsey[11]

[1]Department of Geosciences, University of Rhode Island, RI, USA
[2]School of Earth and Ocean Sciences, Victoria, BC, Canada
[3]Pacific Geoscience Centre, Geological Survey of Canada, Sidney, BC, Canada
[4]Department of Earth and Ocean Sciences, University of North Carolina Wilmington, NC, USA
[5]Department of Mathematics and Statistics, Maynooth University, Kildare, Ireland
[6]Alaska Science Center, U.S. Geological Survey, Anchorage, AK, USA
[7]Geologic Hazards Science Center, U.S. Geological Survey, Golden, CO, USA
[8]Asian School of the Environment, Nanyang Technological University, Singapore
[9]Earth Observatory of Singapore, Nanyang Technological University, Singapore
[10]Sea Level Research, Department of Marine and Coastal Sciences, Rutgers University, NJ, USA
[11]Department of Geology, Humboldt State University, CA, USA

This chapter/manuscript is prepared for submission to the journal *Bulletin of the Seismological Society of America*.

ABSTRACT

Quantitative relative sea-level reconstructions derived from foraminiferal-based Bayesian transfer functions yield precise estimates of coseismic vertical deformation for the Cascadia Subduction Zone (CSZ) 1700 CE earthquake. These estimates inform hypothetical rupture scenarios used in seismic and tsunami hazard models. However, the current CSZ 1700 CE foraminiferal transfer function paleogeodetic database primarily consists of estimates from Oregon (85 %) and has spatial gaps in northern California, Washington, and British Columbia. Therefore, strategically placed transfer function investigations afford the opportunity to progress our understanding of Cascadia rupture and inform hazard characterization. We examine stratigraphic sequences of CSZ 1700 CE earthquake subsidence (abrupt mud-over-peat contacts), from six sites that span ~75 km along strike in southern Washington. We quantitatively reconstruct sudden relative sea-level rise induced by coseismic subsidence across stratigraphic contacts by applying a Bayesian transfer function (BTF) to fossil foraminiferal assemblages.

We analyzed CSZ 1700 CE earthquake contacts at; Copalis River, Ocean Shores, Johns River, Smith Creek, Bone River, and Naselle River. At these sites, coseismic subsidence estimates ranged from 0.39 m (±0.37 m) at Johns River to 1.52 m (±0.51 m) at Smith Creek. The new estimates of the CSZ 1700 CE earthquake from southwest Washington are added to a margin-wide BTF paleogeodetic database (n=14), and increases (43%) the number of reconstructions from Vancouver Island to Humboldt Bay (n=20). The updated BTF paleogeodetic database is used to constrain 3-D elastic dislocation models. Starting from a previously published model, we developed three alternate 3-D elastic dislocation models. The new models improved

agreement between reconstructed and modeled coseismic subsidence. However, we also identify that there are multiple non-unique solutions that fit to the coastal coseismic subsidence estimates. Even with the new coseismic subsidence constraints, a four-patch slip distribution still provides the simplest solution but the amount of slip in each patch has to be modified to fit the new BTF data. Our results highlight the need for additional high quality subsidence estimates from locations in-between high-slip and low-slip patches (e.g., Nehalem-Netarts; Tillamook Bay, ~45.5° N), and within remaining geospatial gaps, e.g., in-between Coquille River and northern Humboldt Bay (~43.1° N to ~40.9° N).

1. INTRODUCTION

The Cascadia subduction zone (CSZ) has not ruptured during the recent instrumented and historical (written) time period (McCrory et al., 2012). Earthquake hazard assessments are informed by past earthquake information and not having a historical record presents difficulties when attempting to forecast future CSZ rupture scenarios (Leonard et al., 2004, 2010; Wang et al., 2013). A number of recent megathrust ruptures have had non-uniform rupture distributions (e.g., 2004 M_w 9.2 Sumatra-Andaman, 2010 M_w 8.8 Maule, Chile, 2011 M_w 9.0 Tohoku-Oki, Japan), which suggests that past megathrust rupture has likely been heterogeneous. However, in order to define past rupture slip distributions, a spatially dense network (paleogeodetic database) of past coseismic deformation estimates is required. Fortunately, due to the moderate rates of relative sea-level (RSL) rise over the late Holocene (e.g., Engelhart et al., 2015; Dura et al., 2017), many Cascadia coastal

wetlands host a remarkable archive of past coastal subsidence caused by megathrust rupture (Atwater, 1987; Peterson and Darienzo, 1991; Nelson, 1991; Nelson et al., 1996; Atwater and Hemphill-Haley, 1997; Kelsey et al., 2002; Witter et al., 2003). Estimates of past megathrust-induced land subsidence (referred to as paleogeodetic estimates) can be derived from analysis of coastal stratigraphic records (e.g., Guilbault, 1995, 1996; Shennan et al., 1996; Hawkes et al., 2010, 2011). These estimates can then inform hypothetical rupture scenarios used in seismic and tsunami hazard models (Hyndman and Wang, 1995; Wang et al., 2003; Leonard et al., 2010, Wang et al., 2013, Witter et al., 2013). However, fundamental questions regarding past great (M_w >8.0) CSZ earthquake magnitude, segmentation, and heterogenous rupture remain unanswered because we lack geospatial coverage of high-precision coastal stratigraphic analysis in many parts of the subduction zone even for the most recent earthquake in AD 1700 CE (e.g., Witter et al., 2012; Wang et al., 2013; Kemp et al, 2018). Therefore, it is critical to develop the highest-quality and most-widespread paleogeodetic datasets possible.

Leonard et al., (2004, 2010) were the first to test consistency of elastic dislocation models for the CSZ 1700 CE earthquake using coastal coseismic subsidence estimated from a margin-wide dataset of paleo-elevation studies. They concluded that coastal subsidence estimates can be used as constraints for elastic dislocation rupture models. Leonard et al., (2004, 2010) considered the best resolution of the data available at that time, much of which had large uncertainties (0.5-1.0 m) and, therefore, early CSZ elastic dislocation models were limited to uniform slip distributions. The large increase in quantitative estimates post-2010 allowed Wang et

al. (2013) to compile a margin-wide paleogeodetic database of higher-precision coseismic subsidence estimates of the CSZ 1700 CE earthquake. These estimates were derived from both semi- and fully-quantitative statistical techniques used to reconstruct past relative sea-level (RSL) from microfossil (diatom and foraminifera) assemblages in coastal stratigraphy. The highest-precision (~±0.3 m) estimates were derived from foraminiferal transfer function analysis (Hawkes et al., 2010; 2011) and the majority of the estimates were from Oregon with more limited data coverage to north and south. The paleogeodetic database of Wang et al., (2013) was used to produce a preferred model of rupture during the CSZ 1700 CE earthquake, which demonstrated a heterogenous slip distribution with low slip areas at both Alsea Bay and Netarts, Oregon. Although there are non-unique rupture solutions that fit the coastal subsidence estimates, the preferred model was a conservative solution. Wang et al., (2013) concluded that improvements to the preferred dislocation model would result from the addition of high-precision subsidence estimates from the geospatial gaps within the paleogeodetic database. e.g., northern California, Washington, and Vancouver Island. Therefore, strategically placed high-precision transfer function investigations within the remaining geospatial gaps afford the opportunity to significantly progress our understanding of Cascadia rupture and inform hazard characterization.

Since the publication of the Wang et al., (2013), there have been further developments in the statistical techniques used to reconstruct RSL based on microfossil data that may influence the preferred rupture model scenarios (e.g., Cahill et al., 2016; Holden et al., 2017; Kemp et al., 2018). Following the approach of Cahill

et al., (2016), Kemp et al., (2018) generated a foraminiferal-based Bayesian transfer function (BTF), which further improved RSL reconstructions. The BTF approach benefits from two functional improvements over previous foraminifera transfer functions; 1) flexibility to model non-uniform species distributions along the intertidal gradient, i.e., allows the modern data to define unique species-elevation relationships and 2) ability to incorporate priors, e.g. lithology, which further constrains the RSL reconstruction. The assignment of informative priors reduces errors due to mixed foraminiferal assemblages below contacts (e.g., Engelhart et al., 2013) and potentially above contacts (e.g., Padgett et al., in-prep). Although Kemp et al., (2018) applied the BTF to the fossil foraminiferal database of Wang et al., (2013), and conclude that many of the foraminiferal subsidence estimates increased and no longer fit the preferred rupture model of (Wang et al., 2013). However, they did not revise the rupture model or resolve issues of spatial coverage within the paleogeodetic database.

To address these limitations in our knowledge of the CSZ 1700 CE earthquake, this research aims to: 1) focus on a spatial data gap within the paleogeodetic database of coseismic subsidence estimates of the CSZ 1700 CE earthquake by applying BTF methodologies to fossil foraminifera assemblages from coastal stratigraphic sequences throughout southwestern Washington and 2) refine 3D elastic dislocation models of the CSZ 1700 CE earthquake based on the new data from Washington presented here, as well as new data from northern California (Padgett et al., *in-prep*). Here we produce 8 new coseismic subsidence estimates from six new locations in southwest Washington to the paleogeodetic database of the CSZ 1700 CE earthquake, which increases the number of estimates along the margin by ~43%. The new BTF coseismic

subsidence estimates require revisions to a previously preferred simple four-patch rupture scenario of the 1700 CE earthquake elastic dislocation model of Wang et al., (2013).

2. STRATIGRAPHY OF THE CASCADIA SUBDUCTION ZONE 1700 CE EARTHQUAKE AT SIX ESTUARIES

Along the Cascadia coastline, laterally extensive and spatially-correlated abrupt *mud-over-peat* and *mud-over-forest soil* contacts have been interpreted to be lithostratigraphic evidence of a rapid rise in RSL (land subsidence) during past great (M_w >8.0) CSZ earthquakes (Atwater, 1987; Darienzo and Peterson, 1990; Atwater et al., 1992; Nelson et al., 1996). Over three decades of coastal paleogeodetic research has greatly improved our understanding of Cascadia plate boundary processes (Atwater, 1987; Peterson and Darienzo, 1991; Atwater et al., 1992; Nelson, 1992; Nelson et al., 1996; Shennan et al. 1996; Atwater and Hemphill-Haley, 1997; Kelsey et al., 2002; Witter et al., 2003; Hawks et al., 2010; 2011; Engelhart et al., 2013, Wang et al., 2013; Milker et al., 2016). For example, Atwater et al., (1987) first documented coastal stratigraphic evidence consistent with past Cascadia megathrust induced subsidence and since then researchers have identified that the most recent CSZ earthquake occurred at ~9:00 pm on January 26th 1700 CE, based precise tree ring and radiocarbon dating combined with inverse tsunami modeling (Nelson et al., 1995; Satake et al., 2003; Atwater et al., 2005). Due to the size of the tsunami in Japan, estimates of the triggering Cascadia earthquake magnitude range from ~8.7 to 9.2 M_w (Satake et al., 2003; Atwater et al., 2005). Because it is the most recent CSZ

earthquake, stratigraphic evidence of the CSZ 1700 CE earthquake is the best preserved, shallowest, and most widespread coastal stratigraphic sequence of past Cascadia earthquake deformation and such stratigraphic evidence can be observed throughout Cascadia wetlands.

In this study we focus on wetland stratigraphy of the CSZ 1700 CE earthquake from six sites in southwest Washington; Copalis River, Ocean Shores, Johns River, Smith Creek, Bone River, and Naselle River. Wherever possible we use previous stratigraphic studies of the same or nearby sites in order identify key stratigraphic intervals. We employ coastal paleoseismic criteria discussed by Atwater et al., (1995); Nelson et al., (1996), and Shennan et al., (2016) throughout our stratigraphic mapping.

The lower Copalis River marsh coring site is ~3.5 km upstream from the Pacific Ocean and protected by a 3 km-long, 0.7 km-wide vegetated and forested sand spit (Fig 1b). We studied a sediment core that was collected ~50 m east of Highway 109 on the north side of the river. Atwater (1992), found lithostratigraphic and plant macrofossil evidence for subsidence during the CSZ 1700 CE earthquake in outcrops and in standing dead western red cedar trunks rooted in the shallowest buried organic-rich unit. A laterally extensive sharp upper contact of a buried organic-rich unit that is capped by a silt to fine sand 1-7cm thick deposit are stratigraphic evidence used to infer sudden earthquake-induced subsidence and tsunami. Seven radiocarbon-dated ages of plant remains from the shallowest buried organic-rich unit have the mean age of 139 ±17 and the age interval using tree-ring data and the mean of four ages on stumps rooted in the horizon is AD 1680-1720 (Atwater et al., 1991; Atwater, 1992).

The Ocean Shores Airport site is ~ 8 km north of the mouth of Greys Harbor and ~450 m east of the Albatross Street NE and Duck Lane Drive NE intersection in Ocean Shores, Washington (Fig 2c). Our sampled bank section was collected ~240 m east of the north-east corner of the Ocean Shores airport runway. Adams (2017), found lithostratigraphic and macrofossil evidence for subsidence during the CSZ 1700 CE earthquake in outcrop and in dead conifer snags rooted in the shallowest buried organic-rich unit. A laterally extensive sharp upper contact of a buried organic-rich unit that is capped by a silt to fine sand 2-6 cm thick deposit are stratigraphic evidence used to infer sudden earthquake-induced subsidence and tsunami (Adams, 2017).

The lower Johns River marsh is located along the south shore of Grey Harbor. We studied two stratigraphic sections that span the shallowest buried organic-rich unit, which were collected from both sides of the main channel (Fig 1d). Shennan et al., (1996) found lithostratigraphic, plant macrofossil, and microfossil (diatom, foraminifera, and pollen) data within wetland stratigraphy that are evidence for sudden and lasting subsidence during the CSZ 1700 CE earthquake in outcrop and sediment cores of the shallowest buried organic-rich unit. Using fossil diatom, foraminifera, and pollen data Shennan et al., (1996) estimate subsidence to be 1.0 ±0.5 m during the CSZ 1700 CE earthquake. Three bulk peat radiocarbon ages taken from the top cm of the shallowest organic-rich unit define its' age; 360 ± 60 cal yrs BP (Table 1, Beta 22008; Atwater, 1992), 390 ± 60 cal yrs BP and 450 ±60 cal yrs BP (Shennan et al., 1996). Although these radiocarbon ages on bulk peat samples pre-date the timing of the CSZ 1700 CE earthquake, they are inherently combined organic plant material that

accumulated over >10's-100 year time periods and are therefore supportive of the 1700 CE age assignment.

The lower Smith Creek marsh is located along the north shore of Willapa Bay just east of the mouth of North River. Reinhart, (1992), briefly mentions observations of the stratigraphy at Smith Creek of a mud that overlays the shallowest buried organic-rich unit which supported a coastal forest 1km upstream. We studied a sediment core collected ~50 m west of Highway 105 and ~35 m north of the Smith Creek that spanned the shallowest buried organic-rich unit (Fig. 1f). To our knowledge Reinhart (1992) is the only report on the wetland stratigraphy of the lower Smith Creek.

The lower Bone River marsh is located ~11 km east of the opening of Willapa Bay and ~4 km north of the Niawiakum River estuary. Reinhart, (1991), describes wetland stratigraphy of the CSZ 1700 CE earthquake and tsunami at the lower Bone River marsh; where the shallowest buried organic-rich unit is capped by a mud laminated sand as much as 2.5 km upstream. We studied a core sample collected ~80 m east of highway 101 and ~275 m north of the boat launch that spanned the shallowest buried organic rich-unit (Fig. 1g). Other than stratigraphy of the tsunami sand above the shallowest organic-rich unit,

The Naselle River coring site is located along the southern shore of the river ~1-1.5 km upstream from the Highway 101 bridge (Fig. 1h). Reinhart (1991) observed a tsunami deposit at Stanley Point which is at southern shore of the confluence of the Naselle River and Willapa Bay. Although. The shallowest buried organic-rich unit has been dated, the wetland stratigraphy has not been formally reported up on. Eight

radiocarbon-dated radiocarbon ages of plant remains from the shallowest buried organic-rich unit have the mean age of 162 ±17 (Nelson et al ., 1995), which is falls within radio carbon calibration curve plateau and suggest the upper contact of the shallowest buried organic rich unit represents seismic subsidence the 1700 CE earthquake. We studied two cores, one collected 20 m north of Parpala Road across from the intersection with Ellens Worth Road and the other ~20 m east of Ellens Worth Road and ~75 m south of Parpala Road.

3. METHODS AND MATERIALS

3.1 Stratigraphic analysis

Our stratigraphic research approach is two-fold; 1) undertake lithostratigraphic analysis (describe subsurface contact stratigraphy), 2) produce relative sea-level reconstructions (estimate paleoenvironmental elevation changes using fossil foraminiferal data and an existing BTF; Kemp et al., 2018).

3.1.1 Stratigraphic Description and Sampling

Based on stratigraphic mapping across six sites, over a 75 km transect along southwestern Washington, we selected 8 representative stratigraphic sections that span the CSZ 1700 CE earthquake induced-subsidence contact from Copalis River (1), Ocean Shores (1), Johns River (2), Smith Creek (1), Bone River (1) and Naselle River (2). At the investigated wetland locations, we mapped the shallowest, laterally extensive, abrupt (~1mm) to sharp (<3mm) *mud-over-peat* and *mud-over-forest soil* contacts that represent subsidence during the 1700 CE earthquake. We selected

representative stratigraphic sequences, collected in 50 cm length core sections, for foraminiferal analysis.

Wetland stratigraphy was observed within outcrop and hand core auguring equipment. Representative stratigraphy was collected preferentially by an Eijkelkamp peat sampler because the it allows for the collection of an uncontaminated sample because it captures material directly adjacent to the primary stress direction of coring apparatus. However, in outcrop and across stiff stratigraphy the 60 mm gouge core was used for sediment core collection.

Sediment sequences that contained the 1700 CE contact were described using the Troels-Smith (1955) method for describing organic-rich sediment combined with general stratigraphic methods for describing grain size, sedimentary structures, contacts, thickness, and facies changes. The encountered stratigraphy consisted of clastic mud and interbedded organic-rich units. A "mud unit" refers to a grey to brown-grey massive to finely bedded silt and clay lithology. An "organic-rich unit" refers to a brown to black salt marsh peat or forest soil. Lithologic unit descriptions within this investigation include peat, muddy peat, peaty mud and mud, with organic percentages of 100-75%, 75-50%, 50-25%, and <25%, respectively.

Typically, at Cascadia, one coseismic subsidence estimate has been used to represent subsidence for an estuary (Hemphill-Haley 1995; Guilbault et al., 1995, 1996; Shennan et al., 1996; Sabean, 2004; Hawkes et al., 2011; Wang et al., 2013). However, Shennan et al., (2014) and Padgett et al., (*in-prep*), show that there can be variability in coseismic subsidence estimates derived from the same stratigraphic sequence both within a marsh and across an estuary and that confidence will be gained

from an average of multiple spread-out RSL reconstructions. Therefore, we follow the recommendation of Padgett et al., (in-prep) where possible and perform multiple spread-out RSL reconstructions across the same stratigraphic sequence at Johns River and Naselle River and at Ocean Shores we compare to a reconstruction from Adams, (2017).

3.1.2 Stratigraphic Imaging

Stratigraphic contact sharpness and through-core continuity is not always apparent and representative on the surface of a sediment core. In order to identify through-core continuities we follow recent paleoseismic studies (e.g., Goldfinger et al., 2012; Patton et al., 2013; Briggs et al., 2014; and Milker et al., 2016) and obtained computerized tomography (CT) high-resolution density imagery of the selected representative sediment core samples. The CT scan analysis were performed at Oregon State University College of Veterinary Medicine and Rhode Island South County Hospital, following standard methodologies (Rockwell and Rack, 2006; Davies et al., 2011). The Oregon State University College of Veterinary Medicine used a Toshiba Aquilion 64 Slice at 120 kVp, 200 mA, and a pitch of 0.5s (100 mAs). At Rhode Island South County Hospital used a 32 Slice GE Light speed Scanner with technical factors set at 120 kVp and 200-400 mA and a pitch of 0.969:1. Sediment core images were processes with a "bone" algorithm to generate coronal images every mm across the core. The imagery were produced and stitched together using Horos and Adobe software.

3.1.3 Foraminifera analysis

Standard foraminiferal preparation and analysis followed Scott and Medioli (1982), de Rijk, 1995 and Horton and Edwards, (2006). We concentrated foraminifera by washing 1 cm intervals of sediment (~3cm^3) dissected from fossil sediment cores, over 500- and 63-micron sieves and retained materials between those size fractions. For each interval analyzed, we identified up to 200 specimens or until the entire sample was enumerated (Fatela and Taborda, 2002). Only samples that contained >30 foraminifera were used in the production of a quantitative RSL reconstruction because low abundances may reflect a non in-situ assemblage and/or may not be representative of the depositional environment (Kemp et al., 2018). We follow the foraminifera taxonomy based on Hawkes et al., (2010) and Milker et al., (2015). We also follow Kemp et al, (2018), by combining *Haplophragmoides spp.* and *Ammobaculites spp.* In order to evaluate if a fossil assemblage has a modern analog, we used the Bray-Curtis distance metric (Kemp and Telford, 2015). Due to the low species diversity of salt-marsh foraminifera, a threshold of less than the 20th percentile is appropriate for determining whether a fossil sample has a modern analog in the modern dataset (Kemp and Telford, 2015).

3.1.4 Bayesian transfer function

Transfer functions allow us to use the relationship between microfossil assemblages and elevation in the present to reconstruct intertidal elevations in the past using fossil assemblages. Microfossil transfer function RSL reconstructions usually have errors that are ~10% of the tidal range for an individual sample (Barlow et al., 2013; Watcham et al., 2013; Kemp and Telford, 2015). This resolution is appropriate to refine our understanding of past CSZ rupture by constraining rupture scenarios

within earthquake deformation models (e.g., Wang et al., 2013). For typical Cascadia tidal ranges (2-3m) foraminifera-based transfer functions (e.g., Guilbault et al, 1995, 1996; Hawkes et al., 2010, 2011; Engelhart et al., 2013) produce estimates of subsidence with a precision of ~±0.3m. In 2018, Kemp et al., introduced a BTF that allows for flexible species-response curves and can formally incorporate prior information from additional proxies, e.g., other microfossil groups, $\delta^{13}C$, or stratigraphic context, which combine to produce high-precision of RSL reconstructions and extends applicability of the methodology (Cahill et al., 2016; Holden et al., 2017). We assign stratigraphic context as informative priors with ranges from either organic-rich high salt marsh, which accumulates at elevations around MHW to the highest occurrence of foraminifera or clastic dominated (tidal flat) to low salt-marsh sediment, which accumulates at elevations between mean low water (MLW) and MHHW (20-200 SWLI, Kemp et al., 2018).

3.2 Modeling methods

3.2.1 Basic assumptions

To model coseismic subsidence deformation, we use a 3D megathrust combined fault geometry of McCrory et al., (2004), Gao et al., (2017), and Hays et al., (2018). Coastal paleoseismic estimates of coseismic subsidence are the only constraints for past megathrust rupture in Cascadia. Therefore, the data coverage is in a margin-normal orientation and can only provide limited data on the downdip extent of rupture. Previous Cascadia modeling efforts (Hyndman and Wang, 1993; 1995; Satake et al., 2003; Priest et al., 2010; and Leonard et al., 2010; Wang et al., 2013) have used the 450°C isotherm to limit the down dip rupture extent. However, the

450°C isotherm has been breached in recent earthquakes, e.g., 2003 8.3 M_w Hokkaido, Japan and by attempting to confine rupture in-between the deformation front and 450°C isotherm we were unable to fit modeled rupture to the coastal paleoseismic coseismic estimates. Therefore, we used the 450°C isotherm as a guide to limit down dip slip. Following previous modeling efforts (e.g., Wang et al., 2003; Satake et al., 2003; and Priest et al., 2010), all model runs the coseismic slip is assumed to be in the convergence direction between Juan de Fuca plate and the Cascadia forearc as Wang et al., (2013).

3.2 Slip distribution and strike direction

We are attempting to assess along-strike slip variation according to the updated foraminiferal-based BTF paleogeodetic estimates from Kemp et al., 2018, a new northern Humboldt Bay estimate of Padgett et al., (*in-prep*), and our six new subsidence estimates from southwest Washington. Slip is assigned with the bell-shape distribution in a strike normal orientation (equation) in Wang et al (2013). Where possible we represent slip in the simplest manner possible, i.e., elliptical patches with strike-normal bell-shaped slip distributions. We follow Wang et al., (2013), with patches orientated such that the principle axis are approximately parallel to the local strike. Where the geometry of the strike inhibits an ellipse, e.g., southern Vancouver Island and the Olympic Peninsula, we try different rupture patch shapes in our attempts to fit the updated paleogeodetic database.

3.3 Modeling procedure

There are written observations of damage and flooding that report tsunami heights reached 1-5 m during the 1700 CE Cascadia tsunami at seven locations in

Japan (Satake et al, 2003). Satake et al., (2003) tested several uniform-slip Cascadia rupture model scenarios that could replicate these tsunami heights in Japan. Although the models could not resolve rupture details, they do provide constraints on rupture size and indicate that a moment magnitude on the order of 8.7-9.2 is required. Therefore, we limited the modeled scenarios to this magnitude range.

Models presented in this paper are summarized in Table 2. Following Wang et al., (2013), coseismic slip is measured in terms equivalent to slip accumulation time multiplied by the convergence rate. We attempt to fit the paleoseismic coseismic subsidence estimates with four different rupture scenarios. Following Wang et al., (2013), we apply slip the simplest way using elliptical patches where slip is distributed with peak slip at the center and tapers towards the edges of the patch. We also follow Wang et al. (2013) by using the $(W/Wmax)^2$ equation for the elliptical patches where W is the local width and Wmax is the maximum width. For the non-the elliptical patches, slip is applied in a similar fashion as the uniform slip distribution models (Wang et al., 2013). However, for the non-elliptical northern patches (Figs. 8-9), slip is assigned using $(W/Wmax)^2$ scaling factor of 30% from the north end of the patch and 5% from the south end of the patch, which extends the gradient of slip distribution from peak slip to the edge of the rupture patch. We then apply uniform slip in-between the northern and southern peak slip locations.

Even though we have addressed a spatial data gap of coseismic subsidence estimates in southwestern Washington, there are still substantial data gaps from northern California to southern Oregon, northwest Washington to Vancouver Island, Canada. The model assumes that slip is constant between subsidence estimate

constraints. Future paleoseismic investigations that address these remaining spatial gaps will likely impact the rupture model scenarios.

4. STRATIGRAPHIC RESULTS

Based on stratigraphic mapping we observed *mud-over-peat* and *mud-over-forest soil* contacts at six marshes; three in Grays Harbor and three in Willapa Bay, which collectively span across southwest Washington's Pacific coast. In hand-augured cores we observed, dark organic-rich units overlain in sharp contact to grey mud units. In general, the organic-rich units contain relatively abundant plant macrofossils and the clastic muds contained sparse plant macrofossils and were often massive and occasionally finely bedded. We observed sand layers in-between an organic-rich unit and overlying mud at three locations (Copalis River, Johns River and Ocean Shores). At each marsh, we map the shallowest organic-rich unit within marsh locations, correlate stratigraphy within marshes based on our mew mapping (Fig. 2) and select representative sediment cores for foraminiferal analyses. By applying the BTF to fossil foraminiferal assemblages, we derived quantitative coseismic-subsidence estimates from RSL reconstructions (Table1; Figs. 3-6). Pairwise comparison of modern and fossil foraminiferal assemblages were below the 20th percentile threshold, indicating that all fossil assemblages had modern analogs. Below, we describe the stratigraphic and biostratigraphic characteristics which influenced the RSL reconstructions of each core analyzed within this investigation.

4.1 Relative sea-level reconstructions

We refine the paleogeodetic database of Wang et al., (2013) by contributing subsidence estimates from six new locations from this investigation as well as incorporating the updated BTF estimates from Kemp et al., (2018; Table 1) and exclude locations that lack transfer function estimates of subsidence but the new models are consistent with the broad estimate error ranges. The new paleogeodetic database replaces two of four non-transfer function estimates from Wang et al., (2013) with BTF estimates (Johns River and Humboldt Bay).

4.1.1 Copalis River

At Copalis River, we sampled a buried organic rich unit that was abruptly (contact <2 mm) buried by a medium-fine grain sand during the 1700 CE earthquake (Atwater 1987, Atwater et al., 1992). The shallowest buried organic rich unit is 8-~20 cm thick is at ~1.0-1.6 m core depths and consists of a dark brown muddy organic-rich unit that a western red cedar "ghost forest' is rooted into ~4-6.5 km up stream (Atwater et al., 1992).

At *CR.01*, the upper contact of the shallowest buried organic-rich is at 71.5 cm core depth (Fig. 3a). The picture and CT image of *CR.01* show an abrupt 1-2 mm contact with ~5 mm of relief. The contact is overlain by a 3 cm thick sand, that sharply grades (~6mm) into a mud unit. Foraminifera in the mud unit dominantly consist of *Haplophragmoides spp.* (27-48%), *T. inflata* (11-44%), and *M. fusca* (14-27%), which is consistent with sediments accumulating below MHW (Kemp et al., 2018). The organic-rich unit is 8 cm thick and grades from a dark brown soil unit to light brown muddy organic rich unit at the base. There are no foraminifera present within the organic-rich unit. Due to the lack of fossil foraminifera within the organic-rich unit we

interpret that the organic-rich unit represents a depositional environment that formed above the highest occurrence of foraminifera (HOF; Kemp et al., 2018). Therefore, using the first interval that contains in-situ fossil foraminifera above the organic-rich unit and tsunami sand, we subtract the reconstructed RSL elevation predicted by the BTF from the elevation of the highest occurrence of foraminifera in Copalis River estuary, which is 3.39 m (NAVD 88). This results in a limiting estimate for subsidence of ≥0.91 m.

4.1.2 Ocean Shores

At *OCE.15.*Y3, the shallowest buried organic-rich unit upper contact is at 60.5 cm core depth (Fig. 3b). The photo and CT imagery display an abrupt contact, 2 mm that undulates with 5 mm of relief, as well as 2-3 cm of denser sediments at the base of the >25 cm thick overlying grey mud unit. Foraminifera in the mud unit dominantly consist of *Haplophragmoides spp.* (38-44%) and *J. macrescens* (18-35%) but also contain *M. fusca* (10-15%), which is consistent with sediments accumulating below MHW (Kemp et al., 2018). The organic-rich unit is 12 cm thick black to dark brown soil. There are no foraminifera present within the organic-rich unit. Due to the lack of fossil foraminifera within the organic-rich unit we interpret that the organic-rich unit represents a depositional environment that formed above HOF. Therefore, using the first interval that contains in-situ fossil foraminifera above the organic-rich unit, we subtract the reconstructed RSL elevation predicted by the BTF from the elevation of the highest occurrence of foraminifera at Ocean Shores, which is 3.39 m (NAVD 88). This results in a limiting estimate for subsidence of ≥0.82 m.

4.1.3 Johns River

We collected two sediment cores at Johns River (one from the west and one from the east side of the river) using the Johns River stratigraphy of Shennan et al., (1996) as a guide. Shennan et al. (1996), describe the shallowest buried organic rich unit as a "well-developed peat", observed it at 15 of 19 core sites, and report a 2 cm thick layer of sand on the contact at a core from the north-eastern side of the river. Reinhart (1992) also report sand over the shallowest buried organic-rich unit at several core sites on the north-eastern side of the main channel of river.

At *JR.17.01*, the upper contact of the shallowest buried organic-rich unit is at 101 cm core depth (Fig. 4a). The organic-rich unit is 8 cm thick and ranges from a dark brown peat to a grey brown muddy peat. Foraminifera in the peat unit dominantly consist of *Haplophragmoides spp.* (46-51%) and *B. pseudomacrescens* (12-31%), which is consistent with a peat soil forming near MHHW. The overlying grey mud unit is >25 cm thick. Foraminifera in the mud unit dominantly consist of *M. fusca* (34-40%) and *Haplophragmoides spp.* (26-32%) which is consistent with sediments accumulating below MHW (Kemp et al., 2018). For the subsidence estimate, we use the reconstructed RSL elevations that are 2 cm apart, which are the first full centimeter intervals above and below the contact that avoid the relief of the *mud-over-peat* contact. The fossil foraminifera BTF reconstruction shows 0.39 ±0.37 m of subsidence.

At *JR.15.101*, the upper contact of the shallowest buried organic-rich unit is at 73.5 cm core depth (Fig. 4b). the photo and CT image show an abrupt, ~2 mm, contact with has 4 mm of relief. The overlying grey mica-rich mud has grey-brown mottles ≤10 mm thick. Foraminifera in the mud unit dominantly consist of *Haplophragmoides*

(32-50%), *B. pseudomacrescens* (13-18%), *T.* inflata (13-26%) and *M. fusca* (16-20%), but also contain *Reophax spp.* (0-3%), which is consistent with sediments accumulating below MHW (Kemp et al., 2018). The dark brown to black organic-rich unit is 6 cm thick. There are no foraminifera present within the organic-rich unit. Due to the lack of fossil foraminifera within the organic-rich unit we interpret that the organic-rich unit represents a depositional environment that formed above HOF. Therefore, using the first interval that contains in-situ fossil foraminifera above the organic-rich unit, we subtract the reconstructed RSL elevation predicted by the BTF from the elevation of the highest occurrence of foraminifera in Johns River estuary, which is 3.27 m (NAVD 88). This results in a limiting estimate for subsidence of ≥0.80 m.

4.1.4 Smith Creek

At *SC.17.03*, the shallowest buried organic-rich units sharp upper contact is at 77 cm core depth and has 5 mm of relief (Fig. 5a). The dark brown-black organic-rich unit is 7 cm thick. Fossil foraminifera in the organic-rich unit dominantly consist of *Haplophragmoides spp.* (30-45%), *J. macrescens* (23-36%), and *B. pseudomacrescens* (15-20%), which is consistent with a peat soil forming above MHHW. The overlying mica-rich grey to light brown mud is >25 cm thick. Foraminiferal assemblages within the mud unit dominantly consist of *M. fusca* (57-69%) with *Haplophragmoides spp.* (7-26%) but also contain *Ammobaculites spp.* (7-12%), which is consistent with sediments accumulating between MTL and MHW (Kemp et al., 2018). For the subsidence estimate, we use the reconstructed RSL elevations that are 3 cm apart, which are the first full centimeter intervals above and below the contact that avoid the

relief of the *mud-over-peat* contact. The fossil foraminiferal BTF reconstruction is 1.52 ±0.51 m of subsidence.

4.1.5 Bone River

At *BR.15.06*, the upper contact of the shallowest buried organic-rich unit is at 109 cm core depth (Fig. 5b). The picture and CT imagery show a sharp contact with 14 mm of relief. The organic-rich unit is 23 cm thick that grades from a dark brown-black peat to a brown muddy peat towards the base of the unit. Fossil foraminifera in the organic-rich unit dominantly consist of *B. pseudomacrescens* (40-55%) and *Haplophragmoides spp.* (31-41%), which is consistent with a high salt marsh peat. The overlying grey mud is >25 thick an contains laminations 2-5 mm thick ≤ 12 cm above the lower contact. Foraminifera light brown-grey rooted mud dominantly consist of *M. fusca* (57-74%), but also contains *B. pseudomacrescens* (9-22%) which optima elevation overlap around MHW (Kemp et al., 2018). For the subsidence estimate, we use the reconstructed RSL elevations that are 2 cm apart, which are the first full centimeter intervals above and below the contact that avoid the relief of the *mud-over-peat* contact. The fossil foraminiferal BTF reconstruction is 0.91 ±0.50 m of subsidence.

4.1.6 Naselle River

At *NR.15.05*, the upper contact of the shallowest buried organic-rich unit is sharp, ~5 mm, at 80.5 cm core depth, and has 14 mm of relief (Fig. 6a). The overlying dark grey mud is >25 cm thick and contains sporadic organics. Foraminifera assemblages in the grey mud unit dominantly consist of *M. fusca* (72-80%), which is consistent with sediments accumulating between MTL and MHW. The black organic-

rich unit is 19 cm thick. There are no foraminifera within the organic-rich unit, therefore we interpret that the organic-rich unit represents a depositional environment that formed above HOF. We use the first interval that contains in-situ fossil foraminifera above the organic-rich unit and subtract the reconstructed RSL elevation predicted by the BTF from the elevation of the highest occurrence of foraminifera at Naselle River estuary, which is 3.84 m (NAVD 88). This results in a limiting estimate for subsidence of ≥1.38 m.

At *NR.15.11*, the upper contact of the shallowest buried organic-rich unit is abrupt at 101 cm core depth and has 4 mm of relief (Fig. 6b). The overlying dark grey mud is >25 cm thick and contains orange mottles. Foraminifera assemblages within the grey mud dominantly consist of *Haplophragmoides spp.* (24-31%), *T. inflata* (20-30%), and *M. fusca* (25-28%), which is consistent with sediments accumulating below MHW. The black organic-rich unit is 12 cm thick. Foraminifera assemblages within organic-rich unit dominantly consist of *Haplophragmoides spp.* (58-70%) and *J. macrescens* (23-36%), which is consistent with a peat forming above MHHW. For the subsidence estimate, we use the reconstructed RSL elevations that are 2 cm apart, which are the first full centimeter intervals above and below the contact that avoid the relief of the *mud-over-peat* contact. The fossil foraminifera BTF reconstruction shows 0.74 ±0.47 m of subsidence.

4.2 Modeling results

We first reconstruct the preferred rupture model of Wang et al., (2013) with the newly integrated fault geometry and updated deformation front (Sypus, *in-prep*). The mid points of the preferred model of Wang et al., (2013) overlapped with all of the

coastal paleogeodetic coseismic subsidence estimates. However, within the 200-700 year deficit window for the preferred model of Wang et al., (2013) overlaps with only 85% of the BTF estimates and only 75% of the paleoseismic subsidence estimates overlap with modelled deformation midpoints (Fig. 7). In order to fit the modeled deformation to the coastal estimates, we try 4, 5, and 6 slip patch rupture solutions (Figs. 8-10). For the rest of the paper, per each model, we refer to the rupture patches in ascending order, south to north.

In the first model we modified the four-patch scenario (Fig. 8). All BTF subsidence estimates overlap with the 200-700 year deficit window and ~89% of the BTF estimates overlap with the midpoint of the modeled deformation. We attempted to increase the fit to the modeled coastal deformation by bringing slip patches 1, 2, and 3 further east. The new fault geometry requires a small change in strike for patches 1 and 2 with increasing landward orientation. The shape of patch 3 has a shortened ~north-south axis and slip accumulation is set to 550 years, in order to distribute relatively high slip proximal to Siletz, Salmon River, and Nestucca, which is in-between low slip of Alsea and Netarts. By applying slip in a more uniform distribution along strike across patch 4, the modeled coastal deformation was able to fit the estimated coastal deformation with an overall thinner down dip patch but the patch. We also had to move the patch further east in the southwest corner to fit the large (>1m) Nehalem estimate. Although, the five patch (Fig. 9) and six patch rupture scenarios (Fig 10) do not improve the modeled deformation overlap with subsidence estimate ranges from the modified four patch rupture scenario, they do combine to exemplify the non-unique nature of the rupture solutions to fit the coastal constraints.

Although future work will improve the overlap between the modeled deformation 200-700 year slip deficit window and the coseismic subsidence estimate ranges, the simplest slip distribution model that fits the coastal estimates is the aim.

4.2.1 Limitations of the Current Paleogeodetic Database

A difficulty for all the CSZ rupture scenario models presented here is attempting to distribute slip across adjoining high- and low- slip areas; e.g., Nehalem (1.16 ±0.55 m) and Netarts (0.39 ±0.41 m). Are such differences in the high and low estimates the result of heterogeneity in coseismic deformation or are such differences in the high and low estimates the result of intra site variability in the estimates?

It is reasonable for coastal paleogeodetic investigations to anticipate that sites closer together, within the same fault segment, should have similar coseismic subsidence for the same earthquake sequence. However, at northern Humboldt Bay, California, Padgett et al., (in-prep), observe inter-site averaged foraminiferal BTF coseismic subsidence estimate variability to be as much as 0.59 m across a 6 km estuary-wide transect. Based on their variability and assessment results, Padgett et al., (in-prep) suggest at least two (and ideally three) quantitative microfossil RSL reconstructions will increase confidence in an coseismic subsidence estimate.

Therefore, replicated microfossil reconstruction across the same marsh as performed here (Johns River and Naselle River) provides confidence in the assigned subsidence estimates (e.g., Padgett et al., *in-prep*). With the exceptions of Johns River, Naselle River, Nestucca, Alsea and northern Humboldt Bay, most estimates within the updated BTF paleogeodetic database have not been replicated. If replicate reconstructions were conducted at locations where only one RSL reconstruction exists,

the results would substantiate and perhaps refine our understanding of slip distribution for the CSZ 1700 CE earthquake.

5. REMAINING GAPS IN OUR KNOWLEDGE OF CSZ 1700 CE EARTHQAUKE

5.1 Spatial Gaps

Inherently rupture models are spatially biased around data constraints and models must interpolate deformation in-between data points. Although, it is the goal to have dense and margin-wide data coverage, there are geographical limitations to where constraints can be obtained. The accommodation space along the Cascadia coastline is not constant north-to south (e.g., Engelhart et al., 2015; Dura et al., 2016) and there are several coastal stretches where RSL over the late Holocene has not permitted wetland stratigraphy to continuously accumulate. For example, Dura et al., (2016) show that the Cascadia coastline has been experiencing two different GIA relaxation regimes over the late Holocene; near-field RSL fall from northwestern Vancouver Island south to the Olympic peninsula in northwest Washington, and intermediate-field RSL rise from southern Washington south to northern California. Moreover, there are additional complications within these two zones, e.g., intermittent headland uplift punctuated in-between coastal low-land areas (e.g., Kelsey, 1990; Kelsey and Bockheim, 1994; Kelsey et al., 1994, 1996). However, there are sites along the Cascadia coastline that could potentially increase our understanding of past CSZ rupture patterns.

Although we have supplemented the CSZ 1700 CE paleogeodetic database, there remain several sites that likely archive past CSZ deformation and would address

spatial data gaps within the paleogeodetic database. For example in southern Cascadia, the Coquille River and northern Humboldt Bay are separated by ~275 km along strike and in-between there are several coastal paleoseismic sites that not have quantitative microfossil RSL reconstructions, e.g., including Euchre Creek (~42.55° N) and Sand Mine Marsh (~41.74° N). Moreover, positioned south of Nehalem Bay and north of Netarts Bay, Tillamook Bay is a relatively large bay with two salt marshes separated by ~8 km along strike; Miami Cove marsh near Garibaldi, Oregon and the marsh at the confluence of Wilson River and Tillamook River near Tillamook, Oregon. The aforementioned spatial gaps are areas that represent areas with large uncertainties of 3-D elastic dislocation models and are close to hypothetical patch boundaries.

5.2 Limiting data

Within the updated BTF paleogeodetic database there are five minimum subsidence estimates; Copalis River, Johns River, Naselle River, South Slough, and Coquille. Minimum coseismic subsidence estimates are derived from subsidence stratigraphy, where the buried organic-rich units are forest soils that do not contain fossil foraminifera but the intertidal sediments that bury the forest soil are within the intertidal zone (e.g., Hawkes et al., 2010; Engelhart et al., 2013). Forest soils do not contain foraminifera because it is an environment that forms above the upper limit of foraminiferal habitation. Therefore, at locations with buried forest soil units, other microfossil groups can provide additional constraints on RSL reconstructions and confidence in an assigned subsidence estimate for an estuary. For example, diatom species not only span intertidal elevations but also freshwater and upland environments, which implies that fossil diatom assemblages can provide elevation

information beyond the elevation range of foraminifera (Hemphill-Haley, 1995; Shennan et al., 1996; Atwater and Hemphill-Haley, 1997; Sawai, 2001; Dura et al., 2016, 2017). Quantitative diatom RSL reconstructions will be able to substantiate and refine a subsidence estimate derived from a quantitative foraminifera transfer function reconstruction. For example, fossil pollen and diatom data from Johns River (Shennan et al., 1996) that suggest 1.0 ± 0.5m of subsidence support our BTF limiting estimate of ≥0.80 m. Multiple microfossil reconstructions will provide additional confidence in an assigned coseismic deformation estimate for an estuary (Shennan and Hamilton, 2006; Shennan et al., 2014; Padgett et al., *in-prep*).

5.3 Stratigraphic mixing or pre- and post-seismic transient deformation

Do wetland stratigraphic sequences archive a record of pre- and post-seismic land movements (e.g., Shennan and Hamilton, 2006; Horton et al., 2017)? Can mixing of the microfossil record influence our reconstructions by causing centimeter to decimeter variations (e.g., Milker et al., 2016)? Arguments for mixed microfossil assemblages below contacts can be based on the consistency of RSL reconstructions and/ or optical inspection and density imagery. The role of sedimentation, e.g., mixed, when, and how much, is integral to the arguments attempting to address post seismic (above contact) uncertainties.

The possibility that wetland stratigraphy records pre seismic elevation changes has been explored in diatom-based transfer function investigation in Alaska (Shennan and Hamilton, 2006), and foraminiferal-based transfer functions in Cascadia (Nelson et al., 1998; Engelhart et al., 2013; Milker et al., 2016). Shennan and Hamilton (2006) interpret that mixed assemblages below subsidence contacts are not the result of

random pore space infiltration based on the fact that all reconstructions show negative RSL trends. However, mixed microfossil assemblages below subsidence contacts have also been observed in Cascadia stratigraphic sequences (Nelson et al., 1998; Engelhart et al., 2013; Milker et al., 2016) where overlying mud infiltration is observed through optical inspections, density imagery, and microfossil assemblages. Instead of replicate reconstructions Cascadia research has addressed physical mixing below a contact through the development of informative prior assignments in Bayesian transfer functions (Kemp et al., 2018). However, the assignment of an informative prior above a subsidence contact cannot fully address the possibility of a mixed intervals.

Postseismic land level change is difficult to assess in wetland stratigraphy due to the lack of in-situ short-lived datable material accumulation and the time resolution of stratigraphic intervals (10's of years). If salt marshes experienced postseismic land-level changes, it would most likely be encapsulated in the subsidence estimate, which is commonly driven by the microfossil assemblages directly above subsidence contacts except where thee is evidence for mixing above the contact or when tsunami deposits overly a subsidence contact. Therefore, post seismic sedimentation rates and re-habitation time-lag for microfossil groups can influence quantitative RSL reconstructions (Atwater et al., 2001; Milker et al., 2016; Horton et al., 2017: Padgett et al., *in-prep*). For example, rapid post-seismic sedimentation was documented by Atwater et al., (2001), who report sedimentation of 1.4 ±0.2 m thickness over first the 9 years since the 1964 Alaska earthquake and ~1.6 ±0.3 m over 34 years after the 1964 earthquake at a site near Portage, Alaska. These observations imply that the sediment contained within 1 cm interval above the subsidence contact could represent

<one month, which is an order of magnitude different at >1.4 m above the subsidence contact where a 1 cm interval can represent ~10 years.

However, even if sedimentation resumes instantaneously, further complications related to the response time of microfossil groups may impact our reconstructions. Based on an experiment at a reclaimed marsh in southern Oregon, the time of year that an earthquake occurs may also influence a quantitative microfossil RSL reconstruction (Horton et al., 2017). At Ni-les'tun marsh, Oregon, foraminiferal abundances responded to the flooding of reclaimed pasture land after two weeks but did not reach equilibrium with their new tidal elevation for 11 months. In contrast, diatom response time was observed to be 2 weeks and moved rapidly towards equilibrium (Horton et al., 2017). Horton et al., (2017) suggest that this difference may be due to timing of foraminiferal reproduction that typically occurs in late spring and early summer and prior to the flooding of the site in August. However, the study is limited by the analysis of only a single site and the very low sediment accumulation rate (1cm/yr) that is unlikely to be analogous to sedimentation after an earthquake (e.g., Atwater et al., 2001; Benson et al., 2001). Therefore, depending on sediment availability and the time of year that an earthquake occurs, foraminiferal transfer function RSL reconstructions could cause an under- or over-estimate of coseismic deformation depending on the direction of postseismic land motion (Horton et al., 2017). As with coseismic land-level changes, postseismic land-level changes are likely to be reproducible within a marsh because the elevation changes should be fairly constant across the small spatial scale (typically less than a few km) of a site (e.g.,

Shennan et al., 2016). Moreover, inter site variability is likely to vary across sites due to the possibility of varying sediment availability across marshes.

5. CONCLUSIONS

Using fossil foraminifera and BTF we estimate coseismic subsidence during the CSZ 1700 CE earthquake, derived from stratigraphic sequences beneath six tidal marshes along a ~75 km transect in southern Washington. Estimates of coseismic subsidence at Smith Creek (1.52 ±0.51 m), Bone River (0.91 m ±0.50), and Naselle River (0.74 ±0.47 m) are larger than estimates at Johns River (0.39 ±0.36 m). At Copalis River, Ocean Shores, Johns River (replicate), and Naselle River (replicate) we can only make minimum estimates of coseismic subsidence, respectively, ≥0.91 m, ≥0.82 m, ≥0.80 m, and ≥0.91 m, and ≥1.38 m. Locations with minimum foraminiferal-based estimates would benefit from either foraminiferal- based RSL reconstruction across a buried salt marsh peat unit and/or a quantitative diatom-based RSL reconstruction(s).

The six new site estimates of the CSZ 1700 CE earthquake from southwest Washington are added to a margin-wide BTF paleogeodetic database (of 14 site estimates), which increases the number of measurements by 43% to a total of 20 estimates margin wide. Southwest Washington now has a similar density of quantitative foraminiferal-based coseismic subsidence estimates as northern and central Oregon. Within the CSZ 1700 CE paleogeodetic database, sites where previous non-quantitative subsidence estimates were derived, the updated BTF subsidence generally agree, e.g., northern Humboldt Bay. However, at several locations, the

updated BTF estimates are larger than previous foraminiferal-based paleogeodetic estimates using a previous transfer function, e.g., Nehalem, Nestucca, and Salmon River. These differences taken together with the new coverage in southern Washington, necessitate refinement to the preferred four-patch rupture model (Wang et al., 2013; Kemp et al., 2018). We developed three alternate 3-D elastic dislocation models that improve the fit between the quantitative coastal estimates and the modelled coseismic deformation, which produce multiple non-unique slip distribution solutions. Even with the new coseismic subsidence constraints, a four-patch model is still the best hypothetical solution but with different slip within the patches . Our results highlight the need for additional high-quality subsidence estimates from locations in-between high-slip and low-slip patches such as Nehalem-Netarts (Tillamook Bay, ~45.5° N), and within remaining geospatial gaps, for example in-between Coquille and northern Humboldt Bay (~43.1° N to ~40.9° N).

REFERENCES

Atwater, B.F., 1987. Evidence for great Holocene earthquakes along the outer coast of Washington State. *Science*, *236*(4804), pp.942-944.

Atwater, B.F. and Yamaguchi, D.K., 1991. Sudden, probably coseismic submergence of Holocene trees and grass in coastal Washington State. *Geology*, *19*(7), pp.706-709.

Atwater, B.F., 1992. Geologic evidence for earthquakes during the past 2000 years along the Copalis River, southern coastal Washington. *Journal of Geophysical Research: Solid Earth*, *97*(B2), pp.1901-1919.

Atwater, B.F., Nelson, A.R., Clague, J.J., Carver, G.A., Yamaguchi, D.K., Bobrowsky, P.T., Bourgeois, J., Darienzo, M.E., Grant, W.C., Hemphill-Haley, E. and Kelsey, H.M., 1995. Summary of coastal geologic evidence for past great earthquakes at the Cascadia subduction zone. *Earthquake spectra*, *11*(1), pp.1-18.

Atwater, B.F. and Hemphill-Haley, E., 1997. *Recurrence intervals for great earthquakes of the past 3,500 years at northeastern Willapa Bay, Washington* (No. 1576). USGPO; Information Services [distributor].

Atwater, B.F., Yamaguchi, D.K., Bondevik, S., Barnhardt, W.A., Amidon, L.J., Benson, B.E., Skjerdal, G., Shulene, J.A. and Nanayama, F., 2001. Rapid resetting of an estuarine recorder of the 1964 Alaska earthquake. *Geological Society of America Bulletin*, *113*(9), pp.1193-1204.

Atwater, B.F., Musumi-Rokkaku, S., Satake, K. Tsuji, Y., Ueda, K., and Yamaguchi, D.K., 2005, The orphan tsunami of 1700--Japanese clues to a parent earthquake in North America, U.S. Geological Survey Professional Paper 1707, 133 pp. (published jointly by University of Washington Press, Seattle).

Barlow, N.L., Shennan, I., Long, A.J., Gehrels, W.R., Saher, M.H., Woodroffe, S.A. and Hillier, C., 2013. Salt marshes as late Holocene tide gauges. *Global and Planetary Change*, *106*, pp.90-110.

Benson, B.E., Atwater, B.F., Yamaguchi, D.K., Amidon, L.J., Brown, S.L. and Lewis, R.C., 2001. Renewal of tidal forests in Washington State after a subduction earthquake in AD 1700. *Quaternary Research*, *56*(2), pp.139-147.

Briggs, R.W., Engelhart, S.E., Nelson, A.R., Dura, T., Kemp, A.C., Haeussler, P.J., et al., 2014, Uplift and subsidence reveal a nonpersistent megathrust rupture boundary (Sitkinak Island, Alaska): Geophysical Research Letters, doi:10.1002/(ISSN)1944-8007.

Cahill, N., Kemp, A.C., Horton, B.P. and Parnell, A.C., 2016. A Bayesian hierarchical model for reconstructing relative sea level: from raw data to rates of change. *Climate of the Past*, *12*(2), pp.525-542.

Darienzo, M.E. and Peterson, C.D., 1990. Episodic tectonic subsidence of late Holocene salt marshes, northern Oregon central Cascadia margin. *Tectonics*, *9*(1), pp.1-22.

Davies, M.H., Mix, A.C., Stoner, J.S., Addison, J.A., Jaeger, J., Finney, B. and Wiest, J., 2011. The deglacial transition on the southeastern Alaska Margin: Meltwater input, sea level rise, marine productivity, and sedimentary anoxia. *Paleoceanography and Paleoclimatology*, *26*(2).

de Rijk, S., 1995. Salinity control on the distribution of salt marsh foraminifera (Great Marshes, Massachusetts). *The Journal of Foraminiferal Research*, *25*(2), pp.156-166.

Dura, T., Horton, B.P., Cisternas, M., Ely, L.L., Hong, I., Nelson, A.R., Wesson, R.L., Pilarczyk, J.E., Parnell, A.C. and Nikitina, D., 2017. Subduction zone slip variability during the last millennium, south-central Chile. *Quaternary Science Reviews*, *175*, pp.112-137.

Dura, T., Hemphill-Haley, E., Sawai, Y. and Horton, B.P., 2016. The application of diatoms to reconstruct the history of subduction zone earthquakes and tsunamis. *Earth-Science Reviews*, *152*, pp.181-197.

Engelhart, S.E., Horton, B.P., Nelson, A.R., Hawkes, A.D., Witter, R.C., Wang, K., Wang, P.L. and Vane, C.H., 2013. Testing the use of microfossils to reconstruct great earthquakes at Cascadia. *Geology*, *41*(10), pp.1067-1070.

Engelhart, S.E., Vacchi, M., Horton, B.P., Nelson, A.R. and Kopp, R.E., 2015. A sea-level database for the Pacific coast of central North America. *Quaternary Science Reviews*, *113*, pp.78-92.

Fatela, F. and Taborda, R., 2002. Confidence limits of species proportions in microfossil assemblages. *Marine Micropaleontology*, *45*(2), pp.169-174.

Gao, D., Wang, K., Davis, E.E., Jiang, Y., Insua, T.L. and He, J., 2017. Thermal state of the Explorer segment of the Cascadia subduction zone: Implications for seismic and tsunami hazards. *Geochemistry, Geophysics, Geosystems*, *18*(4), pp.1569-1579.

Goldfinger, C., Nelson, C.H., Morey, A., Johnson, J.E., Gutierrez-Pastor, J., Eriksson, A.T., Karabanov, E., Patton, J., Gracia, E., Enkin, R., Dallimore, A., Dunhill, G., Vallier, T., 2012, Turbidite event history: Methods and implications for

Holocene paleoseismicity of the Cascadia subduction zone: USGS Professional Paper 1661-F, 184 pp.

Guilbault, J.P., Clague, J.J. and Lapointe, M., 1995. Amount of subsidence during a late Holocene earthquake—evidence from fossil tidal marsh foraminifera at Vancouver Island, west coast of Canada. *Palaeogeography, Palaeoclimatology, Palaeoecology*, *118*(1), pp.49-71.

Guilbault, J.P., Clague, J.J. and Lapointe, M., 1996. Foraminiferal evidence for the amount of coseismic subsidence during a late Holocene earthquake on Vancouver Island, west coast of Canada. *Quaternary Science Reviews*, *15*(8), pp.913-937.

Hawkes, A.D., Horton, B.P., Nelson, A.R. and Hill, D.F., 2010. The application of intertidal foraminifera to reconstruct coastal subsidence during the giant Cascadia earthquake of AD 1700 in Oregon, USA. *Quaternary International*, *221*(1), pp.116-140.

Hawkes, A.D., Horton, B.P., Nelson, A.R., Vane, C.H. and Sawai, Y., 2011. Coastal subsidence in Oregon, USA, during the giant Cascadia earthquake of AD 1700. *Quaternary Science Reviews*, *30*(3), pp.364-376.

Hemphill-Haley, E., 1995. Diatom evidence for earthquake-induced subsidence and tsunami 300 yr ago in southern coastal Washington. *Geological Society of America Bulletin*, *107*(3), pp.367-378.

Holden, P.B., Birks, H.J.B., Brooks, S.J., Bush, M.B., Hwang, G.M., Matthews-Bird, F., Valencia, B.G. and Van Woesik, R., 2017. BUMPER v1. 0: a Bayesian user-friendly model for palaeo-environmental reconstruction.

Horton, B.P. and Edwards, R.J., 2005. The application of local and regional transfer functions to the reconstruction of Holocene sea levels, north Norfolk, England. *The Holocene*, *15*(2), pp.216-228.

Horton, B.P., Milker, Y., Dura, T., Wang, K., Bridgeland, W.T., Brophy, L., Ewald, M., Khan, N.S., Engelhart, S.E., Nelson, A.R. and Witter, R.C., 2017. Microfossil measures of rapid sea-level rise: Timing of response of two microfossil groups to a sudden tidal-flooding experiment in Cascadia. *Geology*, *45*(6), pp.535-538.

Hyndman, R.D. and Wang, K., 1993. Thermal constraints on the zone of major thrust earthquake failure: The Cascadia subduction zone. *Journal of Geophysical Research: Solid Earth*, *98*(B2), pp.2039-2060.

Hyndman, R.D. and Wang, K., 1995. The rupture zone of Cascadia great earthquakes from current deformation and the thermal regime. *Journal of Geophysical Research: Solid Earth*, *100*(B11), pp.22133-22154.

Kelsey, H.M., 1990. Late Quaternary deformation of marine terraces on the Cascadia subduction zone near Cape Blanco, Oregon. *Tectonics*, *9*(5), pp.983-1014.

Kelsey, H.M. and Bockheim, J.G., 1994. Coastal landscape evolution as a function of eustasy and surface uplift rate, Cascadia margin, southern Oregon. *Geological Society of America Bulletin*, *106*(6), pp.840-854.

Kelsey, H.M., Engebretson, D.C., Mitchell, C.E. and Ticknor, R.L., 1994. Topographic form of the Coast Ranges of the Cascadia margin in relation to coastal uplift rates and plate subduction. *Journal of Geophysical Research: Solid Earth*, *99*(B6), pp.12245-12255.

Kelsey, H.M., Ticknor, R.L., Bockheim, J.G. and Mitchell, E., 1996. Quaternary upper plate deformation in coastal Oregon. *Geological Society of America Bulletin*, *108*(7), pp.843-860.

Kelsey, H.M., Witter, R.C. and Hemphill-Haley, E., 2002. Plate-boundary earthquakes and tsunamis of the past 5500 yr, Sixes River estuary, southern Oregon. *Geological Society of America Bulletin*, *114*(3), pp.298-314.

Kemp, A.C., and Telford, R.J. 2015. Transfer functions. *Handbook of Sea-Level Research.* I Shennan, A.J. Long and B.P. Horton (Editors), John Wiley and Sons, Chichester, United Kingdom, pp.470-99.

Kemp, A.C., Cahill, N., Engelhart, S.E., Hawkes, A.D. and Wang, K., 2018. Revising Estimates of Spatially Variable Subsidence during the AD 1700 Cascadia Earthquake Using a Bayesian Foraminiferal Transfer Function. *Bulletin of the Seismological Society of America*, *108*(2), pp.654-673.

McCrory, P.A., Blair, J.L., Oppenheimer, D.H. and Walter, S.R., 2004. Depth to the Juan de Fuca slab beneath the Cascadia subduction margin: A 3-D model for sorting earthquakes.

McCrory, P.A., Blair, J.L., Waldhauser, F. and Oppenheimer, D.H., 2012. Juan de Fuca slab geometry and its relation to Wadati-Benioff zone seismicity. *Journal of Geophysical Research: Solid Earth*, *117*(B9).

Milker, Y., Horton, B.P., Vane, C.H., Engelhart, S.E., Nelson, A.R., Witter, R.C., Khan, N.S. and Bridgeland, W.T., 2015. Annual and seasonal distribution of intertidal foraminifera and stable carbon isotope geochemistry, Bandon Marsh, Oregon, USA. *The Journal of Foraminiferal Research*, *45*(2), pp.146-155.

Milker, Y., Nelson, A.R., Horton, B.P., Engelhart, S.E., Bradley, L-A., and Witter, R.C., 2016. Differences in coastal subsidence in southern Oregon (USA) during at least six prehistoric megathrust earthquakes. *Quaternary Science Reviews*.

Leonard, L.J., Hyndman, R.D. and Mazzotti, S., 2004. Coseismic subsidence in the 1700 great Cascadia earthquake: Coastal estimates versus elastic dislocation models. *Geological Society of America Bulletin*, *116*(5-6), pp.655-670.

Leonard, L.J., Currie, C.A., Mazzotti, S. and Hyndman, R.D., 2010. Rupture area and displacement of past Cascadia great earthquakes from coastal coseismic subsidence. *Bulletin*, *122*(11-12), pp.2079-2096.

Nelson, A.R., 1992. Discordant 14C ages from buried tidal-marsh soils in the Cascadia subduction zone, southern Oregon coast. *Quaternary Research*, *38*(1), pp.74-90.

Nelson, A.R., Shennan, I. and Long, A.J., 1996. Identifying coseismic subsidence in tidal-wetland stratigraphic sequences at the Cascadia subduction zone of western North America. *Journal of Geophysical Research: Solid Earth*, *101*(B3), pp.6115-6135.

Nelson, A.R., B.F. Atwater, P.T. Bobrowsky, L-A. Bradley, J.J. Clague, G.A. Carver, M.E. Darienzo, W.C. Grant, H.W. Krueger, R. Sparks, T.W. Stafford, Jr., and M. Stuiver, 1995, Radiocarbon evidence for extensive plate-boundary rupture about 300 years ago at the Cascadia subduction zone: Nature, v. 378, p. 371-374.

Nelson, A.R., Y. Ota, M. Umitsu, K. Kashima, and Y. Matshushima, 1998, Seismic or hydrodynamic control of rapid late-Holocene sea-level rise in southern coastal Oregon, USA?: The Holocene, v. 8, p. 287-299.

Peterson, C.D., Darienzo, M.E., Pettit, D.J., Jackson, P.L. and Rosenfeld, C.L., 1991. Littoral-cell development in the convergent Cascadia Margin of the Pacific Northwest, USA.

Patton, J.R., Romsos, C., Black, B., Morey, A.E., Djadjadihardja, Y. and Goldfinger, C., 2013. Seismoturbidite record as preserved at core sites at the Cascadia and Sumatra–Andaman subduction zones.

Priest, G.R., Goldfinger, C., Wang, K., Witter, R.C., Zhang, Y. and Baptista, A.M., 2010. Confidence levels for tsunami-inundation limits in northern Oregon inferred from a 10,000-year history of great earthquakes at the Cascadia subduction zone. *Natural Hazards*, *54*(1), pp.27-73.

Reinhart, M.A., 1991. Sedimentological analysis of postulated tsunami-generated deposits from Cascadia great-subduction earthquakes along southern coastal Washington. *MSc, University of Washington, Seattle, WA*, *77*.

Rothwell, R.G. and Rack, F.R., 2006. New techniques in sediment core analysis: an introduction. *Geological Society, London, Special Publications*, *267*(1), pp.1-29.

Sabean, J. 2004, Application of foraminifera to detecting land level change associated with great earthquakes along the west coast of North America [unpublished M.S, thesis]: Department of Earth Sciences, Simon Fraser University, Vancouver, Canada, 85 pp.

Satake, K., Wang, K. and Atwater, B.F., 2003. Fault slip and seismic moment of the 1700 Cascadia earthquake inferred from Japanese tsunami descriptions. *Journal of Geophysical Research: Solid Earth*, *108*(B11).

Scott, D.B. and Medioli, F.S., 1980. Living vs. total foraminiferal populations: their relative usefulness in paleoecology. *Journal of Paleontology*, pp.814-831.

Shennan, I., Long, A.J., Rutherford, M.M., Green, F.M., Innes, J.B., Lloyd, J.M., Zong, Y. and Walker, K.J., 1996. Tidal marsh stratigraphy, sea-level change and large earthquakes, I: a 5000 year record in Washington, USA. *Quaternary Science Reviews*, *15*(10), pp.1023-1059.

Shennan, I. and Hamilton, S., 2006. Coseismic and pre-seismic subsidence associated with great earthquakes in Alaska. *Quaternary Science Reviews*, *25*(1-2), pp.1-8.

Shennan, I., Barlow, N., Combellick, R., Pierre, K. and Stuart-Taylor, O., 2014. Late Holocene paleoseismology of a site in the region of maximum subsidence during the 1964 Mw 9.2 Alaska earthquake. *Journal of Quaternary Science*, *29*(4), pp.343-350.

Shennan, I., Garrett, E. and Barlow, N., 2016. Detection limits of tidal-wetland sequences to identify variable rupture modes of megathrust earthquakes. *Quaternary Science Reviews*, *150*, pp.1-30.

Troels-Smith, J., 1955. Karakterisering af lose jordarter. Characterization of unconsolidated sediments.

Watcham, E.P., Shennan, I. and Barlow, N.L., 2013. Scale considerations in using diatoms as indicators of sea-level change: lessons from Alaska. *Journal of Quaternary Science*, *28*(2), pp.165-179.

Witter, R.C., H.M. Kelsey, and E. Hemphill-Haley, 2003, Great Cascadia earthquakes and tsunamis of the past 6700 years, Coquille River estuary, southern coastal Oregon, Geological Society of America Bulletin, v. 115, p. 1289-1306, doi: 10 .1130 /B25189 .1.

Witter, R.C., Zhang, Y.J., Wang, K., Goldfinger, C., and Priest, G.R., 2012, Coseismic slip on the southern Cascadia megathrust implied by tsunami deposits in an Oregon lake and earthquake-triggered marine turbidites: Journal of Geophysical Research, v. 117, p. B10303, doi: 10.1029 /2012JB009404.

Witter, R.C., Zang, Y.J., Wang, K., Priest, G.R., Goldfinger, C., Stimely, L., English, J.T., and Ferro, P.A., 2013, Simulated tsunami inundation for a range of Cascadia megathrust earthquake scenarios at Bandon, Oregon, USA: Geosphere, v. 9, p. 1783-1803, doi: 10.1130/GES00899.1.

Wang, K., Wells, R., Mazzotti, S., Hyndman, R.D. and Sagiya, T., 2003. A revised dislocation model of interseismic deformation of the Cascadia subduction zone. *Journal of Geophysical Research: Solid Earth*, *108*(B1).

Wang, P.L., Engelhart, S.E., Wang, K., Hawkes, A.D., Horton, B.P., Nelson, A.R. and Witter, R.C., 2013. Heterogeneous rupture in the great Cascadia earthquake of 1700 inferred from coastal subsidence estimates. *Journal of Geophysical Research: Solid Earth*, *118*(5), pp.2460-2473.

Table 1. Paleoseismic subsidence estimates used in this study.

Site	Latitude (°N)	Longitude (°W)	Subsidence (m)	Standard Deviation (m)	Reference	Remarks
Vancouver Island						
Meares Island	49.15	-125.86	0.80	±0.19	*Guilbault et al.* [1996]	Estimate revised by *Kemp et al.* [2018]
Cemetery	49.15	-125.85	0.75	±0.25	*Guilbault et al.* [1996]	Estimate revised by *Kemp et al.* [2018]
Washington						
Copalis River	47.12	-124.17	≥0.91	Minimum	This work	
Ocean Shores	47.0	-124.14	0.81	±0.39	*Adams, 2017*	
Ocean Shores	47.0	-124.13	≥0.82	Minimum		
Johns River	46.90	-123.99	0.39	±0.36	This work	
Johns River	46.89	-123.98	≥0.80	Minimum	This work	
Smith Creek	46.74	-123.89	1.52	±0.51	This work	
Bone River	46.65	-123.918	0.91	±0.50	This work	
Niawiakum River	46.61	-123.91	1.21	±0.84	*Sabean* [1994]	Estimate revised by *Kemp et al.* [2018]
Naselle River	46.42	-123.89	0.74	±0.47	This work	
Naselle River	46.43	-123.89	≥1.38	Minimum	This work	
Oregon						
Nehalm	45.70	-123.88	1.16	±0.55	*Hawkes et al.* [2011]	Estimate revised by *Kemp et al.* [2018]
Netarts Bay	45.70	-123.94	0.39	±0.20	*Hawkes et al.* [2011]	Estimate revised by *Kemp et al.* [2018]
Nestucca	45.18	-123.94	1.09	±0.46	*Hawkes et al.* [2011]	Estimate revised by *Kemp et al.* [2018]
Salmon River	45.03	-123.98	1.41	±0.43	*Hawkes et al.* [2011]	Estimate revised by *Kemp et al.* [2018]
Siletz	44.90	-124.03	0.80	±0.41	*Wang et al.* [2013]	Estimate revised by *Kemp et al.* [2018]
Alsea Bay	44.43	-124.03	0.16	±0.21	*Wang et al.* [2013]	Estimate revised by *Kemp et al.* [2018]
Siuslaw	43.98	-124.06	0.50	±0.41	*Hawkes et al.* [2011]	Estimate revised by *Kemp et al.* [2018]
South Slough	43.33	-124.32	1.21	Minimum	*Hawkes et al.* [2011]	Estimate revised by *Kemp et al.* [2018]
Talbot Creek	43.29	-124.30	0.63	±0.43	*Milker et al.* [2016]	Estimate revised by *Kemp et al.* [2018]
Coquille	43.15	-124.39	1.31	Minimum	*Wang et al.* [2013]	Estimate revised by *Kemp et al.* [2018]
California						
Humboldt Bay	40.87	-124.15	0.58	±0.36	*Padgett et al.* [in prep]	Average of nine subsidence estimates

Table 2. Slip Values and Earthquake Magnitudes of Different Models

Model	Figure	Peak Slip[a] (years)	Moment (N m)	M_w
Preferred	7	450, 400, 550, 450	2.57E+22	8.87
Four patch	8	500, 550, 500, 450	2.68E+22	8.89
Five patch	9	400, 500, 550, 500, 450	2.41E +22	8.85
Six patch	10	400, 500, 550, 550, 500, 450	1.90E +22	8.79

[a]Slip is measured in terms of recovered slip deficit accumulated over a period of time. For multiple high-slip patches, the peak values are listed for north to south.
[b]The moment is calculated using a rigidity of 40 GPa

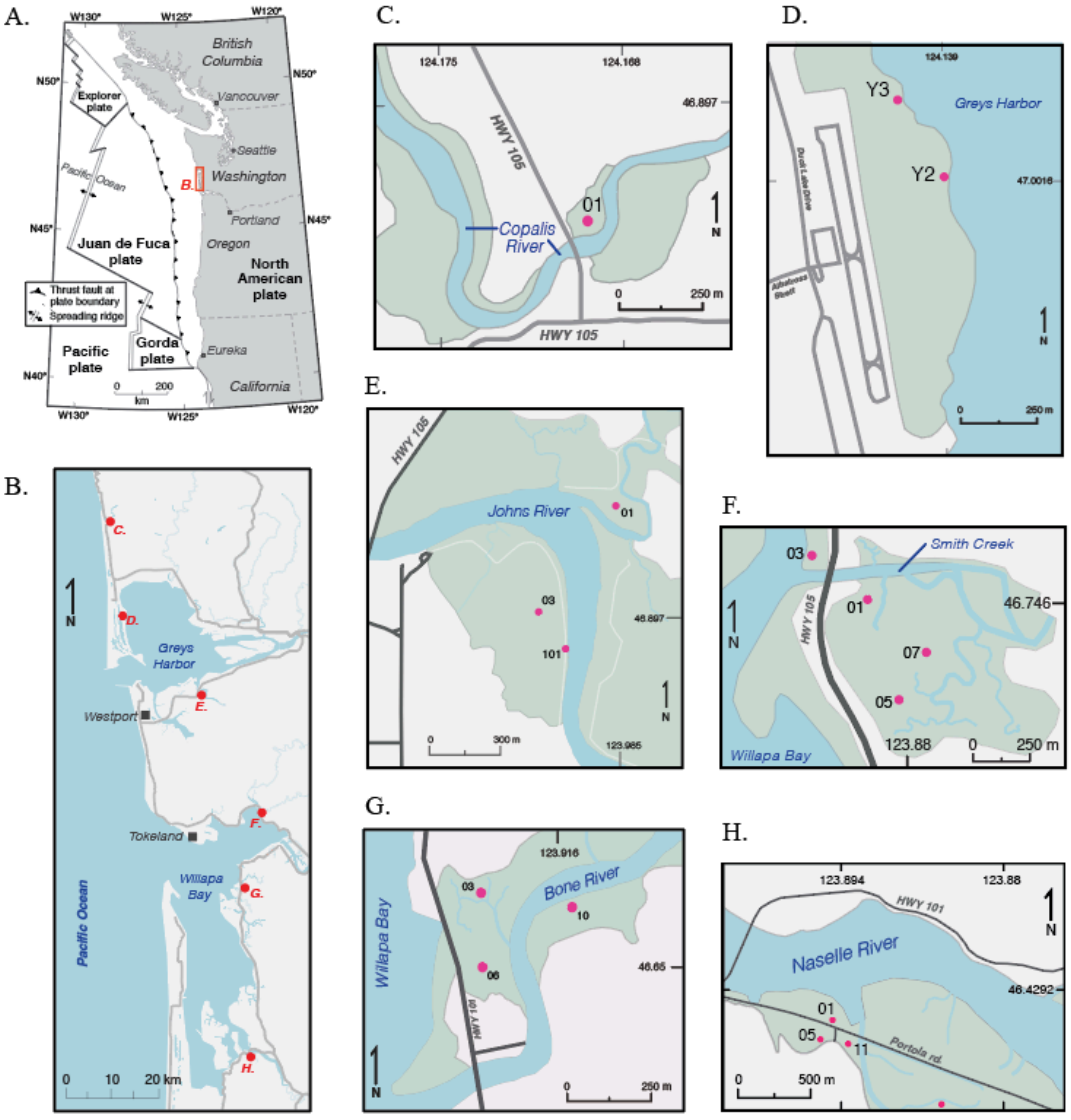

Figure. 1

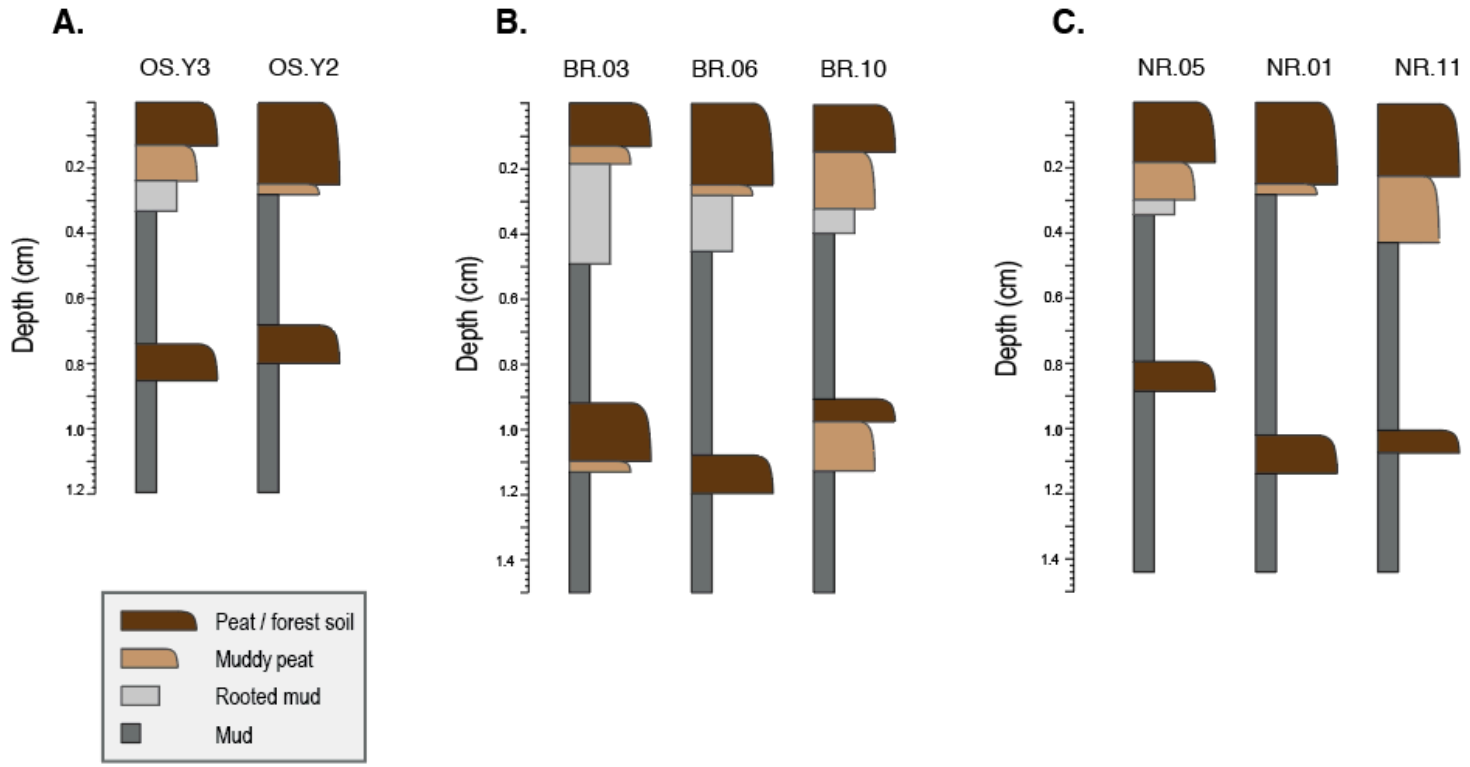

Figure 2.

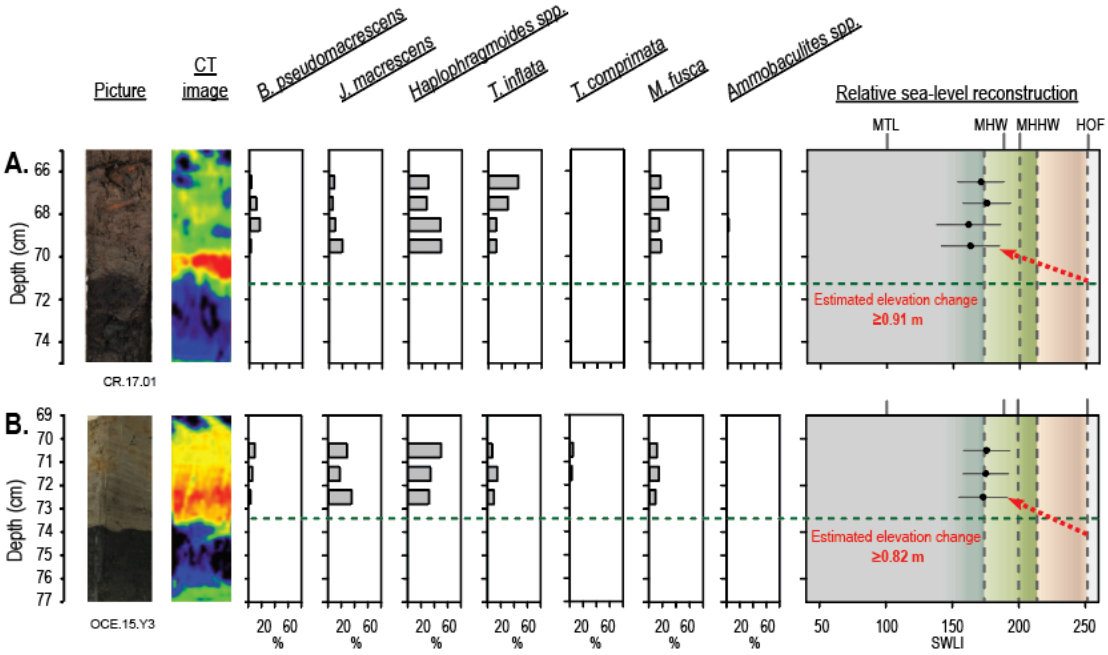

Figure 3.

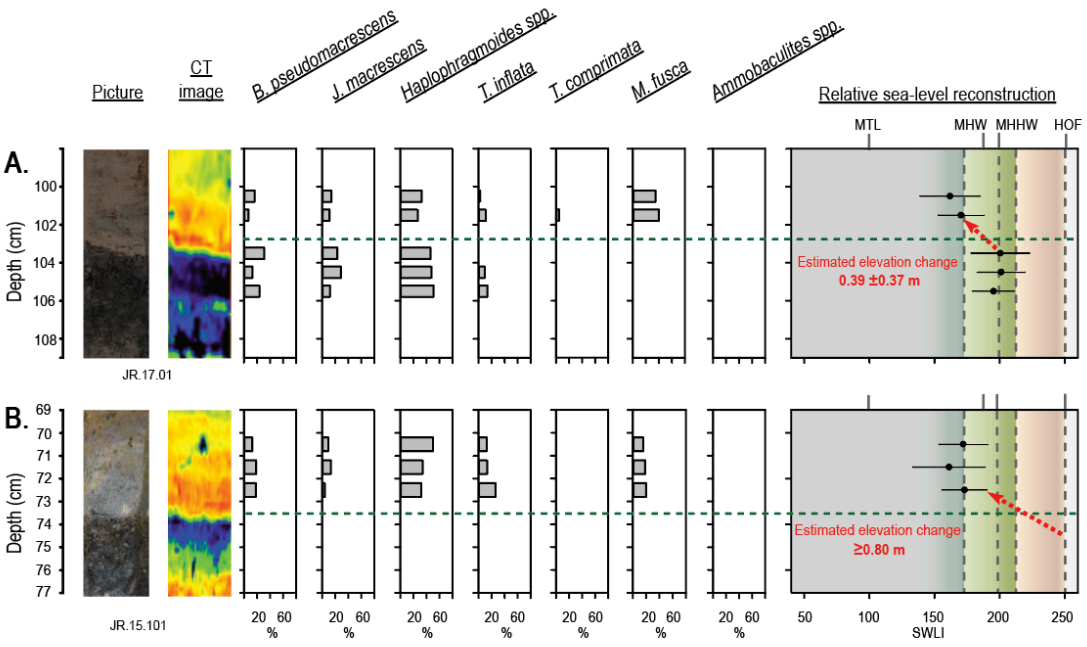

Figure 4.

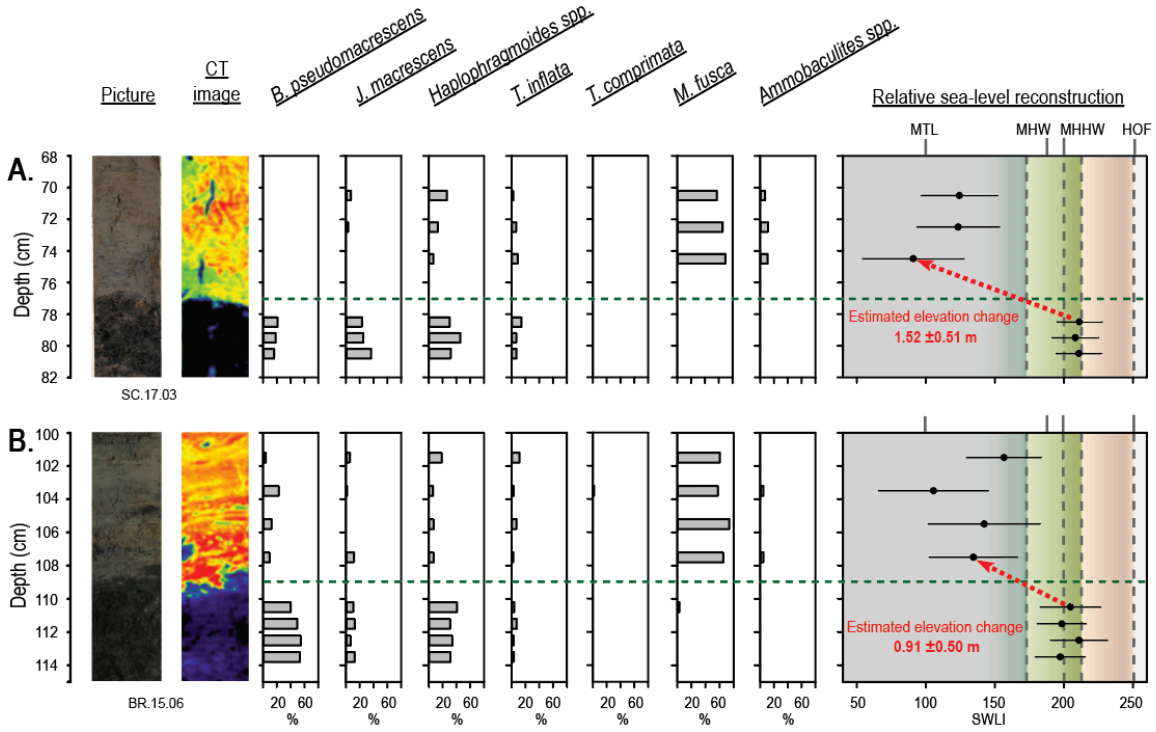

Figure 5.

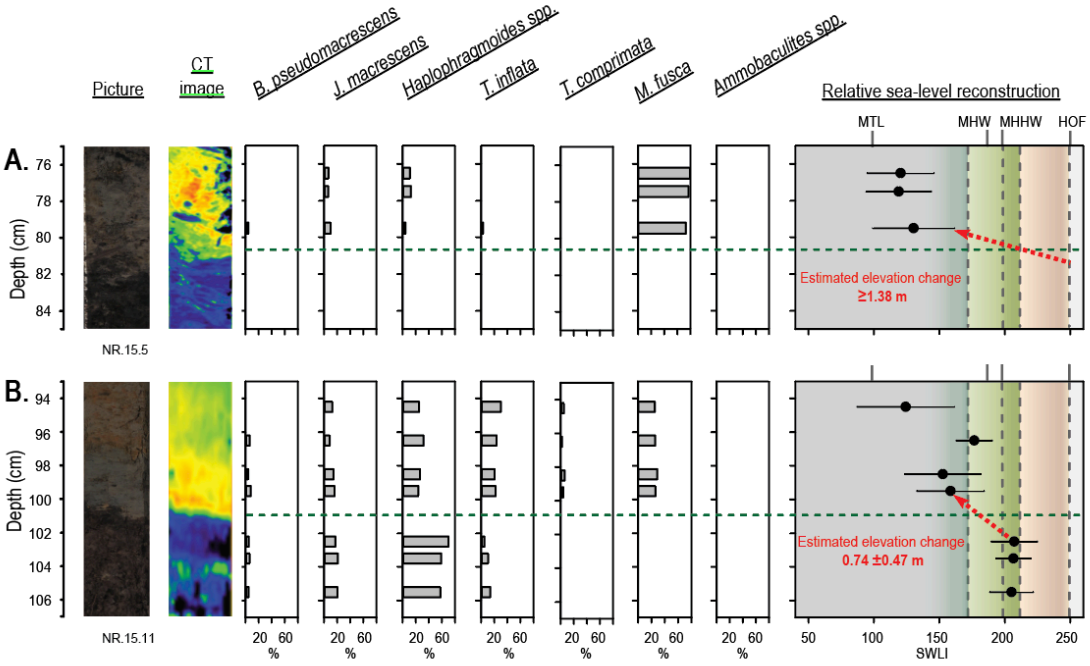

Figure 6.

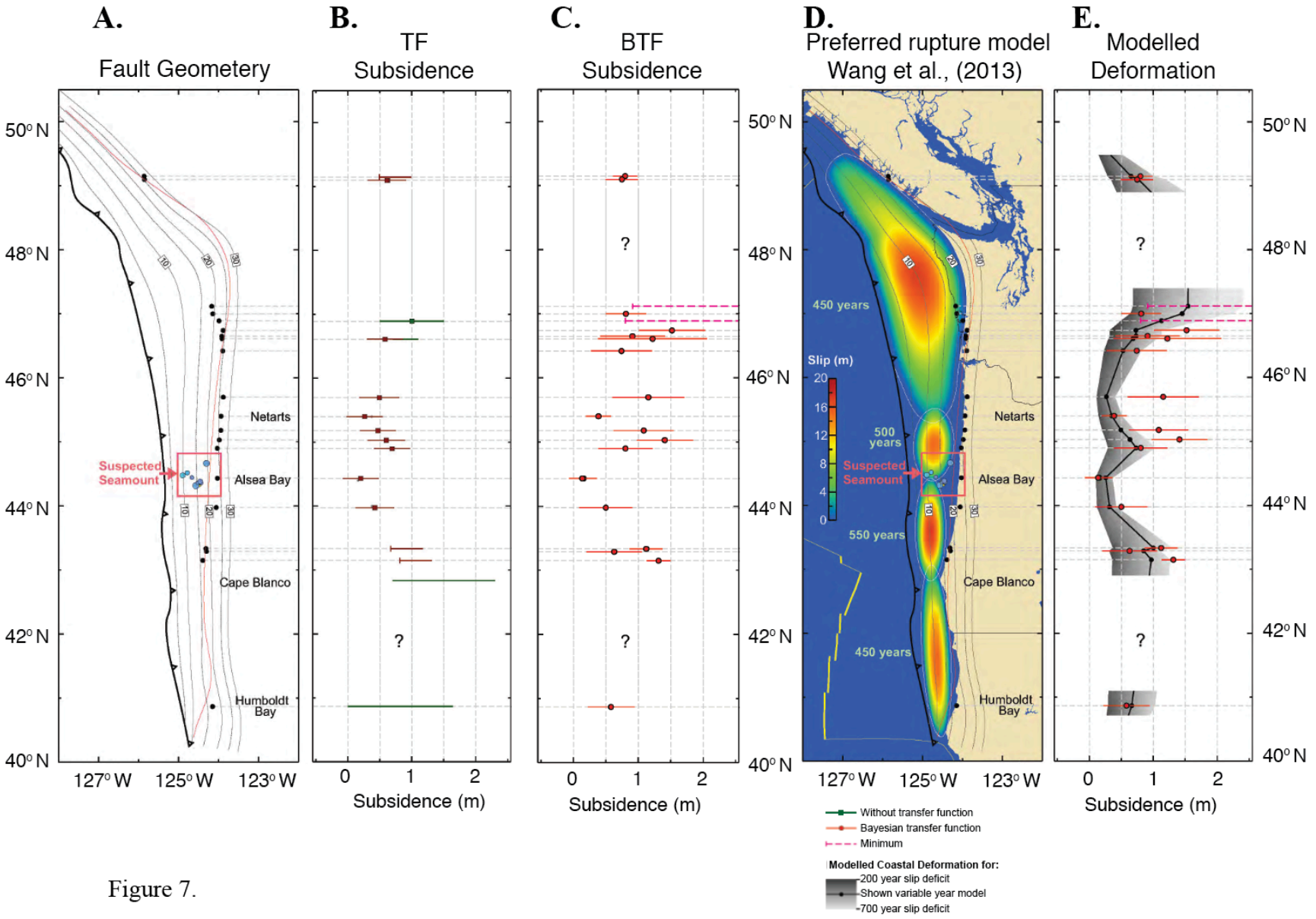

Figure 7.

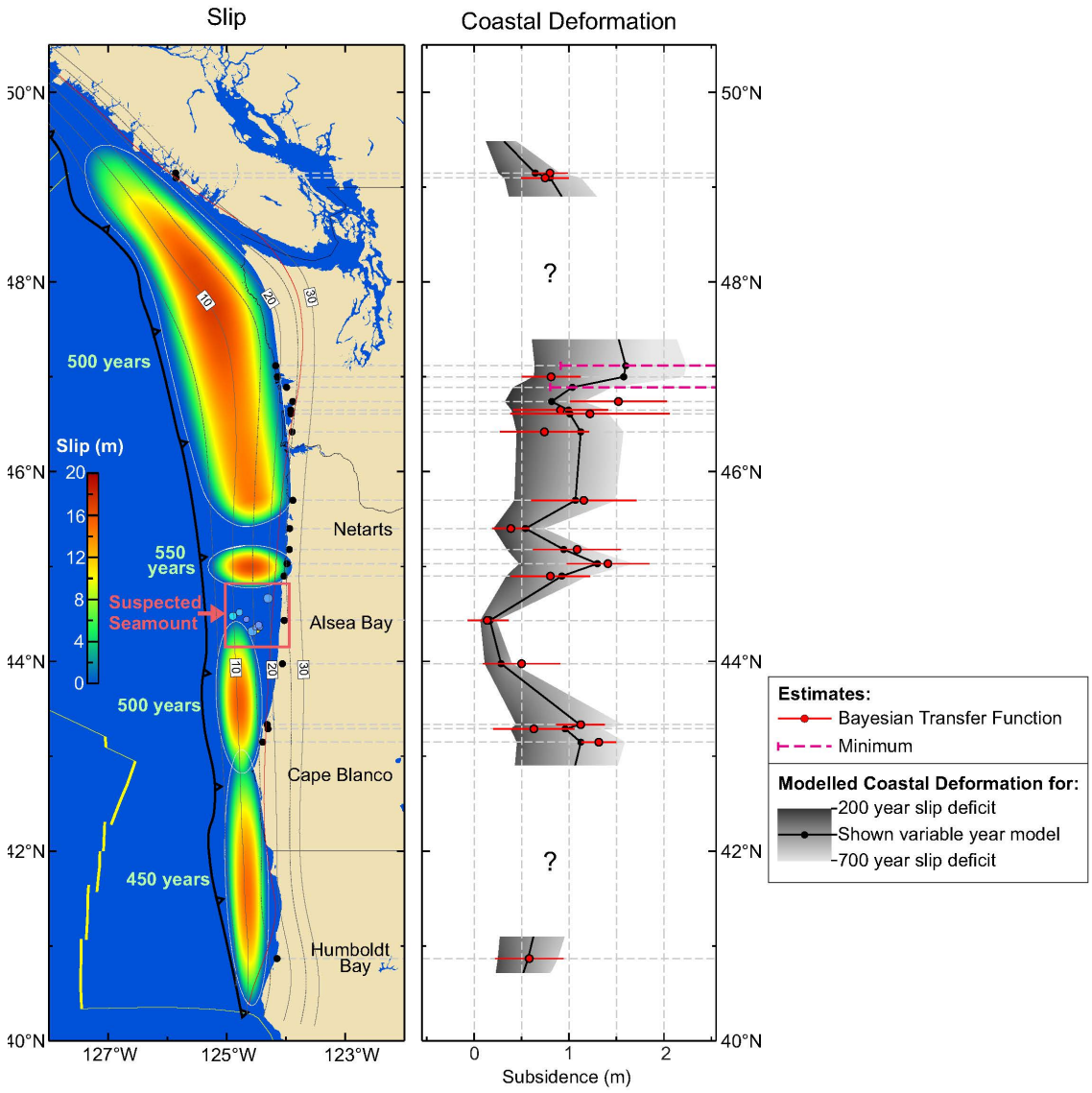

Figure 8.

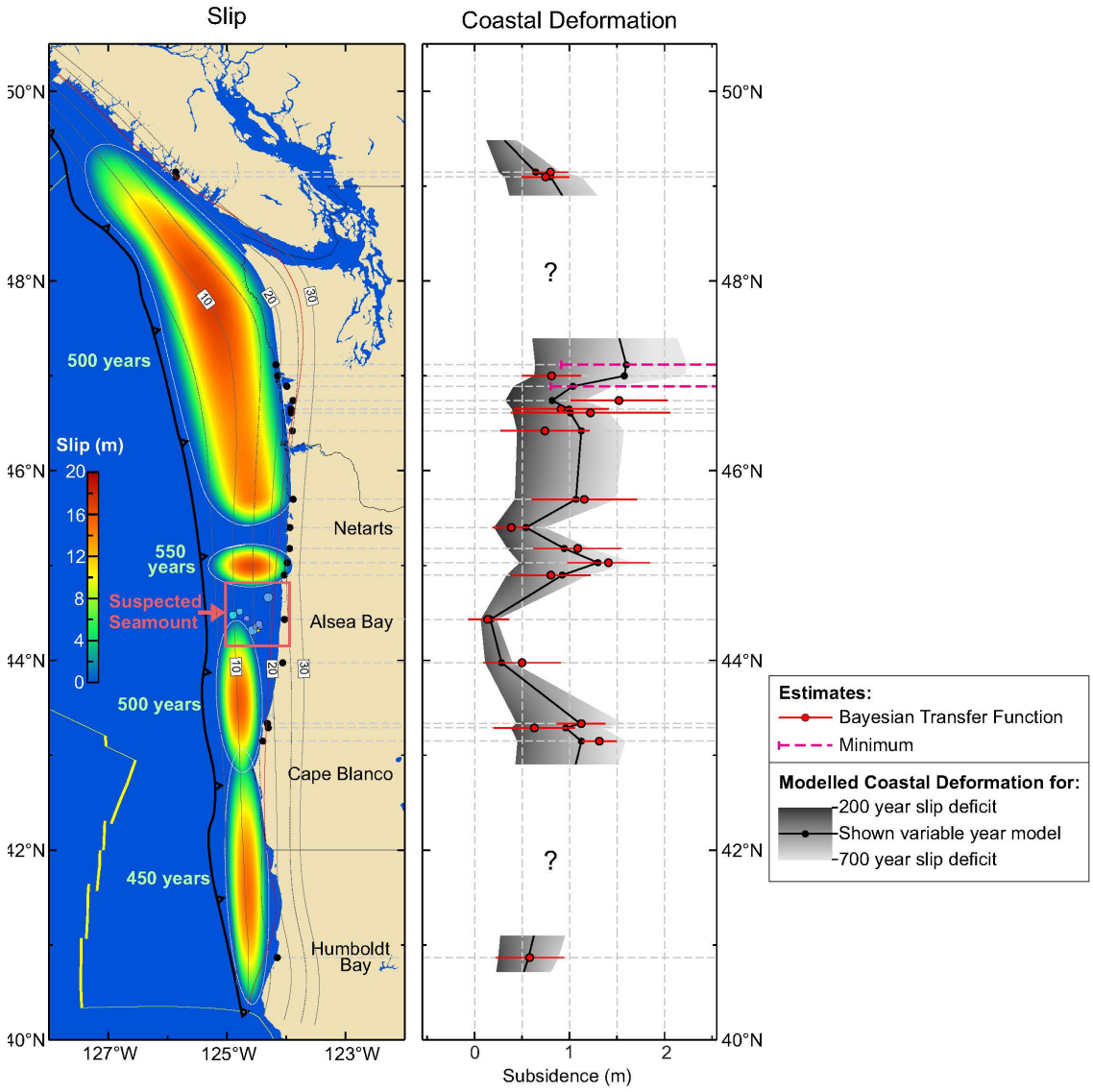

Figure 9.

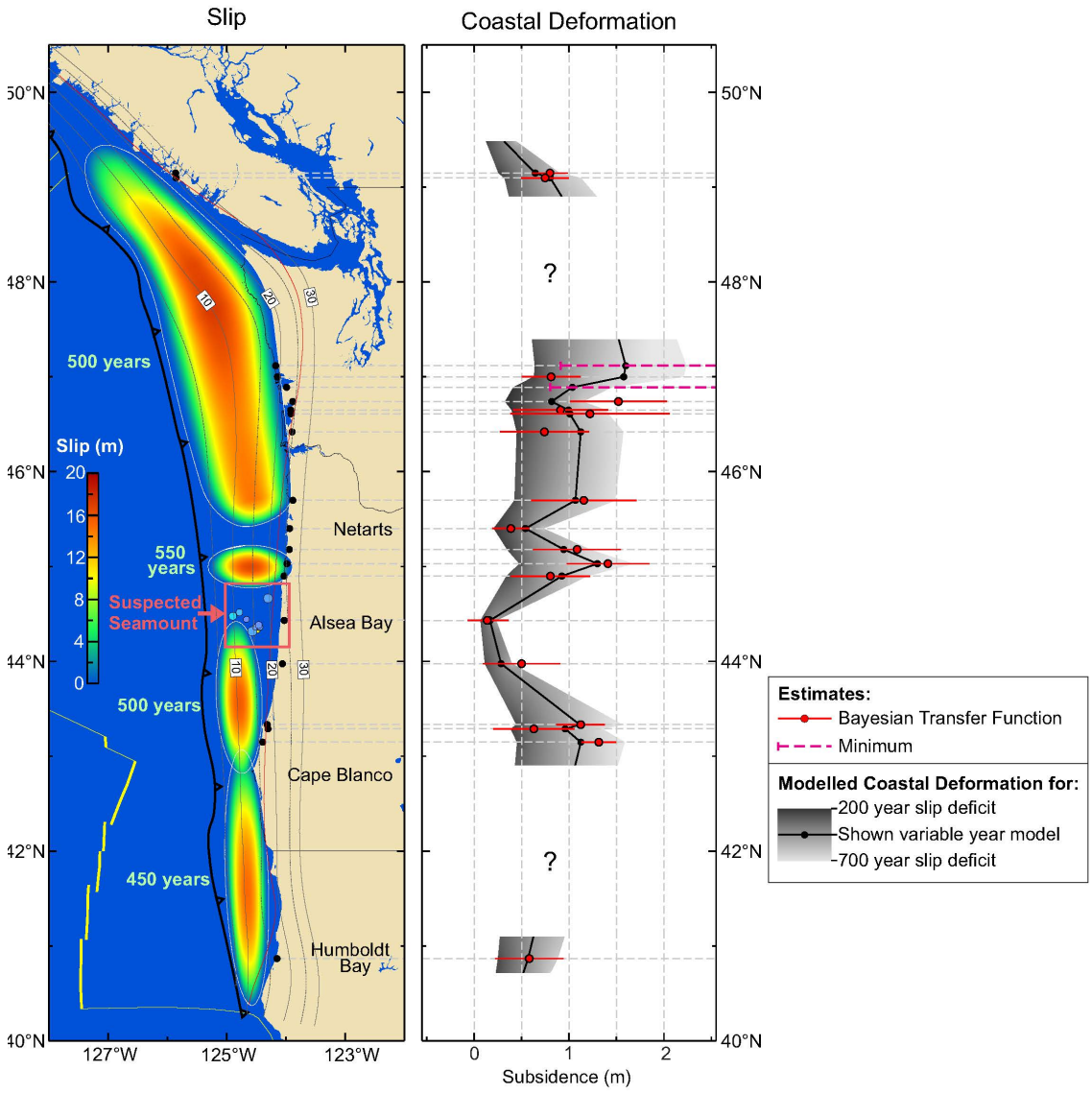

Figure 10.